Aus dem Nephrologischen Zentrum
Medizinische Klinik und Poliklinik IV
Ludwig-Maximilians Universität München
Direktor: Prof. Dr. med. Martin Reincke

Interleukin-1β Inhibition for Chronic Kidney Disease in Obese Mice with Type 2 Diabetes

Dissertation
zum Erwerb des Doktorgrades der Medizin
an der Medizinischen Fakultät der
Ludwig-Maximilians-Universität zu München

vorgelegt von
Yutian Lei
aus Fujian, China
2020

Mit Genehmigung der Medizinischen Fakultät
der Ludwig-Maximilians-Universität München

Berichterstatter:	Prof. Dr. med. Hans-Joachim Anders
Mitberichterstatter:	PD Dr. Jutta Nagel
Mitberichterstatter:	PD Dr. Martin Füchtenbusch
Mitberichterstatter:	Prof. Dr. Susanna Hofmann
Mitbetreuung durch den promovierten Mitarbeiter:	
Dekan:	Prof. Dr. med. dent. Reinhard Hickel
Tag der mündlichen Prüfung:	19.05.2021

The present study was conducted from September 2015 to May 2019 at Nephrologisches Zentrum, Medizinische Klinik und Poliklinik IV, Innenstadt Klinikum der Universität München.

This dissertation was supervised by Prof. Dr. med. Hans-Joachim Anders.

Publication

Lei Y, Devarapu SK, Motrapu M, Cohen CD, Lindenmeyer MT, Moll S, Kumar SV, Anders HJ: Interleukin-1β Inhibition for Chronic Kidney Disease in Obese Mice With Type 2 Diabetes. *Frontiers in Immunology*, 2019;10:1223. DOI: 10.3389/fimmu.2019.01223.

Grant support

LMU-CSC Scholarship Program (2015-2019)

Contents

1 Introduction

1.1 Chronic kidney disease

1.1.1 Definition

A wide range of disorders can induce chronic kidney disease (CKD) and affect kidney structure or/and function in a long term [1]. According the definition of CKD in KDIGO 2012, over 3 months of abnormal manifestations in kidney structure or function is defined as CKD [1]. So far the indication of kidney structural and functional abnormalities is based on various assessments. According to KDIGO 2012, the indication includes reduced glomerular filtration rate (GFR) (<60 ml/min/1.73²), structural changes diagnosed by imaging or histology, kidney transplantation, increased urine albumin excretion, aberrant urinary sediment, and electrolyte, water, acid-base imbalance as a consequence of various tubular disorders [1].

1.1.2 Classification

As CKD population contains a highly heterogeneous group of individuals in terms of primary diseases and kidney damage status, the risks of adverse outcomes, such as cardiovascular diseases, kidney disease worsening, or progression to kidney failure, also differs accordingly [2]. KDIGO recommends to classify CKD by the cause, urine albumin excretion, and GFR levels [1]. In general, the risks of major outcomes increases with the increase of urine albumin excretion rate and GFR loss, as shown in Figure 1.1. The causes of CKD also have a profound effect on prognosis. For instance, a patients with CKD G3 due to diabetes might have a higher risks of adverse events than a patient with CKD G4 due to tubulointerstitial disease [2]. When a patient enters CKD G5 or requires kidney replacement treatment (KRT) such as dialysis or transplantation, this stage is termed as kidney failure with replacement therapy (KFRT) [3].

1.1.3 The burden of chronic kidney disease

The wide prevalence, high mortality and morbidity rate, and high cost of KRT has made CKD a great burden for public health. The worldwide population affected by CKD is large and continues growing. It is estimated that in 2017 there were 843.6 million individuals with CKD, accounting for 11.1% of world's population. Meanwhile around 3.9 million patients received KRT worldwide [4]. A study estimated that the number of individuals receiving KRT will reach 5.44 million by 2030 [5]. Besides, CKD contributes substantially to global mortality and morbidity [6]. It is also an independent risk factor for cardiovascular disease [7]. In 2017, around 4.5% of death was due to CKD or CKD-related cardiovascular disease [6]. Further, the cost for KRT is high and causes a great economic burden to the society [8]. It is estimated that in 2010, around 2.6 million patients received KRT while at the same time there were almost an equivalent number of patients (2.3 million) did not have accessibility to KRT [5].

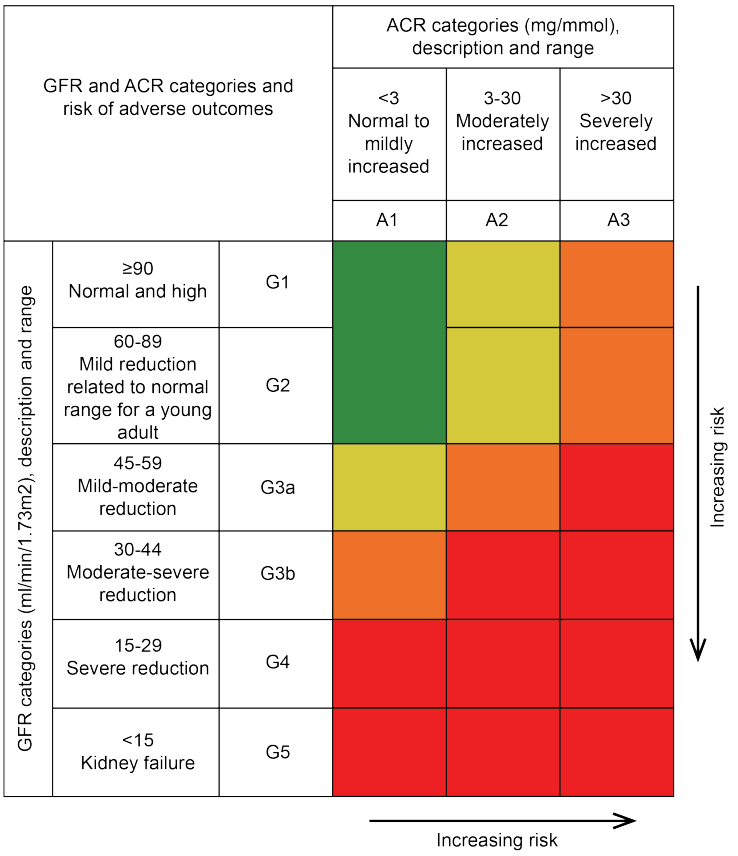

Figure 1.1: A classification of CKD prognosis depending on GFR and urine albumin excretion. This heatmap shows the CKD prognosis classification. CKD risk is classified into low (green color), moderate (yellow), high (orange), and very high (red) dependent on GFR (G1-G5) and ACR (A1-A3) categories. CKD, chronic kidney disease. GFR, glomerular filtration rate. ACR, albumin-creatinine ratio. Adapted from [1].

1.1.4 Diabetes in chronic kidney disease

The past decades, the prevalence of diabetes mellitus (DM) has increased markedly and this growing tendency will continue in the following decades [9]. It is estimated that in 2017, 8.4% adults (451 million adults) had DM globally. The estimated number of diabetic individuals by 2045 is projected to 9.9% of the global population (693 million) [9].

As DM is one of the most common causes for CKD [10, 6], the prevalence of DM also increases the burden of CKD [6]. Of all the DM categories, type 2 diabetes (T2D) predominantly represents 90 to 95% of those with diabetes [11, 12]. In 2017, DM was attributed to around 30% of CKD-related disability, ranking as the largest contributor than any other causes [6]. Compared to patients with non-diabetic kidney diseases, CKD patients with diabetes have higher risks of developing cardiovascular disease and progression to KFRT [13]. Thus, there is a great unmet medical need to improve outcomes for CKD with diabetes.

1.2 Diabetic kidney disease

1.2.1 Natural history

The nature history of diabetic kidney disease (DKD) was described by Mogensen CE, *et al.* in the 1980s. In this classic description, which was mainly based on proteinuria progression among patients with type 1 diabetes (T1D), it illustrated a 5-stage DKD: early hypertrophy-hyperfunction, glomerular lesions without clinical disease, incipient DKD with microalbuminuria (15-300 µg/min) and normal GFR, overt DKD with persistent proteinuria (>0.5 g/day) and declined GFR, and KFRT [14]. This concept evolved due to the heterogeneity of DKD phenotype on the basis of albuminuria and GFR, which are the most prominent markers in predicting risk of KFRT and renal death [15, 16, 17]. For instance, the NEFRON study collected data from 3893 patients with T2D and found of the 48.1% diabetic patients with CKD, only 10% exhibited albuminuria and reduced GFR, 20% exhibited only mildly increased albuminuria, 4.1% exhibited only moderately increased albuminuria, and 12.4% exhibited reduced GFR and normal albuminuria [15]. As shown in Figure 1.2, in a classic phenotype, whole-kidney GFR level increases in the early stage, then drops to normal level, and continuously declines. Microalbuminuria appears in the hyperfiltration stage and progresses to macroalbuminuria as GFR declines. In non-classic phenotypes, total kidney GFR declines before the onset of macroalbuminuria or even microalbuminuria. Notably, here total kidney GFR refers to the filtration level as a whole organ or the sum of all single-nephron GFR. Total kidney GFR and single-nephron GFR do not always match. For example, in the early stage of DKD, sodium-glucose cotransporter (SGLT)-mediated dysfunction of tubular-glomerular feedback results in an increase in single-nephron GFR as well as whole-kidney GFR if the total nephron number remains similar. As DKD progresses and total kidney GFR declines but single-nephron GFR increases as less and less nephrons have to handle the same filtration load [15].

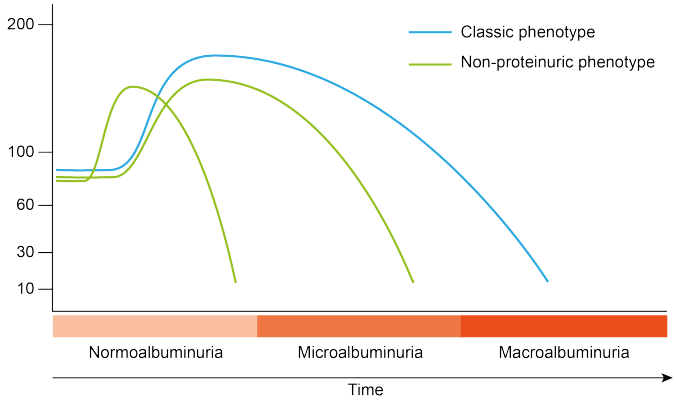

Figure 1.2: Evolution of kidney function in diabetic kidney disease. Increased and subsequent decrease of glomerular filtration rate in patients with proteinuria (classic phenotype), microalbuminuria, and normoalbuminuria (the latter two, non-proteinuric phenotype). Adapted from [16].

1.2.2 Hemodynamic alterations

As mentioned before, a typical GFR evolution in DKD is characterized by an increased whole-kidney GFR in the early phase. After the GFR reaches the maximum, it starts to decline, in parallel with nephron loss [17]. There are at least two distinct elements contributes to hyperfiltration [18, 17]. One is due to nephron loss, the remnant nephron undergoes structural and function changes, resulting in hypertrophy and single-nephron hyperfiltration, as shown in Figure 1.3. By using this strategy, kidneys try to compensate the loss of nephrons, and to maintain overall filtration and absorption levels [18, 17]. The other element is that diabetic conditions (hyperglycaemia, hormones, metabolites), as well as obesity, promote hyperfiltration [17]. How diabetic conditions drive hyperfiltration may comprise several mechanisms and is still not fully understood. One major mechanism is abnormal tubuloglomerular feedback [18, 17]. After glucose passes through glomerular basement membrane (GBM), it is reabsorbed together with sodium at 1:1 ratio via SGLT1/2 at proximal tubule cells [19]. In diabetic patients, excessive glucose filtration causes excessive glucose and sodium reabsorption at proximal tubules. Therefore, less sodium is transported to the distal tubular lumen at the *macula densa*. In response to the reduced sodium level in the tubular lumen, the *macula densa* produces less adenosine. Less adenosine activity at the afferent arteriole leads to vasodilation and increased GFR [19].

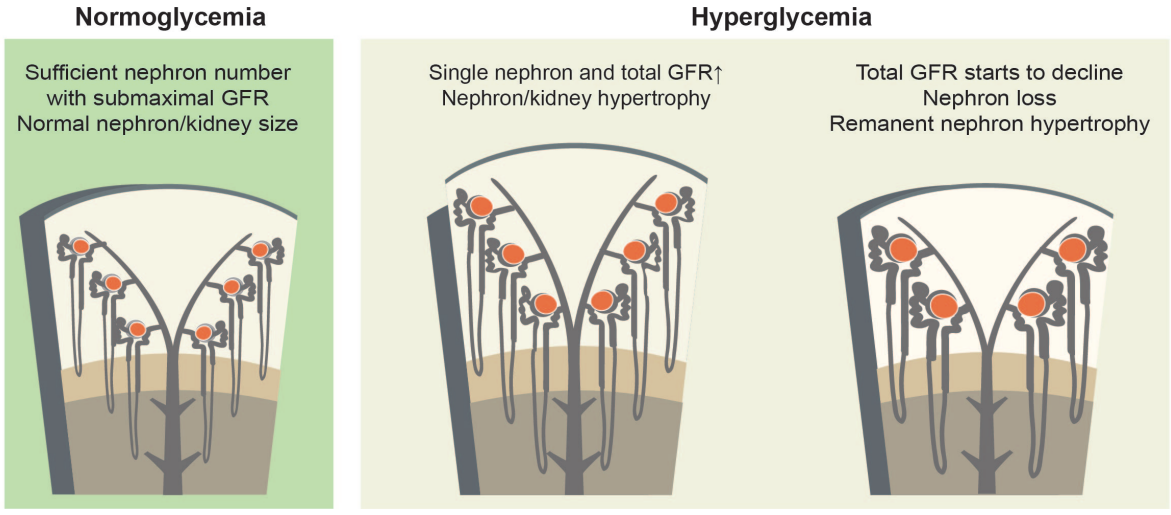

Figure 1.3: Schematic drawing of nephron loss in diabetic kidney disease. In individuals with hyperglycemia, elevated blood glucose and SGLT2-mediated tubuloglomerular feedback disorder increase the single nephron GFR and total kidney GFR, as well as the size of all glomeruli (hypertrophy). As the disease progression continues, some nephrons undergoes sclerosis and lost function. The remnant nephrons attempt to compensate the nephron loss and undergo further hyperfiltration and hypertrophy, which accelerates the nehphron loss. SGLT2, sodium-glucose transport protein 2; GFR, glomerular filtration rate.

1.2.3 Structural alterations

The structural changes in DKD is shown in Figure 1.4. In early stage, the thickness of basement membrane in GBM, tubules, and capillaries increases [20]. Podocytes flatten and undergo foot process effacement [21]. The mesangium expands diffusely due to an accumulation of extracellular material and cells [22]. Glomeruli increase in size [22]. As disease progresses, nodular mesangial expansion, also called Kimmelstiel-Wilson lesions, localize to the mesangium. There are round-shaped lesions with an acellular matrix core and few crescent-shaped nuclei around the periphery. Under scanning electron microscope, the glomerulus of nodular sclerosis site shows a nude and smooth GBM with few or no podocyte coverage [21]. In the more advanced phase, diffuse and nodular expansion leads to glomerulosclerosis. Glomeruli lose functional podocytes and are filled with matrix components [23]. Apart from alteration in glomerular tufts, the Bowman's capsule thickens, and occasionally displays a so-called insudative lesion, characterized by forming a "bridge" between capsule and glomerular tuft. Arteries, arterioles, and glomerular capillaries undergo hyalinosis as a result of deposition of plasma proteins and lipids [22]. Interstitial fibrosis and tubular atrophy follow the alteration in glomeruli. Infiltrated immune cells are present in glomeruli and interstitium [22, 24].

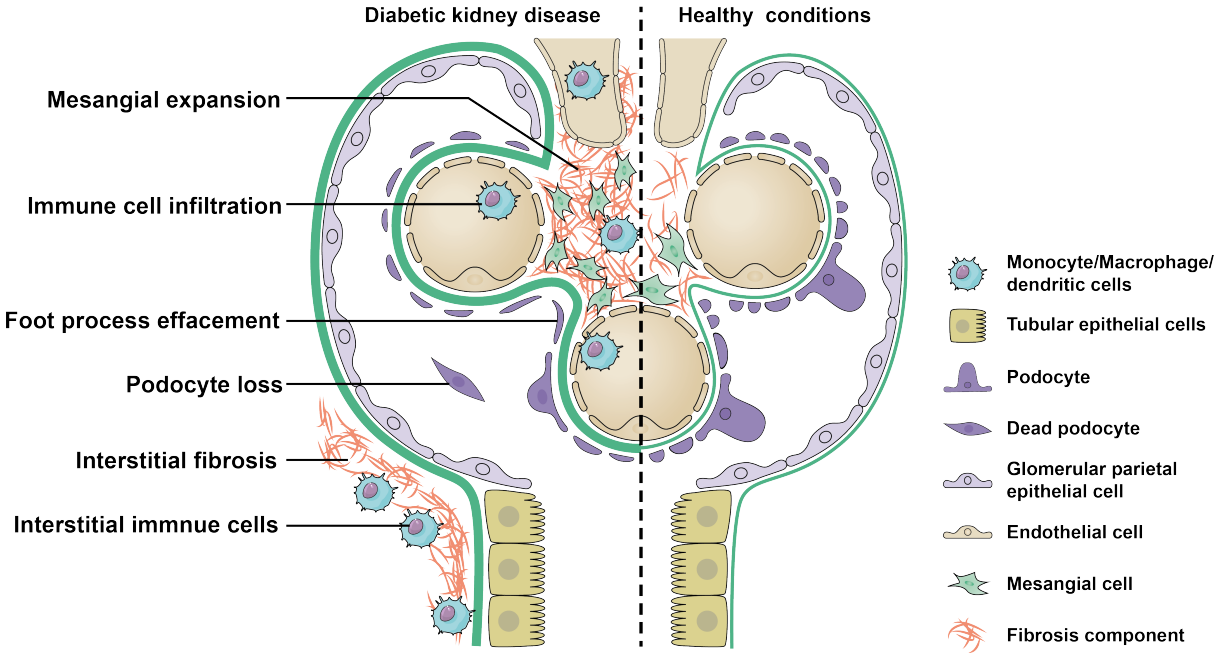

Figure 1.4: Schematic drawing of glomeruli in healthy conditions and diabetic kidney disease. In diabetic kidney disease (left), glomerular volume increases. Immune cells infiltrate to glomeruli as well as interstitium. Excessive mesangial cells, matrix, and immune cells accumulate in mesangial area. Podocyte undergoes foot process effacement and detachment. Interstitium undergoes fibrosis. Modified from reference [25].

1.2.4 Role of inflammation in diabetic kidney disease

A wide range of evidences suggest inflammation is a pathomechanistic contributor to the development of DKD [26, 27, 28]. Apart from the well-documented role of inflammation in established DKD, such as infiltrating immune cells [22] and upregulation of pro-inflammatory mediators [27], some evidences suggest that inflammation may also contribute to the initiation of DKD. One recent publication reviewed 31 urine proteomic/peptidomic studies and summarized robust urine markers in each stage of DKD. It showed that in early stage of DKD, when albuminuria was absent, inflammatory mediators such as α1-antitrypsin and clusterin, appeared in the urine, reflecting an early inflammation activity in kidney [29].

The mechanism by which inflammation leads to the initiation and progression of DKD is complicated and still not fully understood. Recently, Monika A.N., *et al*. analyzed 194 circulating inflammatory proteins by proteomics in diabetic patients with early or advanced DKD, and identified 17 inflammatory cytokines/proteins which were associated with a 10-year risk of KFRT, suggesting circulating cytokines/proteins contributes to kidney disease progression in DKD [30]. Of the 17 inflammatory cytokines/proteins, most were expressed by kidney infiltrating monocytes/macrophages and T cells, as confirmed by another single-nuclei sequence study, highly suggesting a causal role of infiltrated immune cells in pathogenesis of DKD [31]. Thus, systemic inflammation, either by circulating cytokines/proteins or by immune cell infiltration, may contribute to the initiation and progression of DKD [32].

Apart from systemic inflammation, many inflammatory pathways and molecules contribute to local inflammation in DKD (Figure 1.5). These deviations include metabolic abnormalities (hyperglycemia, hyperlipidemia, and numerous metabolites) [33], increased circulating inflammatory cytokines [30], hemodynamic alterations (hypertension, hyperfiltration, increased sheer stress) [34], increased oxygen consumption and kidney hypoxia [35, 36], and hormone dysregulation such as increased synthesis of angiotensin II [13]. These deviations act on almost all parenchymal cells of the kidney, such as podocytes, endothelial cells, tubular epithelial cells, and mesangial cells, and some non-parenchymal cells such as macrophages/dendritic cells. In some circumstance, dead cells or impaired cells release danger-associated molecular patterns (DAMPs) [37], which bind to pattern recognition receptors (PRRs) and activate proinflammatory signal pathways and transcript factors, like JAK-STAT and cytokine-dependent nuclear factor kappa-light-chain-enhancer of activated B cells (NF-κB), and increase the expression and secretion of proinflammatory cytokines [27].

The Evidence from pharmacological blockade or genetic loss in animal models of DKD have identified numerous proinflammatory cytokines as contributors to structural and functional alterations in DKD, such as interleukin-1β (IL-1β) [38], IL-6 [39], and tumor necrosis factor α (TNFα) [40, 41, 42]. The mechanism by which these cytokines lead to kidney impairment may

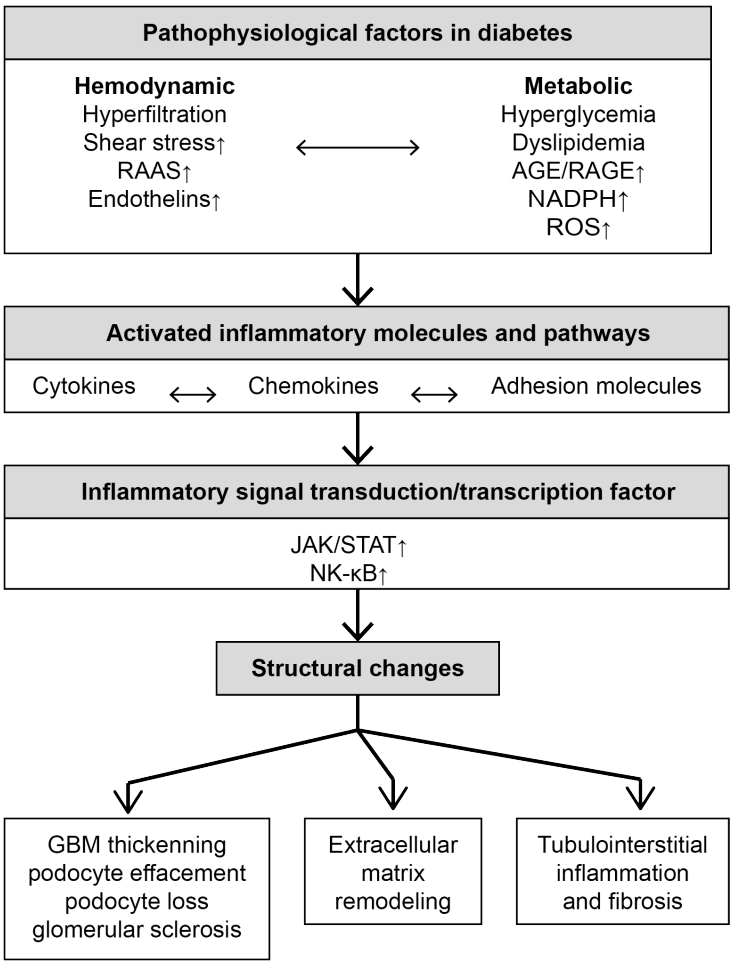

Figure 1.5: Inflammatory mechanisms and pathways leading to DKD. RAAS, renin-angiotensin-aldosterone system. RAGE, receptor for advanced glycation end products. NADPH, nicotinamide adenine dinucleotide phosphate. ROS, reactive oxygen species. AGE, advanced glycation end-products. NK-κB, nuclear factor kappa-light-chain-enhancer of activated B cells. GBM, glomerular basement membrane. JAK, Janus kinase. STAT, signal transducer and activator of transcription. Adapted from [27].

include oxidative stress [42, 38], inflammation amplification, such as upregulation of cytokine receptors and proinflammatory cytokines [42, 41, 40, 39], apoptosis and necroptosis [40], and fibrosis [43]. Proinflammatory cytokines could be novel promising therapeutic targets for DKD [27].

Taken together, inflammation is an essential mechanism in the progression of DKD. Cytokines releasing by numerous activated cell types in diabetes amplify kidney inflammation and contributes to kidney structural changes and functional deterioration, thus serving as potential therapeutic targets.

1.2.5 Current trials and new therapeutic approaches

Even though inflammation mechanism and pathways are well-identified in the past two decades, conventional treatment for DKD, including anti-hypertension therapy,

glucose-lowering therapy, and renin-angiotensin-aldosterone system blockade, remained unchanged. Recently, new therapeutic agents like sodium-glucose cotransporter 2 inhibitors (SGLT2i), have showed prominent kidney protection, as well as reduced cardiovascular events, expanding the treatment choice for DKD. Here I briefly summarized the recent phase-3 or -4 trials, both finished or ongoing, in diabetes or DKD to have an overview of current situation of new therapeutic approaches, as shown in Table 1.1. Notably, through the well-established role of inflammation in DKD, the number of 3- or 4-phase clinical trials using anti-inflammatory medicine is limited.

Sodium-glucose co-transporter 2 inhibitors

SGLT2i blocks glucose reabsorption at proximal tubules, as well as sodium reabsorption, thus restores tubuloglomerular feedback and single-nephron GFR [18]. The EMPA-REG OUTCOME trial found that empagliflozin had significant cardiovascular benefits in T2D patients with established cardiovascular disease [44]. Subgroup analysis found empagliflozin was associated with slower eGFR deterioration, slower albuminuria progression, and less incident KFRT, indicating the kidney benefits of SGLT2i [45]. Similar results were achieved in the CANVAS study using another SGLT2i canagliflozin [46, 47]. Diabetic patients without risks for cardiovascular events or with early stage of CKD also benefited from SGLT2i from less heart failure in another trial [48]. More recently, the CREDENCE trial has further expanded the tested population to individuals with T2D and CKD G1-3 and ≥ A3 and set kidney-related events as the primary outcome. They found that canagliflozin prevented adverse kidney outcomes by 30%, a direct evidence showing the kidney protective effects from SGLT2i [49]. The success of intervention by SGLT2i demonstrates the central role of hemodynamic factors in the progression of DKD.

Endothelin A receptor antagonist

Another novel agent is endothelin A receptor antagonist. It blocks endothelin-1 and/or endothelin A receptor, a pathway mediating sodium retention, fibrosis, and inflammation [49]. In SONAR trail, atrasentan has beneficial effects on serum creatinine increasing or progression to KFRT in CKD patients with T2D.

Glucagon-like peptide 1 analogue

Glucagon-like peptide 1 (GLP1) analogue is a class of glucose-lowering medicine. By binding to the GLP1 receptor on β cells, it can induce the release of insulin and at the same time inhibit the release of glucagon. It improved glycemic control and had cardiovascular benefits in individuals with T2D and high cardiovascular risks [50, 51]. Further, in AWARD-7 trial GLP1

analogue dulaglutide showed an protection effect on ameliorating GFR decline in diabetic individuals with CKD G3-G4 [52].

Dipeptidyl peptidase 4 inhibitors

Dipeptidyl peptidase-4 inhibitor (DPP4i) is another glucose-lowering medication that targeting DPP4, a protease that cleaves GLP1. Through improving glycemic control, DPP4i did not deliver further benefits on cardiovascular outcomes in diabetic patients in trials with cardiovascular events as primary endpoints [53, 54, 55]. A more recent cardiovascular outcome trial CARMELINA had tested an DPP4i linagliptin in T2D patients with moderate or high CKD risks and did not find an evidence of extra cardiovascular benefits [56].

Anti-mineralocorticoid

Anti-mineralocorticoid might be another promising agent for DKD. The PRIORITY trial tested spironolactone in patients with T2D and normal albuminuria [57]. Notably, the trial utilized urinary proteomics as an enrichment method to select high-risk normal-albuminuric diabetic patients for early intervention, which was an innovation in the field of clinical trials on DKD [57]. However, treatment with spironolactone failed to prevent albuminuria progression (ASN Kidney week 2019). Another two Phase 3 trials on finerenone (FIGARO-DKD, FIDELIO-DKD) are still ongoing.

1.3 Mouse models of diabetic kidney disease

1.3.1 Validation criteria

Over many years, researchers have been looking for a DKD animal model that shows characteristic phenotypes of human DKD in an accurate manner [61, 62]. The characteristic phenotypes include at least three aspects [61, 62]. Firstly, it should resemble the functional features of human DKD, such as reduced GFR, elevated albuminuria, and hypertension. Secondly, it should present similar kidney pathology to DKD patients, such as GBM thickening, mesangial expansion or nodular lesions, glomerular sclerosis, and interstitium fibrosis. Lastly, it should also share similar pathogenic pathways, which could be examined at transcription or protein expression levels, or share similar metabolic profiles [61, 62]. Some researchers proposed the goals of an acceptable DKD model [61, 62] as follows:

1. Mice have more than 50% GFR decline compared to their earlier lifetime.

2. Mice have more than 100 times of albuminuria than their age- and sex-matched controls.

Table 1.1: New therapeutic approaches in diabetic kidney disease.

Study	Medicine	Study Participants	Number of Patients	Primary and Secondary Endpoints	Results
EMPA-REG OUTCOME [44, 45]	Empagliflozin	T2D with established CVD	7020	Primary: 3p-MACE Secondary: 4p-MACE	Primary: treatment better. Secondary: treatment better
CANVAS Program [46]	Canagliflozin	T2D with high CVD risks or established CVD	10142	Primary: 3p-MACE Secondary.1: all-cause death secondary.2: CV death secondary.3: albuminuria progression	Primary: treatment better secondary.1: NS secondary.2: NS secondary.3: treatment better
DECLARE-TIMI 58 [48]	Dapagliflozin	T2D with high CVD risks or established CVD	17160	Primary.1: 3p-MACE Primary.2: a composite of CV death and hospitalization for HF Secondary.1: kidney composite outcomes Secondary.2: all-cause death	Primary.1: NS Primary.2: treatment better Secondary.1: treatment better Secondary.2: NS
CREDENCE [58]	Canagliflozin	T2D with CKD G1-3 and ≥ A3	4401	Primary: kidney composite outcomes	Primary: treatment better
CARMELINA [56]	Linagliptin	T2D with high CVD risks and CKD G3b-G4 or GFR 45-75† with UACR ≥ 200‡	6979	Primary: 3p-MACE Secondary.1: kidney composite outcomes	Primary: treatment non-inferior Secondary: NS
SONAR [59]	Atrasentan	T2D with CKD ≥ A3 and GFR 25-75†	2648	Primary: kidney composite outcomes	Primary: treatment better
FIGARO-DKD (NCT02545049)	Finerenone	T2D with CKD A3G1-2 or CKD A2 GFR 25-90†	7437	Primary: 4p-MACE. Secondary: kidney composite outcomes	Ongoing
FIDELIO-DKD (NCT02540993)	Finerenone	T2D with CKD A2 GFR 25-60† or CKD A3 GFR 25-75†	5734	Primary: kidney composite outcomes	Ongoing

Adapted from [60]. T2D, type 2 diabetes. CVD, cardiovascular disease. 3p-MACE, 3-point major cardiac adverse events, including cardiovascular mortality, non-fatal myocardial infarction, non-fatal stroke. 4p-MACE, 4-point MACE, including 3p-MACE + hospitalization for unstable angina. CKD, chronic kidney disease. GFR, glomerular filtration rate. CV, cardiovascular. HF, heart failure. †, unit, ml/min/1.73². ‡, unit, mg/g. NS, not significant.

3. Mice have following changes in kidney pathology:
    (a) more than 50% of GBM thickening
    (b) mesangial expansion
    (c) hyaline arteriolosclerosis
    (d) tubulointerstitial fibrosis

To generate a DKD model, there is a variety of strategies, which can be decomposed into three factors: diabetes platforms, susceptible strains, and accelerators [61].

1.3.2 Diabetes platforms

Diabetes platforms that build up hyperglycemia can be divided into two categories, T1D and T2D. Commonly used models for T1D includes streptozotocin (STZ) induction (pancreatic β-cell injury), non-obese diabetic (NOD) mice (autoimmune insulitis), Akita *Ins2*$^{+/C96Y}$ mice (incorrect folding of insulin), and *OVE26* mice (accumulation of camodulin in β-cell leading to deficient insulin production). For models of T2D, *db/db* mice (leptin receptor deficient) and *ob/ob* mice (leptin deficient) are most widely used [61, 62]. KK-A^{y} mice are sometimes used as an model for T2D and obesity [63]. Tn this mode, the polygenic feature comes from KK strain. The heterozygous for yellow spontaneous mutation (A^{y}) at agouti locus contribute to the abnormal glucose metabolism [63].

1.3.3 Genetic background and permissive strains

The severity of diabetes and kidney phenotypes can be greatly shaped by different genetic backgrounds. For example, male DBA/2 demonstrated more robust hyperglycaemia, urine albumin excretion and glomerular mesangial expansion with STZ than other strains like C57BL/6, MRL/Mp, 129/SvEv, and Balbc [64, 65]. C57BL/Ks, FVB, DBA/2J, and BTBR (black and tan, brachyuric) stains carrying *db/db* or *ob/ob* mutations exhibit more severe diabetes and proteinuria than C57BL/6J or 129/J with the same mutation [66, 67, 68, 69]. C57BL/Ks is a mouse stain sharing approximately 84% C57BL/6J-like and 14% DBA/2J-like alleles [70]. Notably, BTBR *ob/ob* mice develop severe hyperglycaemia and more profound glomerular mesangial expansion than more commonly used C57BL/Ks *db/db* mice [71].

1.3.4 Strategies to accelerate kidney disease

Various strategies have been employed to accelerate the progress of kidney disease. One is to perform an early uninephrectomy to increase the filtration load on the remnant kidney and speed up adaptive glomerulosclerosis similar to what happens in obesity. As endothelial

dysfunction is a key determinant in diabetic kidney progress, the attempt to use *Nos3* gene deficiency as an approach to increase endothelial dysfunction resulted in profound albuminuria, kidney morphology, and GFR decline in either C57BLKS/J *db/db* or C57BL/6 STZ model [72, 73]. Shannon MH, *et al.* used adeno-associated virus delivery of renin (ReninAAV) to superimpose hypertension in three well-built diabetes models and found ReninAAV treatment greatly accelerated DKD [74]. Similar result was achieved by using transgenic mice expressing active human renin in the STZ model or the *OVE26* mouse model [75].

1.3.5 Oxalate-rich diet as a strategy to induce chronic kidney disease

Mulay, *et al.* reported a convenient inducible CKD mouse model by feeding C57BL/6 mice with soluble oxalate-rich diet [76]. Oxalate-rich diet induced ≈85% GFR loss, ≈7 times higher level of blood urea nitrogen (BUN), ≈6 times higher levels of serum creatinine. In the kidney, oxalate-rich diet induced progressive nephrocalcinosis, tubular atrophy, inflammation, and fibrosis. Oxalate-rich diet also induced CKD complications, such as anemia, hyperpotassemia, CKD-related mineral bone disease, hypertension, and cardiac fibrosis [76]. Since then this model has been employed in numerous studies on CKD progression [77, 78, 79, 80, 81, 82].

Taken together, a reliable diabetes platform, a permissive genetic background, and combining with one or more strategies to speed up disease progress make an animal model of DKD more clinical relevant. A main shortcoming of the current DKD mouse models is that disease manifestations are not severe, in many cases due to lacking strategies to accelerate the kidney disease progression. Oxalate-rich diet induces GFR loss and CKD complications, and could be a promising and convenient method to generate an animal model of advanced DKD.

1.4 Interleukin-1β

As mentioned before, anti-inflammatory cytokines are promising therapeutic target for DKD. The therapeutic role of IL-1β is of interest as IL-1β is a well-studied cytokine and contributes to various diseases [83]. In CANTOS trial, patients treated with a monoclonal antibody targeting IL-1β had more cardiovascular benefits than those treated with placebo, confirming that inflammation plays a role in atherothrombosis [84]. Here I briefly summarized the biology of IL-1β and its potential role in DKD.

1.4.1 Biology of interleukin-1β

Discovery

In 1974, Dinarello CA, *et al.* characterized two distinct human leukocytic pyrogens that share similar potencies to induce fever in rabbits. One derived from monocytes, with a molecular weight of ≈38 kDa, and was more acidic. The other pyrogen obtained from neutrophils, with a molecular weight of ≈15 kDa, and was more neutral [85]. In 1984 the amino acid sequences for both acidic and neutral pyrogens were characterized from human macrophages, and these two proteins were termed as interleukin-1α (IL-1α) and IL-1β, respectively [86].

Gene and protein expression

In human, gene *IL1B* encodes IL-1β. Pro-IL-1β is first produced as a 269 amino-acid precursor, which has no bioactivity, accumulates in cytoplasm, and requires caspase-1 to catalyze it into an active form of 153 amino acids [87, 88, 89]. Myeloid cells express IL-1β but not in a constitutive manner [88, 83, 90]. Toll-like receptor (TLR) ligands are the most well-known stimuli that induce both IL-1β mRNA and protein production in monocytes [83]. Besides, upon some non-TLR stimuli, such as hypoxia, monocytes can produce substantial IL-1β mRNA but not with IL-1β proteins [83].

Receptors and endogenous antagonists

The receptors and antagonists for IL-1β are listed in Table 1.2 and illustrated in Figure 1.7. IL-1β has two receptors and one endogenous antagonist. The two receptors are IL-1 receptor type I (IL-1R1) and IL-1 receptor type II (IL-1R2). The endogenous antagonist is interleukin-1 receptor antagonist (IL-1Ra). IL-1R1 is also the receptor for IL-1α. An IL-1β-IL-1R1 signal requires the binding of IL-1 receptor accessory protein (IL1RAP) (also called IL-1R3), which interacts directly with IL-1R1 but not IL-1β itself [83, 91, 92].

As shown in Figure 1.7, both IL-1R1 and IL1RAP have a Toll-IL-1 resistance (TIR) domain in the cytoplasmic side while IL-1R2 lacks it [90]. At resting state, IL-1R1 and IL1RAP are far apart on cell membrane. Upon the binding of IL-1β to IL-1R1, the later undergoes a structure transformation allowing an engagement of IL1RAP to IL-1β-IL-1R1, forming a signaling trimeric complex [91, 92]. The trimeric complex enables the approximation of TIR domains from IL-1R1 and IL1RAP, offering a docking site for the adaptor protein MyD88 [89, 90]. MyD88 triggers the downstream cell signals. This intracellular signaling cascades finally lead to the activation of transcription factors, such as JNK, mitogen-activated protein kinases p38, and NF-κB [83, 88].

On the contrary to IL-1R1 which can conduct pro-inflammatory cell signal, the binding of IL-1β to IL-1R2 converts no cell signals [83]. IL-1R2 consists a IL-1β-interaction domain at the

Table 1.2: Receptors and antagonist for interleukin 1

Ligand	Receptor	Coreceptor	Function
IL-1α, IL-1β	IL-1R1	IL1RAP (IL-1R3)	Proinflammatory
IL-1β	IL-1R2	IL1RAP (IL-1R3)	Antiinflammatory
IL-1Ra	IL-1R1	Not applicable	Antiinflammatory

Adapted from [89].

extracellular side, which is similar to IL-1R1. However, its cytoplasmic domain is short (29 amino acids) and lacks the TIR domain to form a signaling complex to connect to Myd88 [93]. IL-1Ra is a naturally occurring antagonist for both IL-1β and IL-1α [83].

IL-1Ra binds competitively to IL-1R1 but does not recruit accessory protein IL-1R3, thus converting no cell signals [91].

Activation of pro-interleukin-1β

The mechanism of IL-1β activation includes caspase-1-dependent and -independent pathways [94]. Caspase-1 requires activation by protein complexes, called inflammasomes. The organization of an inflammasome follows a routine pattern: a sensor recruits the adaptor ASC and further recruits the effector pro-caspase-1 [95]. So far five inflammasome sensors have been discovered, including nucleotide-binding domain and leucine-rich repeat pyrin containing protein-3 (NLRP3), absent in melanoma 2 (AIM2), NLRP1, NLRC4, and pyrin [95]. Of the inflammasomes, NLRP3 inflammasome is the most well-characterized in diabetes. As shown in Figure 1.6, the NLRP3 inflammasome incorporates three elements: the sensor NLRP3, the adaptor ASC, and the effector caspase-1 [96]. NLRP3 itself can be divided into three domains: the PYRIN domain (PYD) at the N terminus, the NACHT domain at the middle, and the leucine-rich repeat (LRR) at the C terminus [96]. NLRP3 undergoes structure transformation once it senses stress signals and become active. Active NLRP3 is able to oligomerize and several NLRP3 molecules assemble a wheel-like structure with PYD domains at center and LRR at the periphery. Assembled PYD circles are the hubs for the recruitment of the adaptor ASC. ASC consists of two domains for protein interaction, an PYD at the N terminus and a caspase recruitment domain (CARD) at the C terminus [96]. ASC molecules bind to the PYD circle by their own PYD domains, forming a helical filament connected to the wheel-like structure assembled by NLRP3. In this helical filament structure, PYD domains are at the inner side, while CARD domains at the outer side for the recruitment of caspase-1. Once caspace-1 binds to this helical filament structure via the CARD domain, it firstly forms a caspase-1 dimer (p46). Then this dimer undergoes several steps of auto-processing and finally generates the active form of caspase-1 (p33/p10) [97]. The active caspase-1 degrades substrates, such as pro-IL-1β [98], pro-IL-18, and pro-gasdermin D [99, 100] into active forms.

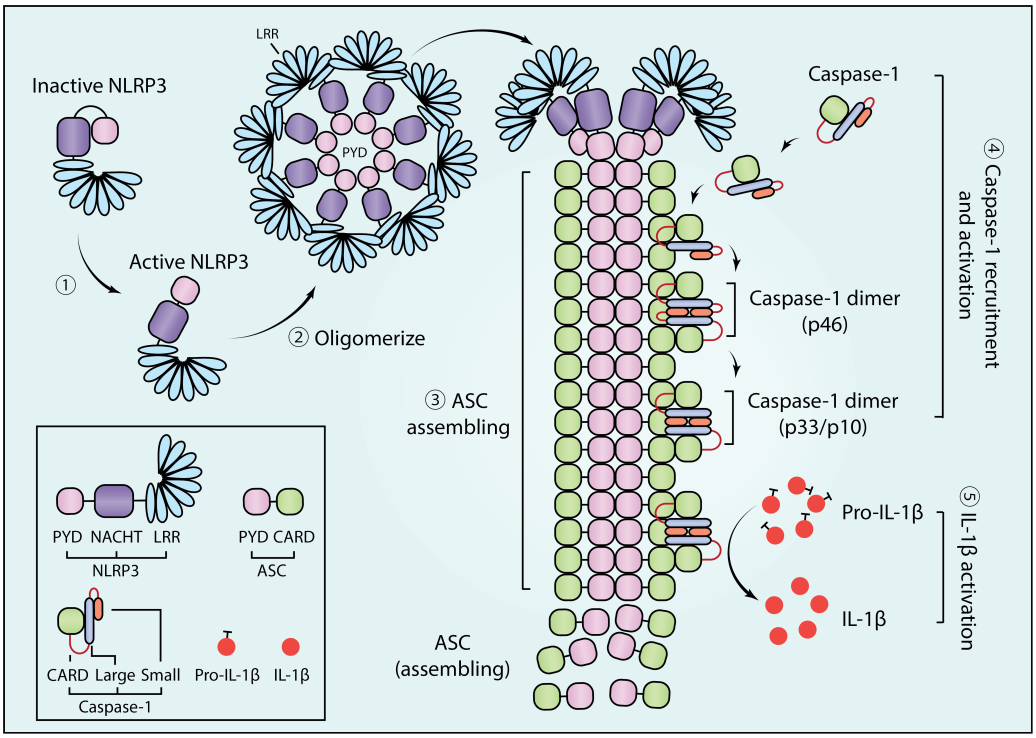

Figure 1.6: NLRP3 inflammasome-mediated interleukin 1β activation. NLRP3, nucleotide-binding domain and leucine-rich repeat pyrin containing protein-3. PYD, pyrin domain, LRR, leucine-rich repeat. ASC, apoptosis-associated speck-like protein containing a CARD, also known as PYCARD. CARD, caspase activation and recruitment domain. Adapted from [97].

Notably, caspase-1-independent pathways can also process pro-IL-1β [94]. In zymosan-induced peritonitis, a complement-mediated inflammation, generation of mature IL-1β mainly depends on caspase-1. While in turpentine-induced tissue necrosis, caspase-1 deficiency only reduces 50% of mature IL-1β production, suggesting that other proteases also participates in processing pro-IL-1β. These findings also suggest that proteases involving in pro-IL-1β are likely environment dependent [94]. Also matrix metalloproteinases, neutrophil proteases such as proteinase-3, granzyme A, cathepsin G are involved in processing IL-1β [101, 94].

Regulation of interleukin-1β activation

NLRP3-dependent IL-1β production is tightly regulated and typically follows two sequential steps [96]. The first step is priming, leading to the transcription of many components, including IL-1β and NLRP3 [102]. Activation of PRRs requires the stimulation form pathogen-associated molecular patterns (PAMPs), such as lipopolysaccharide (LPS), bacterial lipoproteins, and viral RNA, and lead to the priming process [102]. DAMPs, specific molecules released by damaged and dying cells such as ATP, can also lead to this priming process via PRRs [102]. Additionally, this priming step can also be induced by NF-κB activation [103, 104]. The second step is activation of NLRP3 by various stimuli, including a wide spectrum of

PAMPs, self-derived and foreign-derived DAMPs [96].

Besides, NLRP3-dependent IL-1β production is not always following the two-step mechanism [96, 105]. For example, in some circumstances, TLR4-dependent LPS stimulation alone is sufficient release IL-1β from human peripheral monocytes but not from human macrophages [106], or human dendritic cells [106], or mouse monocytes [105], or mouse bone marrow-derived macrophages [105].

Biological activity

Circulating IL-1β is elevated in various diseases including sepsis and burns as well as upon LPS injection into healthy humans [107]. However, circulating IL-1β level is low compared to other cytokines such as IL-6 and TNFα, and the possible reasons could be that pro-IL-1β mainly stays intracellularly and that IL-1β binds to large proteins in plasma, such as IL-1R2 and complement [107]. IL-1β has multiple biologic effects, including inducing fever, myocardial suppression, and hypotension, increasing bone marrow cells and circulating neutrophils and platelets, increasing hepatic acute phase protein production, increasing metastasis, increasing sodium excretion, increasing the non-specific resistance to infections, and many others [107]. The basis for its multi-functions is that it regulates a board range of gene expression, including many cytokines and their receptors, colony-stimulating factors, growth factors, clotting factors, adhesion molecules, complements, extracellular matrix components, pro-inflammatory mediators such as type-2 cyclo-oxygenase, type-2 phospholipase A2, endothelin-1, and inducible nitric oxide synthase, oncogenes, and others [107].

1.4.2 Roles of interleukin-1β in diabetic kidney disease

Interleukin-1β expression and activation

Diabetes-related conditions can act as a stimulus inducing inflammasome priming in immune cells. Lee HM, *et al.* isolated peripheral blood mononuclear cells (PBMCs) from patients newly diagnosed with diabetes and differentiated these cells into macrophages. Without priming, these macrophages already exhibited an elevated mRNA and protein expression of NLRP3, ASC, and IL-1β than cells from healthy controls [108]. Upon stimulation with LPS and some DAMPs, patient-derived macrophages produced and released more mature IL-1β. Furthermore, after these patients received metformin treatment and their blood glucose levels were normalized, PBMCs-derived and LPS-primed macrophages from the same diabetic patients showed reduced mature IL-1β release after the same stimulations [108]. This study confirmed the activation of IL-1β in circulating immune cells in diabetes *ex vivo* and demonstrated that factors affected by metformin treatment, most probably hyperglycemia, are associated with IL-1β activation [108].

IL-1β level in the circulation, as well as in the urine, are increased in DKD patients with albuminuria [38, 109]. Another interesting finding is that diabetic patients with higher circulating IL-1R1 levels were more likely to develop KFRT in a proteomic study including three different cohorts with T1D and T2D [30]. However, the source of circulating IL-1R1, as well as its association to IL-1β activity and kidney function, remains unknown.

In kidneys from DKD patients, protein expression level of IL-1β is uncertain. However, increased expression of its upstream molecules was found in human kidney in diabetes. Immunostaining showed increased NLRP3 expression in glomeruli from DKD patients. DKD patients also showed elevated expression levels of *NLRP3*, *PYCARD*, and *CASP1* in glomerular compartment [110]. Protein expression level of AIM2, another upstream molecule of IL-1β, was increased in leukocytes and tubular cells in kidney biopsies from DKD [110]. For animal models of DKD, *db/db* mice and streptozotocin (STZ)-treated C57BL/6 mice produced more mature IL-1β in kidneys and the expression of IL-1β paralleled with disease progression [38, 111].

Even though traditionally IL-1β is believed to be expression by myeloid cells, some *in vitro* studies also demonstrated kidney cells, such as podocyte [38, 38], glomerular endothelial cells [38], tubular cells [112, 113, 114], were capable to express IL-1β under diabetes-related stimulation. However, it remains controversy [115].

Together, circulating monocytes are a likely source of IL-1β release inside the kidney in DKD. In kidney tissues of DKD, it was not clear whether parenchymal cells also release IL-1β.

Interleukin 1 blockade in functional studies

Treatment with IL-1Ra (anakinra) ameliorated the proteinuria and mesangial expansion in both *db/db* mice and STZ models [38], suggesting an involvement of IL-1α/IL-1β/IL-1R axis in DKD initiation [38].

Targeting upstream of IL-1β also showed kidney protective effects. Shahzad, K, *et al.* found that global depletion of *Nlrp3* or *Casp1* showed kidney protection in uninephrectomized STZ-induced mouse model [38]. Also, diabetic mice treated with caspase-1 inhibitor showed reduced albuminuria, less fractional mesangial area, and lower plasma IL-1β levels. Above observations suggests the involvement of NLRP3/caspase-1 activation in the pathogenesis of DKD [111]. But it was not sure whether the kidney benefit was through blocking NLRP3/caspase-1 on myeloid cell or/and kidney parenchymal cells. The authors further transplanted wild type, *Casp1*$^{-/-}$, or *Nlrp3*$^{-/-}$ bone marrow cells to *db/db* mice. They found that these three groups of *db/db* mice had comparable albuminuria and mesangial expansion, suggesting the kidney benefit of *Nlrp3* and *Casp1* global knockout derives from kidney parenchymal cells but not myeloid cells [38].

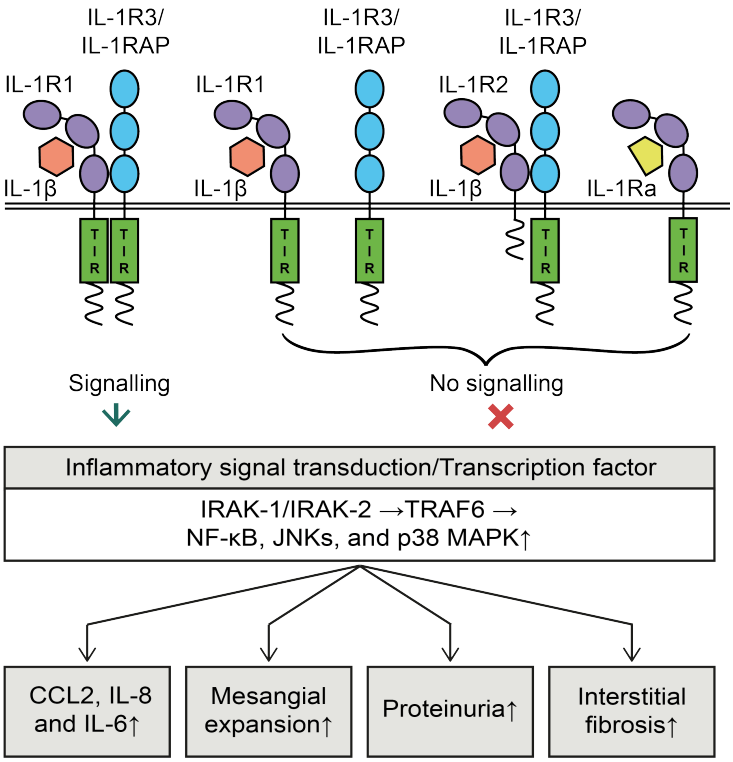

Figure 1.7: Selected actions of interleukin 1β related to diabetic kidney disease. IRAK, Interleukin-1 receptor-associated kinase. TRAF6, tumor necrosis factor receptor associated factor 6. JNKs, c-Jun N-terminal kinases. MAPK, mitogen-activated protein kinase. CCL2, chemokine ligand 2. Partially adapted from [116]

Thus, IL-1 blockade, as well as targeting the pathways upstream of IL-1β, has kidney benefits in animal models of early phase of DKD.

Possible mechanisms leading to interleukin-1β activation

The possible mechanisms leading to IL-1β activation in diabetes include hyperglycaemia-induced mitochondrial reactive oxygen species (ROS) generation. In PBMC-derived macrophages isolated from diabetic patients, the production of IL-1β was associated with elevated blood glucose levels and mitochondrial ROS production [108]. It was thought that enhanced glucose influx, as well as stimulation of advanced glycation end product via RAGE, induced mitochondrial ROS generation and the latter contributed to ROS-dependent NLRP3 and IL-1β activation [38, 117]. The mechanism by which the NLRP3 inflammasome senses mitochondrial ROS involves thioredoxin-interacting protein-dependent NLRP3 activation [117]. Thioredoxin-interacting protein is up-regulated when ROS is over-produced [118]. It activates NLRP3 and inhibits antioxidant thioredoxin, making it a pro-inflammatory molecule and a promoter for oxidative stress [117, 118]. Application of antioxidants reduced ROS production and NLRP3-dependent IL-1β generation in cultured podocytes and mesangial cells [38, 117]. Either using antioxidant or gene modification to reduce ROS production showed reduced NLRP3-dependent IL-1β release and kidney protective effects in diabetic mouse model [38].

ATP might be another stimulus of NLRP3-dependent IL-1β activation in DKD. Extracellular ATP binds to P2X receptors, leading to NLRP3 activation and IL-1β release. P2X expression was upregulated in tubule epithelial cells in patients with DKD. Treatment with apyrase can inhibit high glucose-induced NLRP3 up-regulation and IL-1β release in HK-2 cells by consuming extracellular ATP [109]. Hyaluronan is also an endogenous trigger of NLRP3-dependent IL-1β [119]. Elevated glucose induced proximal tubular cell hyaluronan generation *in vitro* [120].

After all, consistent with the introduction in 1.2.4, triggers in diabetes scenario, such as ROS and ATP, seem to induce IL-1β activation. It is not clear whether it also involves other mechanisms.

1.4.3 Clinical trials using interleukin-1β blockade

Searching for the intervention studies, which tested IL-1β blockade in patients with T2D using the ClinicalTrial.gov database (keyword ”interleukin 1” together with ”type 2 diabetes”, by 21-09-2019) retrieved 16 relevant studies as listed in Table 1.3. Seven different IL-1β inhibitors were used: 1. Anakinra, a recombinant nonglycosylated protein similar to human IL-1Ra, 2. CYT013-IL1bQb, a vaccine consisting a recombinant IL-1β encapsulated in virus-like particles, 3. AC-201, an oral IL-1 modulator inhibiting the activation of IL-1 via interfering with MAPK signaling pathways, 4. Diacerein, a small molecule that inhibits IL-1β secretion and function, 5. Canakinumab, 6. Gevokizumab, and 7. LY2189102, all recombinant, human anti-human-IL-1β monoclonal antibodies.

The anti-diabetic effects of IL-1β blockade in T2D patients were not consistent. As shown in Table 1.3, anakinra [121], AC-201, and diacerein [122] reduced hemoglobin A1C (HbA1c) levels. LY2189102 showed modest effects on improving HbA1c but not on fasting glucose [123]. In the canakinumab trial which enrolled 556 patients, however, a 4-month course of monthly canakinumab did not improve glucose control or insulin secretion [124]. Gevokizumab also did not affect glucose control after a treatment duration of 6 months in a trial of 421 patients. In the CANTOS trial, canakinumab did not reduce incident diabetes among patients with prior myocardial infarction, higher levels of high-sensitivity C-reaction protein (hsCRP), and normoglycemia; it reduced HbA1c levels only over the first 6-9 months but this effect was attenuated over time [125]. Although effects on glucose control were not consistent, IL-1β blockade reduced levels of various inflammation surrogates, including CRP [121, 124, 123, 125] and IL-6 [121, 124, 123]. On patient outcomes, canakinumab reduced cardiovascular events. This benefit might be independent from diabetes [125]. No study used kidney-related events as endpoint.

Searching trials which tested IL-1β blockade in patients with kidney disease on ClinicalTrial.gov database by using keywords ”interleukin 1” and ”kidney”. By 21-09-2019,

there had been four relevant studies listed in the database (Table 1.4). Two IL-1β inhibitors were used: anakinra and rilonacept (a recombinant protein consisting of domains of IL-1R1, IL-1RAP, and the Fc region of human IgG1). No study used kidney-related events as endpoints. Rilonacept improved brachial artery flow-mediated dilation and reduced inflammatory marker expression in a cohort with 34 CKD 3/4 with 12-week treatment [126]. In another trial, rilonacept also reduced plasma hsCRP and IL-6 in patients with CKD G3-G4 (NCT00897715). Anakinra also reduce hsCRP in patients with hemodialysis (NCT00420290).

Taken together, IL-1β blockade demonstrated cardiovascular benefits in patients with cardiovascular disease, which likely resulted from suppressing inflammation but not from hyperglycemia control. The effect of IL-1β inhibition on the development of CKD is still unknown.

Table 1.3: Current clinical trials of interleukin 1 blockade on diabetes

Trial	Medicine	Phase	Patient	Nr.	Endpoint	Treatment Effects
NCT00303394 [121]	Anakinra	2	T2D	72	Primary: HbA1c	Treatment lower
NCT00942188 [127]	Anakinra	4	RA+T2D	41	Primary: ΔHbA1c	Treatment higher
NCT00924105 [128]	CYT013-IL1bQb	1	T2D	48	Primary: adverse events	NS
NCT01276106	AC-201	2	T2D	259	Primary: ΔHbA1c	Treatment higher
NCT01298882 [122]	Diacerein	2	T2D	40	Primary.1: HbA1c Primary.2: fasting glucose Primary.3: insulin secretion	Treatment lower Treatment lower Treatment higher
NCT01068860 [129]	Canakinumab	2	T2D IGT	246	Insulin secretion	NS
NCT00995930 [130]	Canakinumab	2	AS+T2D, AS+IGT	189	Primary.1: adverse events Primary.2: Δaortic distensibility Primary.3: Δplaque burden	NS NS NS
NCT00900146 [124]	Canakinumab	2,3	T2D	556	Primary.1: adverse events Primary.2: ΔHbA1c Primary.2: Δinsulin secretion	NS NS NS
NCT01327846 (CANTOS) [125, 84]	Canakinumab	3	Main:MI hsCRP≥2 mg/l	10071	Primary: 3P-MACE Secondary.1: 4p-MACE Secondary.2: new-onset T2D	Treatment better Treatment better NS
NCT00541983 [131]	Gevokizumab (XOMA 052)	1	T2D	98	Primary: ΔHbA1c	Treatment lower
NCT01066715	Gevokizumab (XOMA 052)	2	T2D	421	Primary: ΔHbA1c	NS
NCT00942188 [123]	LY2189102	2	T2D	106	Primary: ΔHbA1c	NS

T2D, type 2 diabetes. RA, rheumatoid arthritis. IGT, impaired glucose tolerance. AS, arthrosclerosis. MI, myocardial infarction. hsCRP, high-sensitivity C-reaction protein. MACE, major cardiac adverse events. 3P-MACE: cardiovascular mortality, myocardial infarction, stroke. 4p-MACE, 3p-MACE + hospitalization for unstable angina. NS, not significant.

Table 1.4: Current clinical trials of interleukin 1 blockade on kidney disease

Trial	Medicine	Phase	Patient	Nr.	Endpoint	Treatment Effects
NCT01663103	Rilonacept	4	CKD G3-4	42	Primary: Δbrachial artery flow-mediated dilation+Δaortic pulse-wave velocity. Secondary.1: hsCRP. Secondary.2: NADPH expression	Primary: better Secondary.1: lower Secondary.2: lower [126]
NCT00897715	Rilonacept	2	CKD G3-G4	15	Primary: ΔhsCRP	Primary: lower
NCT00420290	Anakinra	N.A.	CKD5 (HD), CHD	14	Primary: hsCRP	Primary: lower
NCT03141983	Anakinra	2	CKD5(HD)	80	Primary.1: safety Primary.2: ΔhsCRP	2021

CKD, chronic kidney disease. CHD, chronic heart disease. eGFR, estimated glomerular filtration rate. HD, hemodialysis. CRP, C-reactive protein. hsCRP, high-sensitivity C-reaction protein. N.A., not applicable.

2 Hypothesis

CKD is a heterogeneous group of disorders and recognized as a global public health priority. DM is a systemic disorder and a common cause for CKD. DKD implicates both systemic and local sterile inflammation, which drives kidney structural and functional deterioration. Sterile inflammation is secondary to DAMPs released from damaged cells and dying cells upon diabetes-associated stimuli activating PRRs and subsequently inflammasomes, leading to the activation of cytokines, chemokines, and adhesion molecules. Some diabetes-related triggers, such as hyperglycaemia and mitochondrial ROS, activate NLRP3-dependent inflammasome and lead to IL-1β maturation and release. IL-1β activates cells expressing IL-1R and induces a board range of proinflammatory mediators. Given the central role of IL-1β in orchestrating inflammation as well as the observation that an up-regulation of IL-1β in diabetic conditions, IL-1 or IL-1R inhibition has been proven protective *in vitro* under diabetes-related conditions and pre-clinical models of early stage of DKD. However, the hypothesis that IL-1β would drive advance DKD has not been tested.

Meanwhile, an animal model with overt DKD is needed for preclinical study. Uninephrectomy is a common tool to accelerate kidney impairment. Its main shortcoming is surgery-related complications, such as lethality and kidney infection. Thus, a non-surgical method which can reduce the number of functional nephrons in *db/db* mice would be desirable. Besides, a non-surgical method is more in accord with 3R of animal welfare (replace, reduce, and refine). Given oxalate-rich diet is a convenient method to generate progressive nephrocalcinosis, tubular atrophy, and CKD in C56BL6 mice, we want to explore the possibility of using oxalate-rich diet as a substitutive and non-surgical approach to accelerate kidney impairment in *db/db*.

Thus, we hypothesize that:

1. An oxalate-rich diet could induce crystal deposition and GFR loss in *db/db* mice.
2. IL-1β blockade by a specific anti-IL-1β IgG would have renoprotective effects in a mouse model of DKD.

Accordingly, the aims of my study include:

1. We would replace uninephrectomy by a non-surgical approach of feeding oxalate-rich diet to induce progressive CKD via triggering nephrocalcinosis and tubular atrophy.
2. We would investigate the therapeutic effects of IL-1β inhibition with anti-IL-1β antibody in a mouse model of advanced DKD.

3 Materials

3.1 Animal studies

Animal anesthesia

Isofluran CP	CP-Pharma, Burgdorf, Germany
Medetomidine	Sanofi-Aventis GmbH, Paris, France
Midazolam	Ratiopharm GmbH, Ulm, Germany
Mentanyl	Zoetis GmbH, Germany
Atipamezol	CP-Pharma, Burgdorf, Germany
Flumazenil	Hexal AG, Munich, Germany
Buprenorphine	Bayer Vital, Leverkusen, Germany

Animal surgery

BD Microlance™ Stainless Steel Needles	Becton Dickinson, NJ, USA
BD Plastipak™ Syringes	Becton Dickinson, NJ, USA
Sterile gauze balls (Mulltupfer)	Verbandmittel Danz, Germany
Sterile swab	Verbandmittel Danz, Germany
ETHIBOND EXCEL Polyester Suture 5-0	Ethicon, Germany
Vicryl™ 5-0 absorbable suture	Ethicon, Germany
Bepanthen Eye and Nose Ointment	Bayer, Germany
Surgical scissors and forceps	Integra LifeSciences, France
Brinsea Octagon 20 Eco Incubator Auto	Brinsea, UK
Infrared 100W Heat Emitting Bulb Healthcare	Philips, Germany
Operation table	Medax, Germany

Animal sample preservation

Histology embedding cassettes	NeoLab, Germany
Formalin 4 %	Merck, Darmstadt, Germany
EDTA	Carl Roth, Germany

Animal diet

Animal diets were purchased from ssniff Spezialdiäten GmbH and stored at 4 °C. The ingredient is as follows.

Standard diet

Ingredient	Quantity
Crude protein	22.0 %
Crude fat	4.5 %
Crude fiber	3.9 %
Raw ash	6.7 %
Calcium	1.0 %
Phosphorus	0.7 %
Vitamin A	25000 U/kg
Vitamin D_3	1500 U/kg
Vitamin E	125 mg/kg
Iron (II) sulphate monohydrate	100 mg/kg
Zinc sulfate monohydrate	50 mg/kg
Manganese (II) sulphate monohydrate	30 mg/kg
Copper (II) sulfate pentahydrate	5 mg/kg
Sodium selenite	0.1 mg/kg
Calcium iodate Anhydrate	2.0 mg/kg

Oxalate-rich and control diet

Ingredients	Quantity	Control food	Oxalate-rich food
Crude protein	17.7%	+	+
Crude fat	6.1%	+	+
Crude fiber	4.0%	+	+
Raw ash	2.4%	+	+
Strength	31.1%	+	+
Sugar	33.8%	+	+
Calcium	0.4%	+	+

Vitamin A	19800 U/kg	+	+
Vitamin D_3	2200 U/kg	+	+
Vitamin E	120 mg/kg	+	+
Vitamin K_3	45 mg/kg	+	+
Vitamin C	350 mg/kg	+	+
Copper	8 mg/kg	+	+
Sodium oxalate	50 mmol/kg	-	+

3.2 Glomerular filtration rate measurement

NIC-Kidney device	Medibeacon, Germany
Double-sided adhesive patch	Lohmann, Neuwied, Germany
FITC-sinistrin	Medibeacon, Germany
Rechargeable miniaturized battery	Medibeacon, Germany
Sterile compress	Verbandmittel Danz, Germany
Medical adhesive tape	BSN Medical GmbH, Germany
Razor blades	Gillette, USA

3.3 Urine and blood measurement

Mouse Albumin ELISA Quantitation Set	Bethyl Laboratories, TX, USA
Creatinine FS	Diasys, Holzheim, Germany
Urea FS	DiaSys, Holzheim, Germany
God FS	DiaSys, Holzheim, Germany
96 well MicroWell™ MaxiSorp™ plate	Thermo Fisher, MA, USA
Nunc™ MicroWell™ 96-Well Microplates	Thermo Fisher, MA, USA
Bovine serum albumin fraction v	Roche, Mannheim, Germany
Tris	Carl Roth, Karlsruhe, Germany
Sodium chloride	Merck, Darmstadt,Germany
Tween 20	Sigma-Aldrich, Munich, Germany
Sodium carbonate	Merck, Darmstadt, Germany

Sodium bicarbonate	Merck, Darmstadt, Germany
TMB Substrate Reagent Set	BD Biosciences, NJ, USE
Sulfuric acid	Sigma-Aldrich, Munich, Germany
pH meter	WTW, Weilheim, Deutschland
Tecan GENios™ Microplate Reader	Tecan, Germany

3.4 RNA isolation, cDNA conversion, real-time qPCR

RNA isolation

2-Mercaptoethanol	Sigma-Aldrich, Munich, Germany
DNase and RNase free water	Thermo Fisher, MA, USA
96% Ethanol	Merck, Darmstadt,Germany
RNase AWAY® spray	Sigma-Aldrich, Munich, Germany
RNA*later*™ Stabilization Solution	Ambion, MA, USA
PureLink™ RNA Mini Kit	Ambion, Darmstadt, Germany
RNase-Free DNase Set	Qiagen, Hilden, Germany
Homogenizer Ultra-Turrax® T25	IKA GmbH, Staufen, Germany

cDNA conversion

NanoDrop™ Spectrophotometer	Biotechnologie, Erlangen, Germany
5x First Strand-Puffer	Invitrogen, Karlsruhe, Germany
Acrylamid	Ambion, Darmstadt, Germany
Dithiothreitol	Invitrogen, Karlsruhe, Germany
dNTP Set	GE Healthcare, Munich, Germany
Hexanucleotid-Mix	Roche, Mannheim, Germany
RNAsin	Promega, Mannheim, Germany
SuperScript II Reverse Transcriptase	Invitrogen, Karlsruhe, Germany
Thermomixer 5436	Eppendorf, Hamburg, Germany

Real-time qPCR

SYBR green I	Sigma-Aldrich, Munich, Germany
PCR Optimizer	Biomol, Hamburg, Germany
$MgCl_2$ 25mM	Thermo Fisher, MA, USA
Bovine Serum Albumin PCR grade	Thermo Fisher, MA, USA
PCR-Primer	Metabion, Martinsried,Germany
Taq-Polymerase	New England BioLabs, Ipswich, USA
10X Taq Buffer	New England BioLabs, Ipswich, USA
Lightcycler 480 PCR plate with 96 wells	Sarstedt, Germany
Optical lid strip for 96-well plates	Sarstedt, Germany
LightCycler 480 Multiwell-Plate 96	Roche, Mannheim, Germany
LightCycler 480 Instrument	Roche, Mannheim, Germany

3.5 Antibodies and reagents used in histology

Antibodies used in histology

Rat anti-mouse Mac-2	Cedarlane, ON, Canada
Anti-mouse Wilms Tumor (WT)-1	Cell signaling, Danvers, MA, USA
Anti-mouse Wilms Tumor (WT)-1	Santa Cruz Biotechnology, CA, USA
Guinea pig anti-mouse nephrin	Acris Antibodies, Herford, Germany
Rabbit anti-mouse alpha smooth muscle actin	Dako, Glostrup, Denmark
HRP-conjugated Anti-Goat secondary Ab	Dianova, Hamburg, Germany
HRP-conjugated Anti-Rabbit secondary Ab	Cell signaling, USA
Rabbit anti-human NLRP3 (ABF23)	Merck, Darmstadt, Germany
Mouse anti-human CD68 (PG-M1)	Dako, Glostrup, Denmark
Mouse anti-human IL1-alpha (LS-B1581)	LifeSpan, Seattle, Washington, USA
Rabbit anti-human IL1-beta (ab82558)	Abcam, Cambridge, UK

Reagents used in histology

Xylene	Merck, Germany
Hydrogen peroxide	Merck, Germany

Paraffin	Merck, Germany
Formaldehyde	Merck, Germany
Fixation solution	Acquascience, Uckfield, UK
DAB substrate chromogen system	Dako, Glostrup, Denmark
Avidin-Biotin Complex Kits	Vector Laboratories, CA, USA
Antigen unmasking solution	Vector Laboratories, CA, USA
Avidin	Vector Laboratories, CA, USA
Biotin	Vector Laboratories, CA, USA
DAB Peroxidase Substrate Kit	Vector Laboratories, CA, USA
Nuclear Fast Red solution	Sigma-Aldrich, Munich, Germany
Antifade Mounting Medium with DAPI	Vector Laboratories, CA, USA
Picro-sirius red solution	Sigma-Aldrich, Munich, Germany
Periodic acid	Carl Roth, Germany
Schiff Reagent	Sigma-Aldrich, Munich, Germany
Nitric acid	Merck, Germany
Silver nitrate	Carl Roth, Germany

3.6 Miscellaneous

Falcon, 15/50 ml	Greiner BioOne, Germany
Reaction tubes, 1.5/2.0 ml	Paul Boettger, Germany
Safe lock tubes, 1.5/2.0 ml (PCR)	Eppendorf, Germany
Cryovial, 2.0 ml	Alpha Laboratories, UK
Refill pipette tips	Greiner Bio-One, Germany
Serological Pipette, 5/10/25/50 ml	Greiner Bio-One, Germany
EpT.I.P.S. refill pipette tips(PCR)	Eppendorf, Germany
PBS	PAN-Biotech, Germany
Tissue culture dish, 100 mm	TPP, Trasadingen, Switzerland
Analytic Balance	BP 110 S Sartorius, Göttingen, Germany
Mettler PJ 3000 Mettler-Toledo	Greifensee, Switzerland
Heraeus, Minifuge T	VWR, Darmstadt, Germany

Heraeus, Biofuge primo	Kendro Laboratory, Germany
Heraeus, Sepatech Biofuge A	Heraeus Sepatech, Munich, Germany
Leica DC 300F	Leica Microsystems, Cambridge, UK
Olympus BX50	Olympus Microscopy, Hamburg, Germany
Microtome HM 340E	Microm, Heidelberg, Germany
Thermomixer 5436	Eppendorf, Hamburg, Germany
Vortex Genie 2™	Bender Hobein, Zurich, Switzerland
Water bath HI 1210	Leica Microsystems, Bensheim, Germany
Easypet® pipette controller	Eppendorf, Germany
Pipetman® pipette	Gilson, Middleton, WI, USA
Research Pro electronic pipettor	Eppendorf, Germany
Multi-channel pipettor, 30-300 μl	Eppendorf, Germany

4 Methods

4.1 Animal studies

4.1.1 Ethical statement

All experiments were conducted according to the European equivalent of the NIH's *Guide for the Care and Use of Laboratory Animals, i.e. EU directive 2010/63/EU*, and received the official permission from local government authorities (*Regierung von Oberbayern*, reference number: 55.2-1-54-2532-15-2014 and 55.2-1-54-2532-15-2017).

4.1.2 Experimental animals

Five- to six-week-old male C57BL/Ks (BKS) diabetic (BKS.Cg-*m+/+Lepr^{db}*/BomTac, genotype: sp/sp) and non-diabetic wildtype mice (BKS.Cg-*m+/+Lepr^{db}*/BomTac, genotype: wt/wt) were purchased from Taconic Biosciences (Lille Skensved, Denmark). Body weight upon arrival was 34.17 ± 2.31 g for diabetic mice, and 20.94 ± 1.31 g for non-diabetic mice.

4.1.3 Housing and husbandry

Mice were housed under standard conditions in a specific pathogen free facility. The facility was equipped with a light system which had a 12 hours-12 hours light/dark cycle. The facility was air-conditioned with target room temperature of 22 ± 4 °C and for relative humidity of 50-70%. Mice were housed in groups of 2-3 in conventional filter top cages. Mice had *ad libitum* access to autoclaved water and autoclaved standard chow diet or specific chow diet (all from Ssniff, Germany); additional food was placed on the floor of cages for easy access. Extra nesting material and wooden sticks for gnawing were provided for the whole study. Transparent red plastic houses were also provided as enrichment except during surgery wound healing. Extra bedding was provided every time and changed 3 times a week. All the bedding, enrichment, cages, water, and food were sterilized before use.

4.1.4 Food and water consumption

Food and water consumption were monitor over one or two days for each measurement. Overall consumption of one cage was calculated by the weight difference between the starting and ending point. The consumption of one mouse was further calculated by dividing the overall consumption of one cage by the total number of mice in each cage. Only mice belonging to the same group were housed in the same cage.

4.1.5 Glomerular filtration rate

GFR was determined by measuring the clearance of exogenous fluorescein isothiocyanate (FITC)-conjugated sinistrin (Mannheim Pharma and Diagnostics) in conscious mice, a method first describe by Schreiber A, *et al.* [132]. The dynamic change of FITC-sinitrin was recorded by a miniaturized device attached to nude mouse skin. Plasma half-life of FITC-sinistrin was then calculated by analyzing the continuous signal change of FITC-sinistrin captured by the chip. We performed the measurement with minor in-house modifications [82]. In brief:

1. Mice were anesthetized with isoflurane. Fur around neck was moisturize with ethanol and carefully shaved to expose skin of around 1.5 × 1.5 cm^2 while avoiding scratching.
2. A miniaturized FITC-sinistrin recording device was connected with a small battery and attached onto the shaved skin via adhesive tapes.
3. Prior to FITC-sinistrin injection, leave the devices recording background signal for 15 min.
4. Mice received intravenous injection of 150 mg/kg FITC-sinistrin.
5. Each mouse was conscious, kept individually in a filter top polypropylene cage without food and water supply, and free to move around. The FITC-sinistrin signal was recorded for 1.5-2.0 hours.
6. Devices were removed and analyzed by MPD Lab software.

A typical FITC-sinistrin signal curve consists three parts: the background signal recording stage (before sinistrin injection), the peak stage (upon sinistrin injection), and decline stage. By analyzing with MPD software, the value of plasma half-life of FITC-sinistrin (t½) was acquired via one-compartment model. GFR (µl/min) was then calculated using following equation [132].

$$GFR(\mu l/min) = \frac{14616.8[\mu l]}{t_{1/2}[min]} \times \frac{BW[g]}{100g} \quad (4.1)$$

4.1.6 Sample collection and storage

Blood samples were collected after 4-hour fasting. Mice were anesthetized with 2.5-3.0 % isoflurane and 2-3 L/h of oxygen flow. By puncture through facial vein using a micro glass capillary, blood drops were collected into an EDTA-containing tube. For the blood collection on the day of sacrifice, each tube contained 10 µl of 0.5 M EDTA for around 800 µl of blood collection; for blood collection at each time point, each tube contained 7 µl of 0.5 M EDTA for 7-8 drops blood (around 100 µl). Tubes containing blood samples were then centrifuged at

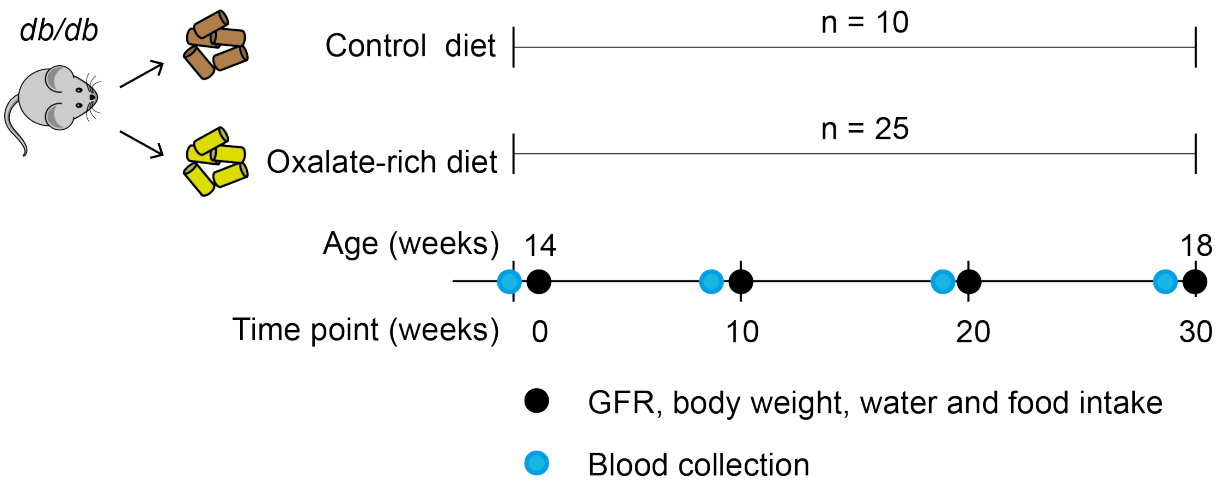

Figure 4.1: Animal study design for diabetic kidney disease by using *db/db* mice fed with oxalate-rich food.

6000 rpm for 6 minutes. The upper plasma was transferred to another clean tube and stored at -20 °C until further use.

Urine was collected through bladder massage. Urine was stored at -20 °C until further use.

Left kidney was taken and cut into 3 pieces. One piece (containing upper pole) was kept in RNA-Later stabilization solution (Thermo Fisher, USA) and stored at -20 °C until further use. One piece (middle parts) was preserved in 4% formalin for 24 hours and transferred to 70% ethanol until paraffin block processing. Another piece (containing lower pole) was kept in liquid nitrogen temporarily and further transferred to and stored at -80 °C.

4.1.7 Animal model: *db/db* mice fed by oxalate-rich diet

Study design, allocation, study outcome, and group size

Fourteen-week-old male BKS diabetic (BKS.Cg-*m+/+Lepr*^{db}/BomTac, genotype: sp/sp) were used. As shown in Figure 4.1, *db/db* mice were randomly distributed into two groups: fed with control diet or with oxalate-rich diet at a ratio of 1 : 2.5 (n=10 for control diet, n=25 for oxalate-rich diet). GFR and blood collection was done every 10 days. After 30 days, mice were sacrificed. GFR was the primary endpoint. Group size calculation was based on GFR as a primary endpoint. The group size was calculated based on previous studies [133, 134, 135].

4.1.8 Animal model of diabetic kidney disease: uninephrectomized *db/db*

Study design

To build up an experimental mouse model of diabetic kidney disease with more clinical meaningfulness, a *db/db* model in BKS strain was utilized in combination with a morning

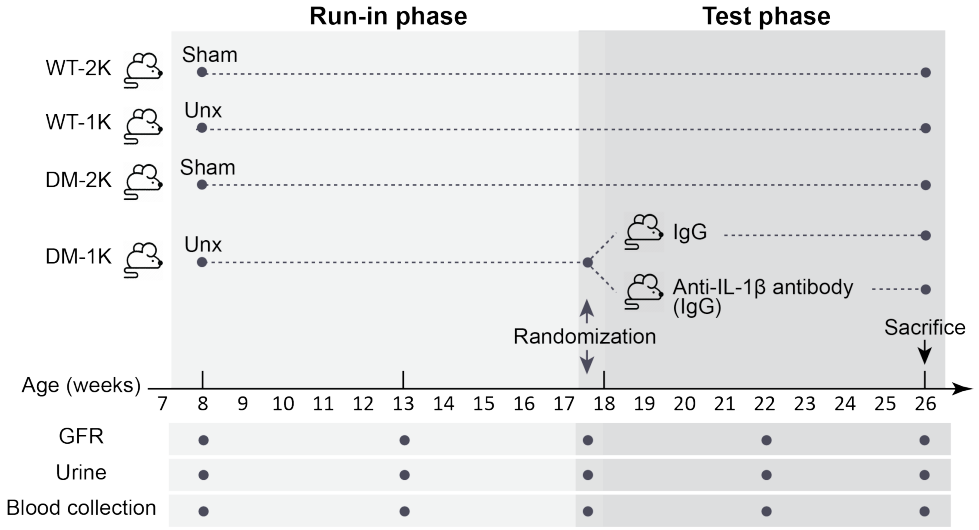

Figure 4.2: Study design for testing anti-IL-1β in a mouse model of diabetic kidney disease

uninephrectomy, as a strategy to accelerate diabetic kidney disease progress. As shown in Figure 4.2, at age 7 weeks *db/db* mice and wild type mice were randomly either received uninephrectomy or sham surgery; thus mice were primarily divided into 4 groups: *db/db* mice with uninephrectomy (DM-1K), *db/db* mice with sham surgery (DM-2K), wild type mice with uninephrectomy (WT-1K), and wild type mice with sham surgery (WT-2K). DM-1K group was further allocated into two groups: at the age of 18 weeks, a time point when kidney impairment in DM-1K mice was prominent, one group received control IgG (DM-1K+IgG (DM-1K+IgG)), the other group received anti-IL-1β IgG (DM-1K+anti-IL-1β (DM-1K+anti-IL-1β)). DM-1K+IgG and DM-1K+anti-IL-1β were intraperitoneally administrated with antibody at 10 mg/kg weekly for a total of 8 weeks, while the other 3 groups remained no treatment. WT-2K, WT-1K, and DM-2K here functioned as healthy control, control of uninephrectomy, and control of *db/db* background, respectively. All mice were sacrificed at age 26 weeks.

Group size and allocation

Base on GFR as a primary endpoint and data from previous studies, sample size was calculated [133, 134, 135]. The group size for WT-2K, WT-1K, DM-2K, DM-1K+IgG, and DM-1K+anti-IL-1β was 5, 5, 9, 8, and 9, respectively. Allocation within DM-1K was performed by matching according to mouse data collected at age 17-18 weeks, including microalbuminuria, GFR, and body weight.

Experimental outcomes

GFR was the primary endpoint. Albuminuria, histology, and gene transcription levels were secondary endpoints.

Uninephrectomy

1. Preoperative analgesia: mice were orally administrated with 2 drops Metamizol (Novalgin) per 30 g mouse weight.

2. Narcosis: mice were intraperitoneally injected with 2.5 ml/kg body weight of narcosis mixture (corresponding to midazolam 5 mg/kg, medetomidine 0.5 mg/kg, fentanyl 0.05 mg/kg) and then placed inside a 37 °C chamber device. Prior to the surgery, depth of anesthesia (anesthesia stage III 2) was checked by the sign of missing pain reaction in the inter-toe reflex.

3. Surgery:

   (a) Mice were immobilized on a heating plate for heat supplying (device temperature set at 40 °C).

   (b) Eyes were applied with Bepanthen creme to protect from drying.

   (c) Fur around the area of incision was moisturized with ethanol, shaved with a blade, and sterilized with povidone-iodide.

   (d) Skin and muscle layers were cut with scissor, thus peritoneal cavity was accessible. Kidney (spleen-side) was pulled out of the peritoneal cavity with swabs and forceps. Renal hilum was then exposed by removing the surrounding adipose tissue.

   (e) A segment of 5-0 non-absorbable suture was placed around the hilum. A ligation was made around the hilum. Kidney was excised. The stump with sutures was put back into the peritoneal cavity.

   (f) Peritoneal and muscle layers were sutured with 5-0 absorbable suture (Vycril). Skin was sutured with non-absorbable 5-0 suture (Ethibond).

4. Mice were subcutaneously injected with Buprenorphin 0.1 mg/kg (=33.34 ml/kg of 0.006 mg/ml solution) 30 minutes before antagonization.

5. Antagonization of narcosis: mice were subcutaneously injected with 8.5 ml/kg body weight of antagonist-mix (containing 0.5 mg/kg of flumazenil and 2.5 mg/kg of atipamezol), and then were accommodated in a 37 °C chamber device until waking up.

6. Post-surgery analgesia: mice were applied with s.c. 0.1 mg/kg (=33.34 ml/kg of 0.006 mg/ml solution) every 12 hours for three days.

Antibody preparation

Antibodies were kindly provided by Hoffmann-La Roche. The antibody is monoclonal antibody and produced by engineered mouse hybridoma cells [136]. The antibody has specificity with

human IL-1β, strong cross reactivity with mouse IL-1β, and no reactivity with IL-1α. All of above was verified by protein-protein interaction assays based on ELISA.

4.2 Histology

As mentioned before, histology samples were first fixed in 4 % formalin for 24 hours and then in 70 % ethanol. Subsequently, tissues were processed, preserved in paraffin blocks, sliced into sections, deparaffinized, and rehydrated. The steps are as follows.

1. Processing: tissues were incubated in alcohol (70%, 96%, 100%) to remove the residual water inside of tissues. Then tissues were treated with xylene to remove the residual alcohol.
2. Embedding: tissues were embedded in lipophilic paraffin to remove xylene and became solid. Until the paraffin blocks were cooled down, sections with certain thickness were made by slicing the blocks with a microtome.
3. Deparaffinization: sliced sections were treated with xylene for 5 minutes for 2 times to remove the paraffin.
4. Rehydration: sections were incubated in in alcohol with gradually decreased concentration for two minutes each (100% for three times, 96% for two times, 70% for one time) to regain hydration. Wash sections with PBS for 7 minutes.

Rehydrated sections were ready for non-immunostaining and immunostainings. For immunostainings, the general procedurs are as follows:

1. Blocking endogenous peroxidase: sections were incubated in 30 % peroxidase for 20 minutes at room temperature in the dark and then washed with PBS for seven minutes.
2. Antigen unmasking: sections were incubated in boiled 10 mM sodium citrate buffer (pH 6.0), cooled down, then washed in PBS for 7 minutes.
3. Blocking avidin and biotin: sections were treated with avidin blocking solution for 15 min and then washed briefly in PBS. Sections were treated with biotin blocking solution for 15 min and then washed briefly in PBS.
4. Blocking non-specific binding: sections were treated with 10 % normal goat serum for 10 minutes at room temperature. Sections were ready for further primary antibody incubation.

5. Primary antibody incubation: sections were treated with primary antibody for one hours at room temperature or 4 °C overnight and then washed in PBS for seven minutes.
6. Secondary antibody incubation: sections were treated with biotinylated secondary antibody for 30 minutes in room temperature and then washed in PBS for seven minutes.
7. Sections were treated with avidin–biotin complex solution for 30 minutes in room temperature and then washed in PBS and Tris-HCl buffer.
8. Staining: sections were stained in staining solution containing 200 mL 37 °C Tris-HCl buffer, 4 mL DAB solution, 1 mL NiCl and 500 µL 3 % peroxidase.
9. Sections were counter-stained with methyl green.
10. Sections were dehydrated by incubation with 96 % for 10 seconds, 100 % ethanol for 10 seconds, and xylene for 10 seconds. Then sections were mounted with cover lips.

Glomerular size measurement in PAS staining

The details for PAS staining are as follows:

1. After rehydration, sections were treated with 0.5 % periodic acid solution for 5 minutes and then washed in distilled water for 5 minutes.
2. Sections were incubated in Schiff reagent for 5 minutes and then washed in 37 °C tap water for 3 minutes. Repeat the washing step.
3. Sections were counter-stained with hematoxylin for 2 minutes and then washed in tap water for 5 minutes.
4. Sections were dehydrated with 90% of ethanol and covered with a cover lip.

In PAS staining, images of at least 25 glomeruli were taken separately with microscope (at 400x magnification). Only glomeruli with a vascular pole or urinary pole were chosen. Glomerular tuft and capsule were outlined and the area were quantified (µm²) with ImageJ software, respectively. Tuft/capsule ratio was obtained by dividing the tuft area (µm²) by Bowman's capsule area (µm²) in percentage.

Mac-2 staining

Sections were stained by Mac-2 antibody to target macrophages (Rat anti-mouse Mac-2, 1:5000, Cederlane). For each section, around 15-20 glomeruli in cortex area and with a

vascular pole or urinary pole were chosen. Glomerular Mac-2 positive cells were counted. Results were reported as positive cells per glomerulus.

WT-1 staining

Sections were stained with anti-mouse Wilms Tumor-1 (WT-1) antibody by immunohistochemistry method (1:200, Santa Cruz Biotechnology). For each section, 15-20 glomeruli in the cortex and with a vascular pole or urinary pole were chosen. WT-1 positive cells at the junction between capsule and tufts were excluded. Results were reported as positive cells per glomerulus.

WT-1/Nephrin staining

Sections were staining by immunofluorescence double staining with WT-1 antibody (anti-mouse WT-1, 1:25, Cell signaling, MA, USA) and Nephrin antibody (guinea pig anti-mouse nephrin, 1:100, Acris Antibodies, Herford, Germany). For each section, 15-20 glomeruli in the cortex were chosen. A typical positve cell showed robust WT-1 staining signal overlapping with DAPI and surrounded by nephrin staining. Results were reported as positive cells per glomerulus.

Alpha smooth muscle actin (αSMA) staining

Sections were staining with αSMA (rabbit anti-mouse αSMA, 1:500, Dako, Hamburg, Germany). By using software Photoshop, a whole-section image was generated by merging series of images taken under low magnitude microscopy. Merged images were then corrected for background by software ImageJ. Area of medulla, especially those containing big blood vessels, was excluded by software Photoshop. Cortex area was measured by software ImageJ in μm^2 (Area-C). Positive area was measured by ImageJ in μm^2 (Area-αSMA). The percentage of Area-C over Area-αSMA was reported as positive area/section, %.

Picro-sirius red staining

The staining procedures are as follows.

1. Sections were warmed in warm bath (56 °C for 1 hour or 37 °C overnight).
2. Sections were washed by xylene for 5 minutes twice, ethanol (100%, 95%, 70%, and 50%) for 2 minutes twice, and distilled water for 2 minutes twice.
3. Sections were treated with adequate picro-sirius red solution and incubated at room temperature for 60 minutes.

4. Sections were washed twice with acidified water. Then Water was removed from sections by shaking.
5. Sections were dehydrated 100% Ethanol for 10 seconds. Repeat twice.
6. Sections were washed in xylene twice.
7. Sections were covered by mounting medium and cover slides.

Quantification was done by software ImageJ. First, glomeruli with urinary pole or vascular pole were selected. Glomerular tuft area was measured in μm^2 (Area-G). Then picro-sirius red area was selected and measured in μm^2 (Area-PG). The percentage of Area-G over Area-PG was reported as positive area/tuft area, %.

Pizzolato staining

A paraffin section of 6 µm was used. The steps are as follows.

1. Paraffin sections were deparaffinized and cover with distilled water.
2. Silver nitrate solution was prepared by mixing equal amounts of 5% silver nitrate and 30% hydrogen peroxide.
3. Sections were treated with sufficient silver nitrate solution so that tissues were totally covered.
4. Sections were heated with a 60-watt bulb for one hour at a distance of 15 cm and then rinsed thoroughly with distilled water twice.
5. Sections were counter-stained for 5 minutes in nuclear fast red solution and then rinsed with distilled water.
6. Sections were dehydrated in 95% alcohol, then 100% alcohol, and in xylene, repeat twice for each.
7. Sections were covered with mounting medium and cover slides.

4.3 Blood and urine measurement

Urine albumin ELISA

Urine albumin levels were measured by ELISA (Bethyl laboratories) following manufacturer's instructions. The procedures are as follows:

1. Goat anti-mouse albumin coating antibodies were diluted in 100 µl 0.05M carbonate-bicarbonate (pH 9.6) at a concentration of 10 µg/ml (100-fold dilution of stock). Diluted antibodies were added to a 96-well plat-bottom plate (MaxiSorp, Thermo Fisher) overnight in 4 °C and then washed for three times.
2. Plates were coated with 200 µl coating buffer which contained 1% bovine serum albumin for at least 30 minutes at room temperature and then washed for 3 times.
3. Samples were diluted for 200-1000 times with ELISA diluent. Plates were coated with 100 µl sample dilution or standards for 1 hour at room temperature and then washed for five times.
4. Plates were coated with 100 µl 10 ng/ml HRP conjugated goat anti-mouse albumin detection antibody (100,000-fold dilution of stock) for one hour at room temperature and then washed for five times.
5. Plates were coated with 100 µl tetramethyl benzidine substrate mix in the dark without covering for around 5-10 minutes.
6. Plates were added with 100 µl of stop solution (2N sulfuric acid).
7. Plates were read by an ELISA reader for measuring the absorbance at 450 nm within 30 minutes.
8. A standard curve of concentration versus absorbance was created by sigmoidal four parameter logistic curve fitting. The albumin concentration of each samples was converted accordingly.

Urine creatinine

Urine creatinine was measured by Jaffe method (Creatinine FS, Diasys, Germany). Urine dilution was prepared by mixing urine and water at 1:9 ratio. A total of 10 µl urine dilution and standards were loaded to a 96-well plate-bottom plate. Reaction reagents were mixed and loaded to the plate at 200 µl. Plates were read by an ELISA reader for measuring the absorbance at 490 nm after 1 minute, 3 minutes, and 15 minutes (endpoint). In our study, only the endpoint reading was used.

Blood urea nitrogen

Blood urea was measured by enzymatic method (Urea FS, Diasys, Germany). Urine (2 µl) and standards were added to a 96-well plate-bottom plate. Reaction reagents were mixed and added to the plate at 200 µl. Plates were read by an ELISA reader for the absorbance at 360 nm after 1 minute (T1), 3 minutes (T2), and 15 minutes (endpoint). In our study, only the

kinetic reading (value difference between T1 and T2) was used for further calculation of urea concentration. Urea nitrogen was converted by multiplying urea concentration by 0.467.

Glucose

Blood glucose was measured by enzymatic photometric method (”GOD-PAP”) (Glucose GOD FS, DiaSys, Holzheim, Germany). Plasma (2 µl) and standards were loaded to a 96-well plate-bottom plate. Reaction reagents were added to the plate at 200 µl. Plates were read by an ELISA reader for the absorbance at 490 nm after 10 minutes.

4.4 RNA isolation, cDNA synthesis, real-time qPCR

RNA isolation

RNA was isolated according to manufacturer’s instruction with minor modifications. The steps are as follows:

1. Lysis buffer containing 10% β-mercaptoethanol and 70% ethanl were prepared.
2. A small piece of kidney was cut and placed in a tube containing 600 µl 10% β-mercaptoethanol lysis buffer.
3. The kidney piece was homogenized for 30-40 seconds for two times.
4. The homogenized produce was centrifuged for 6000 rpm, 5 minutes.
5. The supernatant of centrifuged homogenized product was mixed with 500 µl 70% ethanol and transferred into the isolation column.
6. The tube was centrifuged at 11000 rpm for 30 seconds.
7. A volume of 350 µl of wash buffer I was added to the isolation column.
8. RNase-Free DNase was prepared in RNase-Free Buffer. Eighty µl of RNase-Free DNase was added to each isolation column and incubated at room temperature for 15 minutes.
9. A volume of 350 µl of wash buffer I was added to columns.
10. Columns were centrifuged at 11000 rpm for 30 seconds.
11. The isolation columns were transferred to a new collection tube.
12. Five hundred µl of Wash buffer II into isolation columns and centrifuged at 11000 rpm for 30 seconds. Repeat once.

13. After the waste in the collection tubes was discarded, the columns were centrifuged at 11000 rpm for 1 minute.
14. Isolation columns were transferred to new collection tubes.
15. Thirty-five µl of RNase free water was added to the columns and incubated at room temperature for 1 minute. Tubes were centrifuged at 11000 rpm for 1 min
16. RNA concentration and its purity were measured by Nanodrop. Only samples with A260/280 at 1.95-2.10 and A260/230 at 1.90-2.30 were proceeded to further measurement. Samples were stored at -80 °C.

cDNA synthesis

The detailed procedures of RNA conversion is listed as follows:

1. For a reaction size of 22.45 µl, RNA was diluted to a concentration of 66.67 ng/µl in 15 µl and added to RNase-free tube.
2. Master mix was prepared (for one sample) by mixing 4.5 µl 5x buffer, 1.0 µl DTT, 0.45 µl dNTPs, 0.5 µl Rnasin, 0.25 µl acrylamide, 0.25 µl Hexa, and 0.5 µl superscript reverse transcriptase and added to diluted RNA.
3. Another master mix in which the superscript reverse transcriptase was replaced by RNase-free water in the same volume was added to diluted RNA as a no-reverse-transcriptase control (RT-).
4. Mixed samples were incubated at 42 °C for 1.5 hour on a thermal shaker for reaction and 90 °C for 5 min to terminate the reaction.
5. Samples were stored at -20 °C until further use.

Real-time quantative polymerase chain reaction

Real-time quantative polymerase chain reaction (RT-qPCR) was performed by SYBR Green method in a reaction size of 20 µl. The detailed procedures were as follows:

1. cDNA reaction was diluted 10 times with nuclease-free water and added to a 96-well Lightcycler plate at 2 µl.
2. A master mix was prepared as follows (for one sample): 0.6 µl 10 µM forward primer, 0.6 µl 10 µM reverse primer, 10 µl 2x SYBR green I dye, 0.16 µl Taq DNA polymerase, and 6.64 µl nuclease-free free water. Eighteen µl of master mix were added to the 96-well Lightcycler plate.

3. Plates were sealed and shortly centrifuge to spin down reagents on the wall.
4. We used LightCycler 480 to perform DNA amplification.
   (a) Pre-incubation: the target temperature was 95 °C and held for 5 minutes. This step allows to denaturize cDNA and activate the Taq DNA polymerase.
   (b) Amplification: amplification was set at 40 cycles. For each cycle, it consists of 15 seconds of annealing at 60 °C and 40 seconds of extension at 72 °C.
   (c) Melting curve. First target temperature target was set at 95 °C and held for 5 seconds. Second target was 65 °C and allowed continuous decreased heating over 95 °C-65 °C.

Reference genes (18S rRNA) was carried out under same conditions and same reaction components. No template controls for target and reference genes were also carried out by replacing diluted cDNA by water in the same volume. When the target gene was chemokine or cytokine, cDNA derived from spleen tissues was added as a positive control. Cycle threshold (CT) values for 18s rRNA (CT_{ref}) and target gene (CT_{target}) were measured by LightCycler 480. Relative mRNA/18s rRNA equals to $2^{Ct_{target}-Ct_{ref}}$. Results were presented as relative mRNA/18s rRNA in $\log_{10}$.

Primers

Primers for RT-qPCR were designed by the primer designing tool at NCBI or obtained from published literature or online primer banks. The amplicon size was targeted at 70-150 bp. The primer specificity was checked by primer-BLAST at NCBI before synthesis. All primers were synthesized by a commercial company (Metabion, Germany) at a concentration of 100 µM. Primers were diluted to 10 µM in ultra-pure water. The primer specificity was tested prior to experiment by using cDNA samples derived from tissues expressing target genes (kidney or spleen) to exclude primer-dimer or non-specific products. The sequence of primers used in our study are shown in Table 4.1.

4.5 Human kidney biopsy transcriptomics

The transcriptomics project was under the framework of the European Renal cDNA Bank and approved by local ethical authorities [137, 138, 139]. Kidney biopsy samples were taken from 7 patients with DKD and 18 healthy individuals (living kidney donors) with informed consent [136]. The preservation, isolation, and reverse transcription for kidney RNA samples were described previously [137]. Briefly, Kidney tissues were preserved in RNase inhibition condition at -20 °C (RNA*later*, Ambion, USA). Under a stereomicroscope, tissue sections were

Table 4.1: Primer sequences

Gene	Forward	Reverse
18s	GCAATTATTCCCCATGAACG	AGGGCCTCACTAAACCATCC
Il1a	AGGGAGTCAACTCATTGGCG	ACTGTAGTCTTCGTTTTCACTGT
IL1b	TGCCACCTTTTGACAGTGATG	AAGGTCCACGGGAAAGACAC
Il1r1	CTGTTGGTGAGGAATGTGGCTG	GGCTCAGGATAACAGGTCTGTC
Il1r2	CAGTGCAGCAAGACTCTGGTAC	GCAAGTAGGAGACATGAGGCAG
Nlrp3	ACGTGTCATTCCACTCTGGC	AGGGAGTCAACTCATTGGCG
Acta2	GCTGTTGTAGGTGGTCTCAT	ACCATCGGCAATGAGCGTTT
Col1a1	ACATGTTCAGCTTTGTGGAC	TAGGCCATTGTGTATGCAG
col4a3	GAACCAGGAACCCCTTTCTC	TACCCTGCTGCTGCTACTCCTGG
Synpo	AGGAGCCCAGGCCTTCTCT	GCCAGGGACCAGCCAGATA
Wt1	CTGTACTGGGCACCACAGAG	CCAGCTCAGTGAAATGGACA
Nphs1	CAGCGAAGGTCATAAGGGTC	CACCTGTATGACGAGGTGGA
Tjp1	CCTGTGAAGCGTCACTGTGT	CGCGGAGAGAGACAAGATGT
Il6	TGCCACCTTTTGACAGTGATG	AAGGTCCACGGGAAAGACAC
Tgfb	TGATACGCCTGAGTGGCTGTCT	CACAAGAGCAGTGAGCGCTGAA
Ccl2	TTAAAAACCTGGATCGGAACCAA	GCATTAGCTTCAGATTTACGGGT
Cx3cl1	CAGTGGCTTTGCTCATCCGCTA	AGCCTGGTGATCCAGATGCTTC
Ccl5	CCTGCTGCTTTGCCTACCTCTC	ACACACTTGGCGGTTCCTTCGA

cut into glomerular and tubulointerstitial parts. Then total RNA from each compartments was lysed in guanidine thiocyanate, isolated with silica-gel column, and underwent reverse transcription [137]. The microarray was performed on Affymetrix HG-U133 Plus 2.0 microarrays system following the instruction from manufacturer. An initial data processing such as background correction and normalization was performed by robust multichip analysis method [138, 139, 136]. Gene annotation was analyzed with Human Entrez Gene custom CDF annotation version 18 [136]. Significantly expressed genes were identified with significance analysis of microarrays [140, 139]. A q-value ≤ 5% was considered significant.

4.6 Immunohistochemistry of human kidney biopsies

The details for immunohistochemistry was described previously [136]. Kidney biopsies were from the sample library at the Service of Pathology, University Hospital Geneva. The project was approved by local ethical committee (CEREH number 03-081). Tissues were obtained from eight diabetic patients and one healthy control with informed consent. Of the eight diabetic patients, all developed proteinuria; 2 were female and 6 were male; 2 were T1D and 6 were T2D. The tissue for healthy control was a tumor-free part from a patient who was diagnosed with neoplasia and underwent nephrectomy. Tissues were preserved in paraffin blocks and cut into 3 µm serial sections. The deparaffinization and antigen retrieval procedure were performed in a standard manner. Serial sections were treated with following four primary antibodies: 1. rabbit anti-human NLRP3 (1:1500), 2. mouse anti-human IL-1α (1:500), 3. rabbit anti-human IL-1β (1:400), 4. mouse anti-human CD68 (1:100). Sections were incubated with above antibodies for 1 hour at room temperature, incubated with second antibodies for 30 minutes at room temperature. Then sections were stained with DAB and counter-stained by Mayer's hematoxylin. We also perform negative controls which were performed in the same condition except omitting the primary antibodies.

4.7 Statistical analysis

Data from dropouts were included in analysis. Data are presented as mean ± standard deviation (SD). A p value ≤ 0.05 was considered statistically significant. Comparison between two groups was performed sequentially by normality test, homoscedasticity test (equality of variance), and comparison test as shown in Table 4.2. Comparison between more two groups was performed sequentially by normality test, homoscedasticity test (equality of variance), comparison test, and post hoc analysis as shown in Table 4.2. Statistical analysis and data visualization were performed with R studio or Graphpad Prism.

Table 4.2: Statistical methods for comparing the means between two or multiple groups

Normality	Homoscedasticity	Comparison Test	Post-hoc-test	Note
Comparison between two groups				
Shapiro-Wilk test	Levene's test	Student's *t*-test	n.a.	P>0.05 for Shapiro-Wilk test and P>0.05 for Levene's test
		Welch's *t*-test	n.a.	P>0.05 for Shapiro-Wilk test and P<0.05 for Levene's test
		Wilcoxon rank-sum test	n.a.	P<0.05 for Shapiro-Wilk test
Comparison between multiple groups				
Shapiro-Wilk test	Levene's test	One-way ANOVA test	Tukey	P>0.05 for Shapiro-Wilk test and P>0.05 for Levene's test, comparing the mean to every other group's mean
			Dunnett	P>0.05 for Shapiro-Wilk test and P>0.05 for Levene's test, comparing the mean to a specific group's mean
		Kruskal–Wallis test	Dunn	P<0.05 for Shapiro-Wilk test or P<0.05 for Levene's test

n.a., not applicable

5 Results

5.1 Part I. *db/db* mice fed by oxalate-rich food

In order to see, whether we could replace surgical kidney mass reduction by an oxalate-rich diet to cause GFR decline and progressive nephrocalcinosis also in *db/db* mice, mice received oxalate-rich diet, GFR was measured periodically, and kidney histology was analysed after 30-day feeding. GFR was indistinguishable between control and oxalate diet during 30 days of observation (Figure 5.2E). Oxalate-rich diet did not induce massive crystal deposition in kidney as known from C57BL/6N mice (Figure 5.2A-B). Mortality between these two diets was similar (Figure 5.2A). There was no difference in water intake (Figure 5.2B). Oxalate diet group consumed less food at day 10 and day 30 (Figure 5.2C). Body weight was similar between oxalate-rich diet and controls (Figure 5.2D). Thus, oxalate-rich diet did not induce GFR decline and nephrocalcinosis in *db/db* mice.

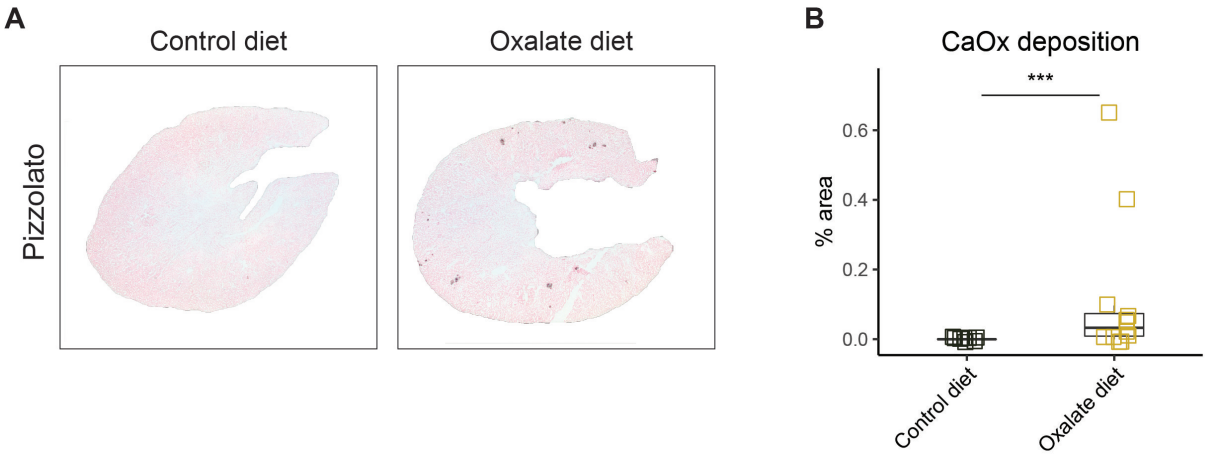

Figure 5.1: Oxalate-rich diet did not induce massive crystal deposition in mouse kidney. A, Pizzolato staining for oxalate crystals. After 30-day feeding, mouse kidney sections were stained with pizzolato staining. Magnification 100x. B, Quantification of pizzolato staining. Crystal deposition was quantified and presented as percentages of positive area over total kidney area. N=8 in control diet group, n=12 in oxalate-rich diet group. ***p <0.001.

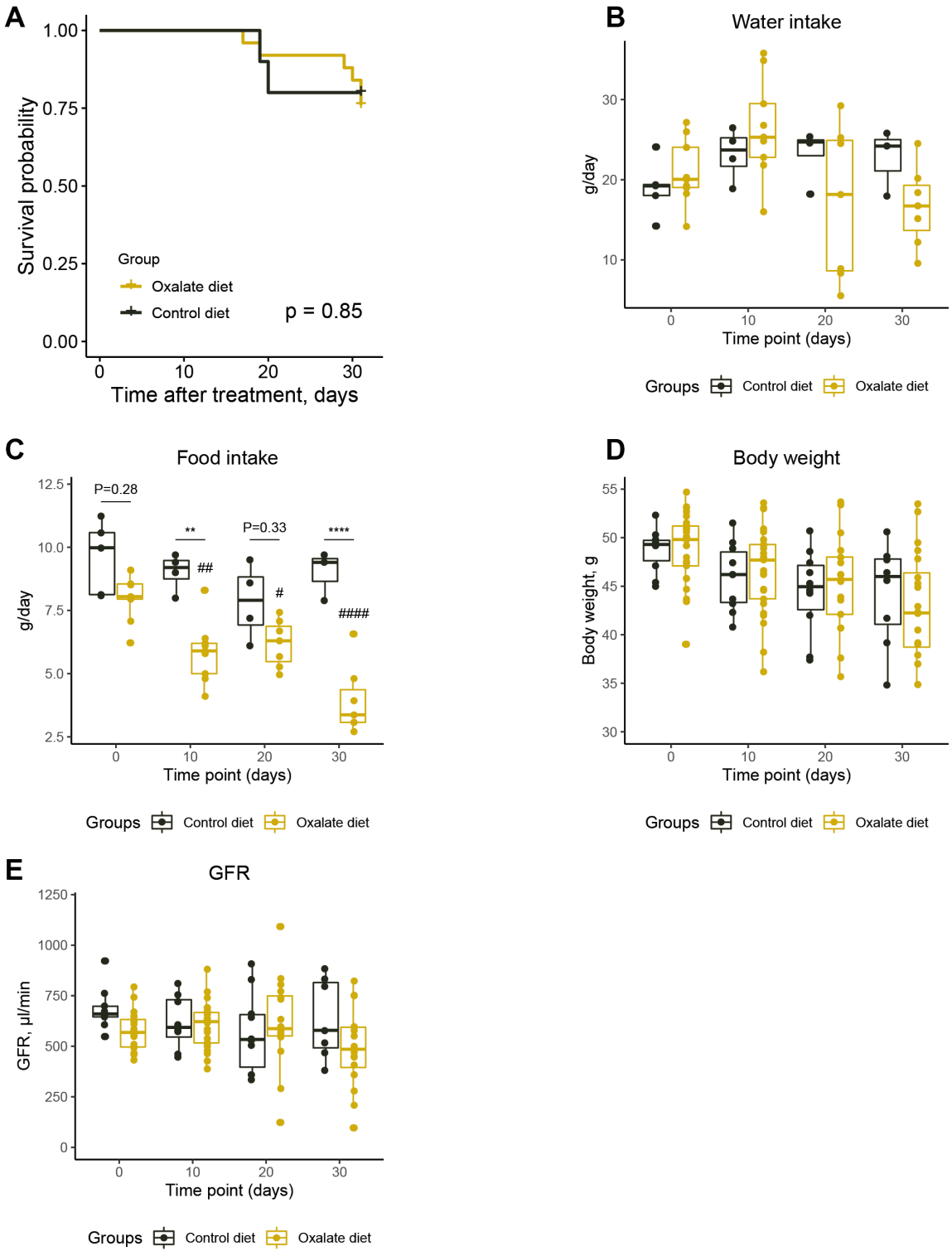

Figure 5.2: Effects of oxalate-rich diet on *db/db* mice. A, Kaplan-Meier survival curves. The survival was compared by a standard rank test between mice fed with regular food (black) and oxalate-rich food (yellow). N=10 in regular food, n=25 in oxalate food. B, Water intake. C, Food intake. Water and food intake were measured by recording the consumption over 24 hours from each cage. Each cage housed 2-3 mice from the same group. Each value in the figure represented the average consumption of each cage. $^{**}p$ <0.01, $^{****}p$ <0.0001. D, Body weight. E, GFR. GFR was measured every 10 days. GFR, glomerular filtration rate.

5.2 Part II. Interleukin-1β blockade in diabetic kidney disease

5.2.1 Interleukin-1β expression in diabetic kidney disease

Interleukin-1β gene expression in patients with diabetic kidney disease

First, in order to see whether IL-1 pathway is activated inside the kidney in the clinical scenario of diabetes, gene expression levels of IL-1α/β, their receptors, and NLPR3 were analyzed in human kidney biopsies from DKD patients and living donors by micro-dissected microarray. Kidney biopsies were collected from 7 patients with DKD, and from 18 living donors served as healthy controls. Result was shown in Figure 5.3. Glomerular and tubulointerstitial *IL1B* expression levels in DKD patients were 1.808 times and 1.273 times higher than those in living donors, respectively. *IL1R1* expression in glomeruli and tubulointerstitium from DKD patients were 1.226 times and 1.302 times higher, respectively, compared with living donors. DKD patients also expressed a higher level of *NLRP3* in glomeruli, which was 1.274 times of that in living donors. *IL1A* expression level was too low to detect. *IL1R2* expression levels, either in glomeruli or in tubulointerstitium, was similar between DKD patients and living donors. Together, kidney gene expression of IL-1β, IL-1R1, and NLRP3 are increased in human DKD.

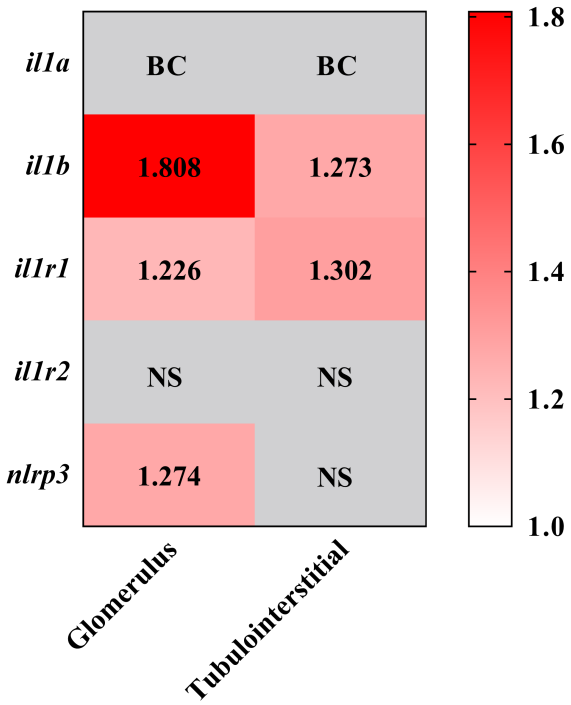

Figure 5.3: IL-1β gene expression in human kidney. Kidney biopsies were obtained from 7 DKD patients with or from living donors, micro-dissected into glomerular and interstitial compartments, and further proceeded to RNA microarray analysis. Gene expression levels of each compartment in diabetic kidneys were normalized to those in healthy kidneys and presented as average fold changes in the heat map. BC, below cut-off; NS, not significant. DKD, diabetic kidney disease.

Interleukin-1β protein expression in patients with diabetic kidney disease

To further confirm if IL-1β pathway is induced in DKD, protein expression levels of IL-1β, IL-1α, and NLRP3 were tested by immunohistochemistry in human kidney biopsies.

First, a total of 8 biopsies were collected, which were from patients diagnosed with DKD and varying severity of interstitial fibrosis and tubular atrophy (IFTA), including 1 case with 0% IFTA, 1 with 15 % IFTA, 2 with 30% IFTA, 1 with 50% IFTA, 2 with 60% IFTA, and 1 with 70 % IFTA. Then the specificity of antibodies for immunohistochemical staining was tested. As shown in Figure 5.4, compared with negative control omitting primary antibodies, staining with each antibody showed clear and specific signals.

Biopsy tissues were stained for CD68, IL-1α, IL-1β, and NLRP3, and the representative figures from 0% IFTA and 70% IFTA was shown in Figure 5.5 A. Here CD68 staining was performed additionally to see if macrophages are the cell origin of IL-1α, IL-1β, and NLRP3. The biopsy with 70% IFTA showed stronger CD68, IL-1α and IL-1β staining than biopsy with 0% IFTA. The NLRP3 staining was similar between 0% IFTA and 70% IFTA.

Further, a semi-score (0-3) was made to quantify the staining intensity in each biopsy in 5 compartments, including: glomerular tuft, Bowman's capsule, distal tubule, proximal tubule, and interstitium. Results were shown in 5.5B. Biopsies with higher IFTA score tended to have higher scores of CD68 staining. This tendency was also true in IL-1α and IL-1β, but not in NLRP3 staining. Of note, staining pattern of IL-1α was diffuse while that of IL-1β was more condensed and mainly located in some cells scattered in glomeruli tufts and tubulointerstitium, suggesting that IL-1β might originate from macrophages. IL-1β staining was also found in some tubular cells but to a lesser extent.

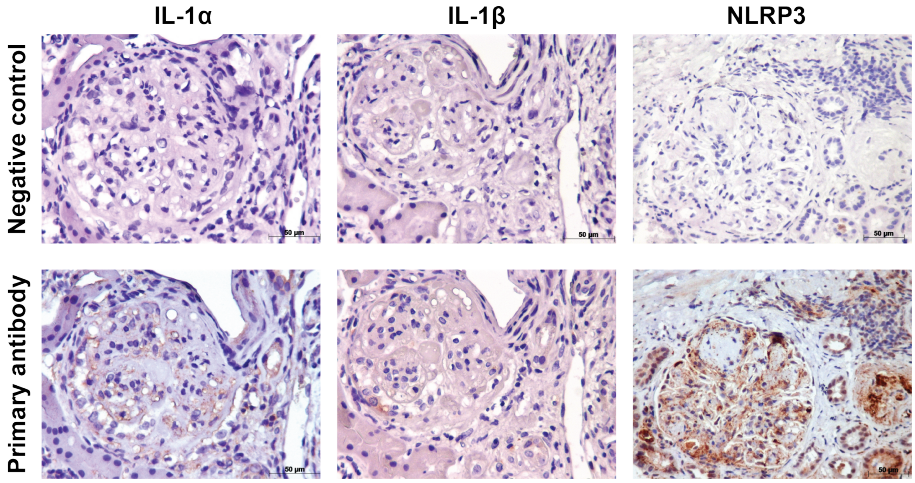

Figure 5.4: Specificity of IL-1α, IL-1β, and NLRP3 staining in human kidney biopsies. For IL-1α and IL-1β staining, kidney tissue was obtained from a patient with diabetic kidney disease and with 60% IFTA; for NLRP3 staining, kidney tissue was obtained from a patient with DKD and 40% IFTA. Upper: negative control; primary antibody was omitted. Lower: primary antibodies were added. Original magnification 320x in IL-1α and IL-1β staining, and 250x in NLRP3 staining. IFTA, interstitial fibrosis and tubular atrophy.

Linear regressions of IFTA score and the sum of score from each staining was made as shown in Figure 5.5C. Score of CD68 (R=0.82, p=0.012) and score of IL-1β (R=0.73, p=0.042) was significantly correlated with IFTA.

Thus, IL-1β protein expression is increased in human DKD. IL-1β mainly derives from infiltrating immune cells in glomeruli and interstitium and also from few tubular epithelial cells.

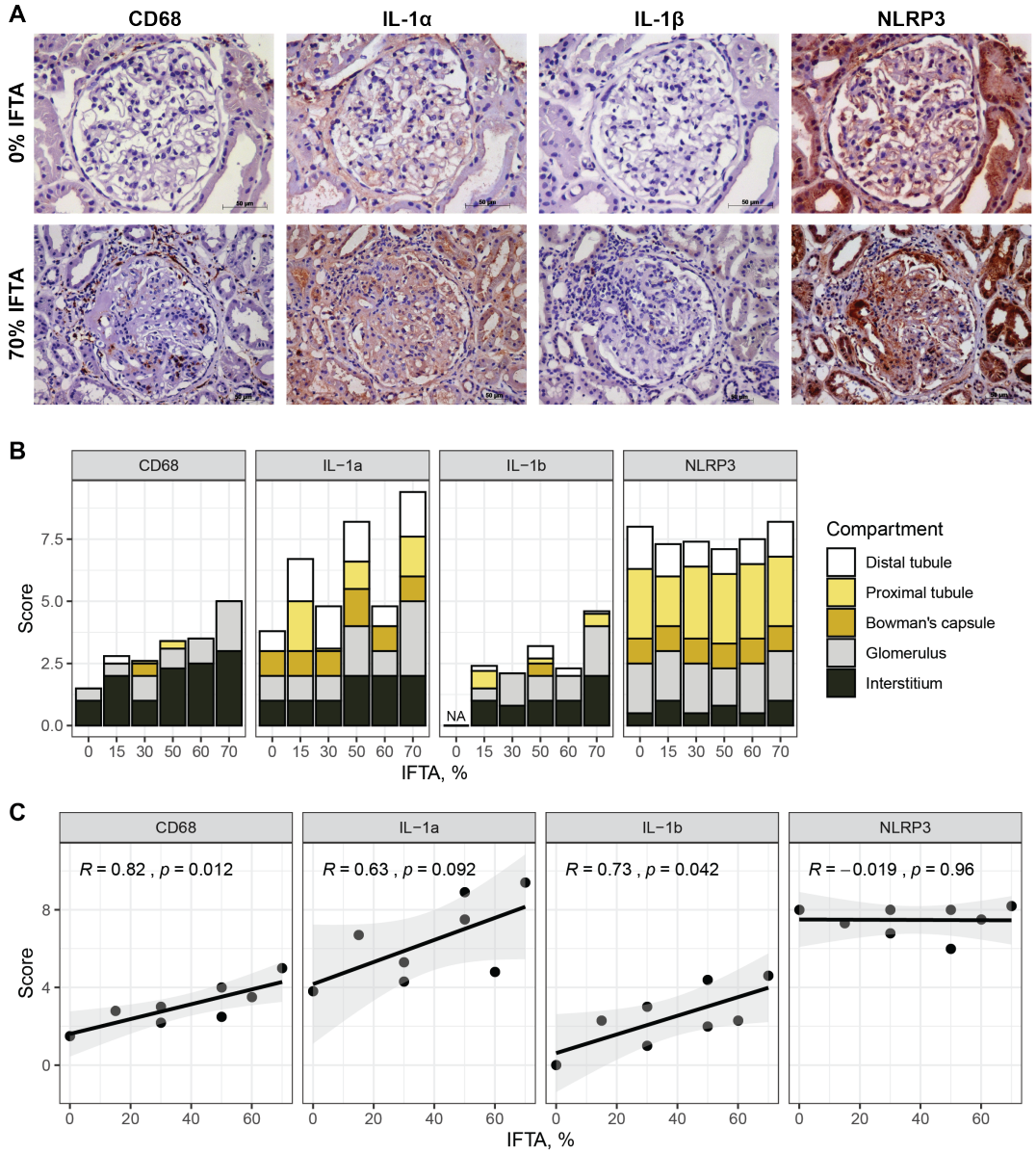

Figure 5.5: IL-1α, IL-1β, and NLRP3 protein expression in human kidney biopsies. A, Immunohistochemistry staining. Kidney biopsy tissues were stained for CD68, IL-1α, IL-1β, and NLRP3. Representative images were from biopsies scored with IFTA 0% and IFTA 70%, respectively. Original magnification 320x in IFTA 0% and 200x in IFTA 70%. B, Semi-quantification for immunohistochemistry staining. Staining results were semi-quantified by scoring 0-3 points for five kidney compartments: glomerular tuft, Bowman's capsule, distal tubule, proximal tubule, and interstitium. Zero point represents for no positive staining, 3 for very strong staining. Base on the scores, stacked bar charts were generated. NA, not applicable. C, Linear regression of IFTA and score of staining. The correlation of the sum of staining scores from all five kidney compartments and IFTA was analyzed by linear regression. N=1 in 0%; n=1 in 15%; n=2 in 30%; n=1 in 50%; n=2 in 60%; n=1 in 70%. IFTA, interstitial fibrosis and tubular atrophy.

Interleukin-1β expression in diabetic mice

Next, in order to see, if our animal model of DKD also has the feature of increased IL-1β expression in kidney, we analyzed transcription levels of IL-1β in kidneys from *db/db* mice by RT-qPCR. We analyzed kidney gene expression in 26-week-old *db/db* mice that had uninephrectomy at age 8 weeks (DM-1K). Age controlled *db/db* mice with sham surgery (DM-2K), age controlled wild type mice with a morning uninephrectomy at the age of 8 weeks (WT-1K), as well as age controlled wild type mice with sham surgery (WT-2K) served as controls.

As shown in Figure 5.6, expression level of *IL1b* in DM-1K was higher than that in DM-2K group and reached a statistical significance. A significant higher level of *Il1r1* expression was also shown in DM-2K when comparing to WT-2K. Expression levels of *Il1a*, *Il1r2* and *Nlrp3* were similar between each group. Together, IL-1β gene expression is increased in *db/db* mice with uninephrectomy.

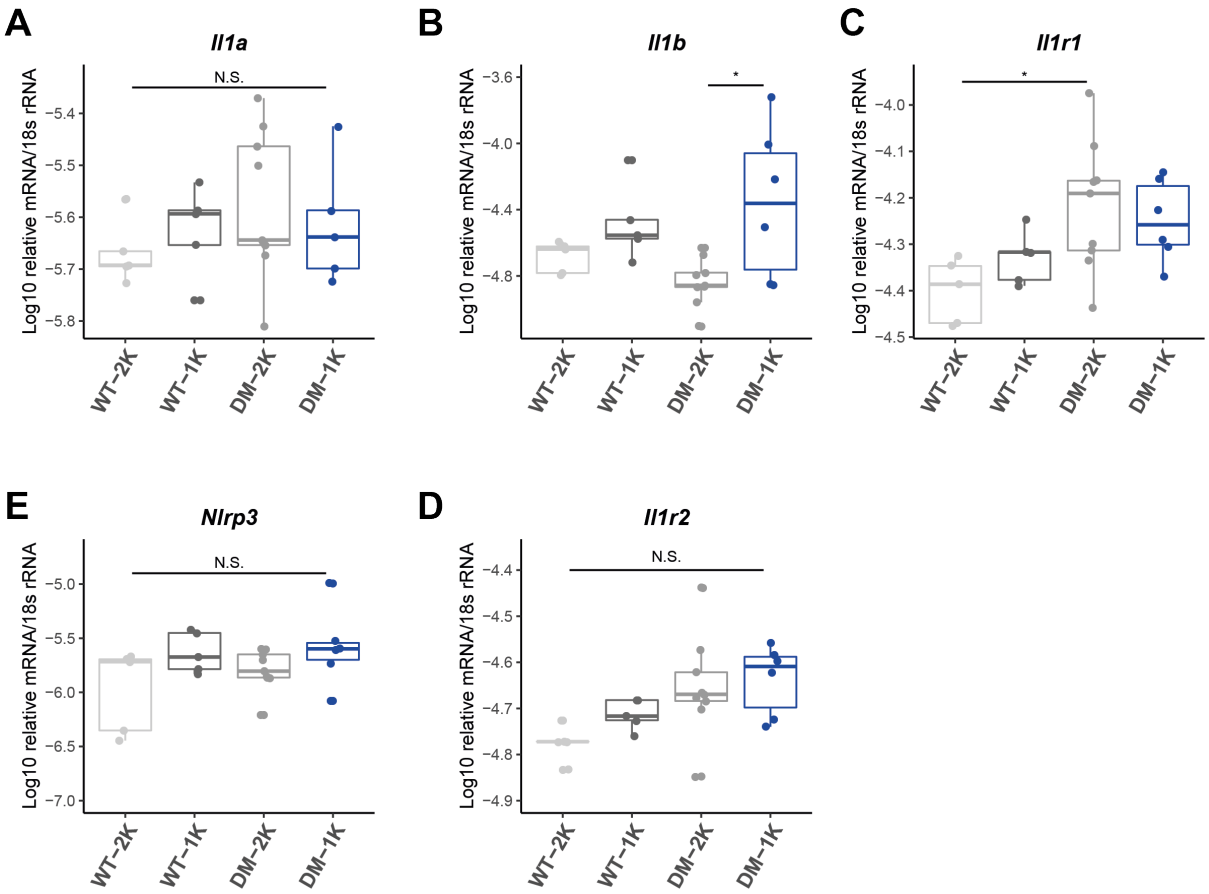

Figure 5.6: Kidney IL-1β expression in *db/db* mice. Kidneys RNA from 26-week-old wild type mice and *db/db* mice with or without uninephrectomy were isolated and measured for *Il1a*, *Il1b*, *Il1r1*, *Il1r2*, and *Nlrp3* expression levels by real-time quantitative PCR. Data were presented as log10 transformation of relative gene expression to 18S rRNA. N.S., statistically not significant; *p <0.05.

5.2.2 Effects of interleukin-1β blockade on metabolic parameters

In order to see if IL-1β blockade has an effect on DKD, 18-week-old DM-1K mice were intraperitoneally administrated with anti-IL-1β IgG antibody or control IgG for 8 weeks. First, effects of IL-1β blockade on metabolic parameters were analyzed to see if treatment influenced obesity and hyperglycemia.

Body weight was monitored every week. Before the treatment, *db/db* mice with uninephrectomy (Unx) (DM-1K) had a lower body weight than their sham surgery controls (Figure 5.7 A). Mice receiving anti-IL-1β IgG had similar body weight compared to those received IgG treatment (5.7 B).

Food and water intake were also monitored periodically after treatment initiation. Mice with anti-IL-1β IgG treatment had similar food and water consumption compared to mice in IgG controls (Figure 5.7 C-D).

Fasting blood glucose levels was also measured periodically after treatment initiation. Compared with sham surgery group, *db/db* mice with uninephrectomy had similar fasting blood glucose levels, indicating uninephrectomy did not affect glucose metabolism. Compared with mice receiving control IgG, mice receiving anti-IL-1β IgG had similar fasting glucose levels during the 8-week treatment period (Figure 5.7 E).

Taken together, anti-IL-1β IgG treatment has no effects on body weight, food or water consumption, or fasting blood glucose in uninephrectomized *db/db* mice.

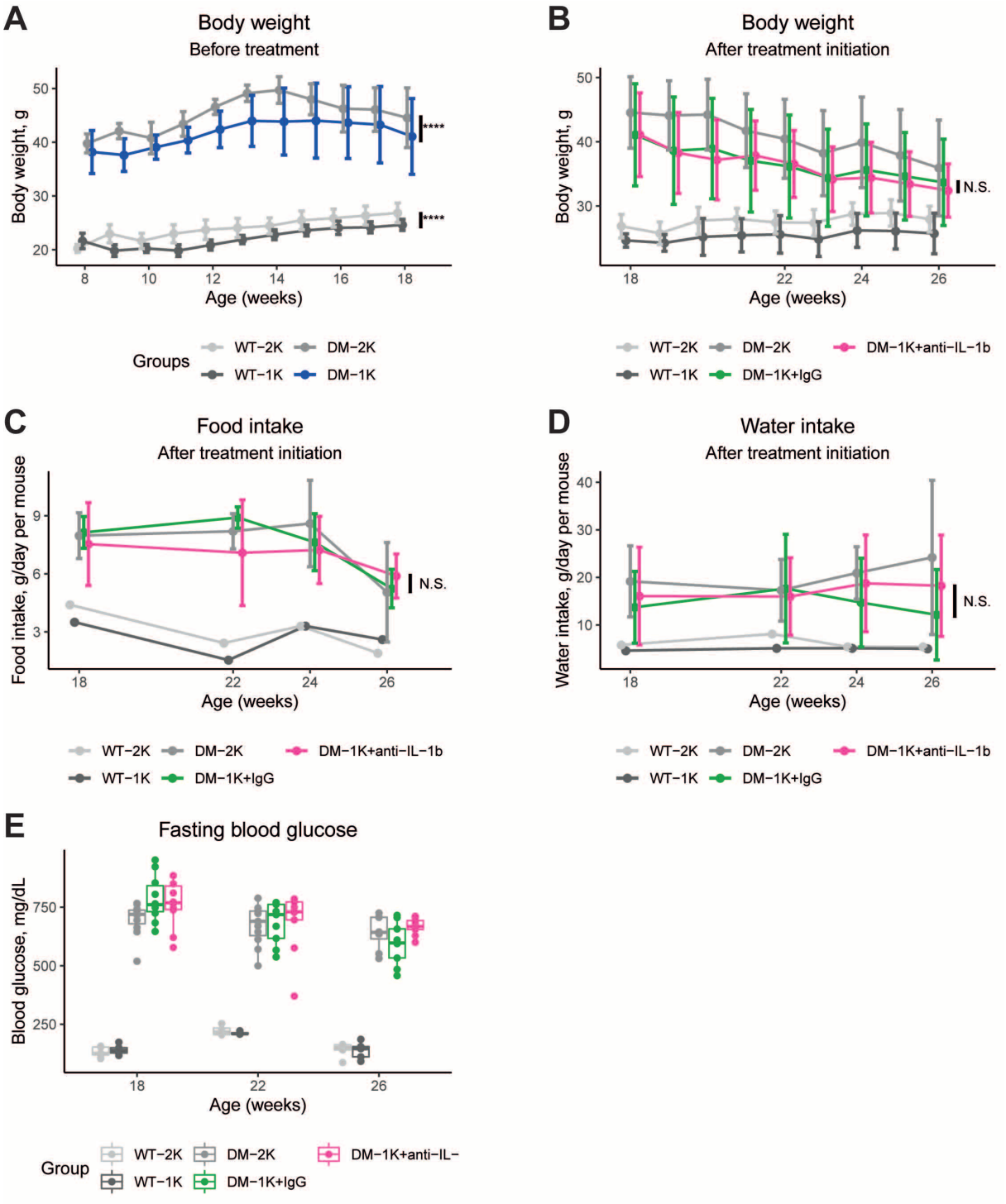

Figure 5.7: Body weight, food consumption and water intake, fasting blood glucose. A, Body weight before the initiation of treatment. Body weight was recorded every week until treatment started. ****p <0.0001 in two-way ANOVA test. B, Body weight after treatment started. After anti-IL-1β IgG or control IgG treatment initiated, body weight was recorded until the end of treatment. N.S. represents for not significant in the two-way ANOVA test. C, Water intake. D, Food intake. Water and food intake were measured by recording the consumption over 24 hours. N.S., not significant in the two-way ANOVA test. E, Fasting blood glucose. Mice were fasted for 4 hours and plasma was collected. Glucose was tested by enzymatic photometric method.

5.2.3 Effects of interleukin-1β blockade on kidney function

Next, GFR was tested periodically to see if anti-IL-1β IgG has an effect on kidney function in diabetic mice.

GFR was measured with a transdermal miniaturized monitor recording the signal of exogenous FITC-sinistrin in conscious mice. As few studies had used this technique and analyzed GFR evolution in this model, GFR evolution in this model was closely examined. Table 5.1 and Figure 5.8 A showed the effect of diabetes and uninephrectomy on the evolution of GFR. First is the effect of diabetes on GFR. GFR in healthy wild type mice was relatively stable from 8 to 26 weeks of age, which increasing gradually from 199.2 ± 21.6 µl/min to 274.6 ± 21.3 µl/min. Due to hyperglycaemia, obesity, and polyphagia, GFR in DM-2K mice started with a twice higher level compared to their wild type controls (431.6 ± 58.3), dramatically increased to the peak at 13 weeks of age (685.0 ± 106.5), and gradually decreased to 422.7 ± 86.7 at 26 weeks of age, which was comparable to their baseline GFR level. Next is the effect of uninephrectomy on GFR. Five weeks after surgery, *db/db* mice with uninephrectomy (DM-1K) had a GFR level equivalent to around two third, but not half, of that in *db/db* mice with sham sergery. The GFR level in DM-1K group gradually declined to 275.3 ± 52.4 at the age of 26 weeks, which was similar to that in age-controlled wild type control (WT-2K) group.

For the treatment effect of anti-IL-1β on GFR, compared to mice receiving control IgG, mice receiving anti-IL-1β IgG had indistinguishable GFR level after 4-week treatment but had a higher GFR level after 8-week treatment (5.8 C). The difference was around 50 µl/min (334.3 ± 31.7 vs. 275.3 ± 52.4, $p = 0.02$).

Table 5.1: Evolution of glomerular filtration rate in *db/db* mice.

Group	Age, weeks				
	8	13	18	22	26*
WT-2K	199.2 ± 21.6	239.3 ± 22.3	249.0 ± 58.2	274.5 ± 47.8	274.6 ± 21.3
WT-1K	190.2 ± 18.6	154.6 ± 17.4	169.6 ± 11.7	175.7 ± 16.9	202.7 ± 23.3
DM-2K	431.6 ± 58.3	685.0 ± 106.5	659.2 ± 180.8	405.1 ± 143.8	422.7 ± 86.2
DM-1K	407.8 ± 58.8	432.4 ± 128.3	442.1 ± 81.1	306.8 ± 78.2	275.3 ± 52.4

* Data represent as Mean ± SD. Mouse numbers for WT-2K, WT-1K and DM-2K were 5, 5, 8, and 11. Mouse number for DM-1K was 20 from 8 weeks to 18 weeks , and 8-11 from for 22 to 26 weeks which was taken from DM-1K+IgG group.

Excretory kidney function was also evaluated by BUN measurement. As demonstrated in Figure 5.8 D, at the age of 26 weeks, mice from all groups had no significant difference in BUN. When comparing BUN only between DM-1K+anti-IL-1β and DM-1K+IgG group, there was still no between-group difference (Figure 5.8. Considering that GFR levels in diabetic mice were still higher than wild type controls at the age of 26 weeks, BUN might not be an sensitive parameter reflecting excretory kidney function.

Thus, anti-IL-1β IgG treatment in *db/db* mice with uninephrectomy preserves more GFR than control IgG.

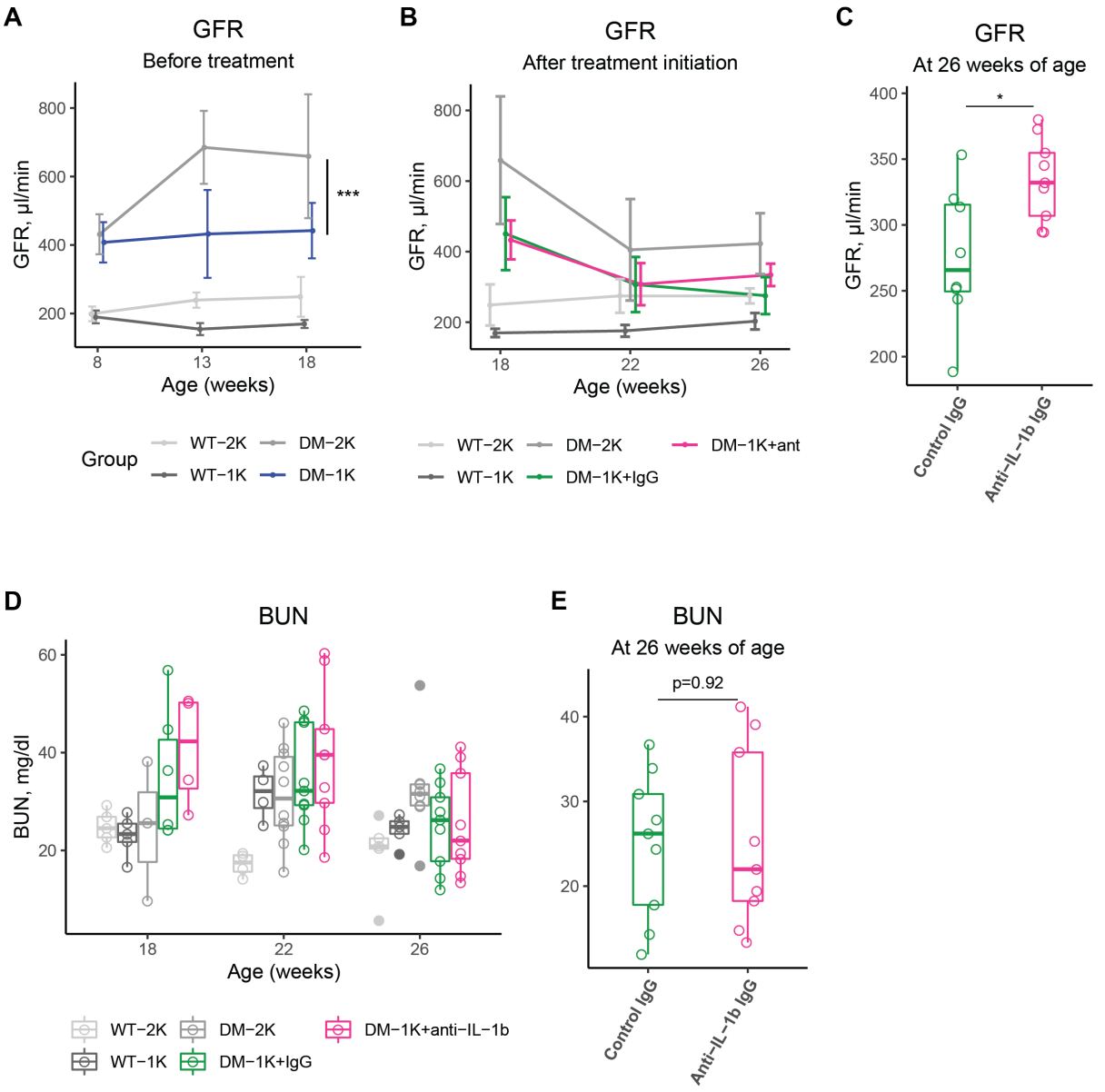

Figure 5.8: Effects of anti-IL-1β IgG treatment on kidney function in *db/db* mice. A, GFR before treatment. GFR was measured before treatment began (from 8 to 18 weeks of age). Uninephrectomy was performed shortly after 8 weeks old. ****p <0.0001 in a two-way ANOVA test. B, GFR after treatment. GFR was measure after treatment started. C, GFR at the age of 26 weeks. Comparison was calculated by t test. D, BUN. E, BUN at 26 weeks of age. GFR, glomerular fitlration rate.

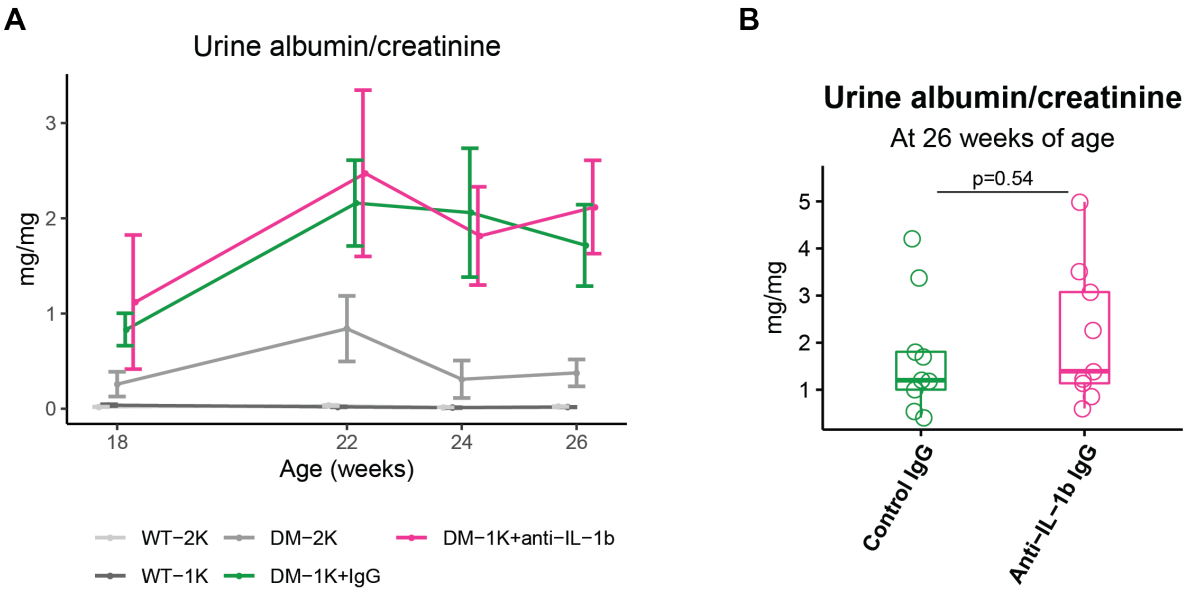

Figure 5.9: Effect of anti-IL-1β antibody on albuminuria in *db/db* mice. A, UACR. Concentration of albumin and creatinine in spot urine were determined by ELISA and Jaffe method, respectively. B, UCAR at 26 weeks of age. UACR, urine albumin to creatinine ratio.

5.2.4 Effects of interleukin-1β blockade on proteinuria

Proteinuria is a critical parameter for kidney disease progress and a predictor for kidney outcome. In the current study, albuminuria was measured by urine albumin ELISA normalized to urine creatinine. The Time course of urinary albumin-creatinine ratio (UACR) during 8-week treatment was shown in Figure 5.9 A. Mice receiving anti-IL-1β IgG treatment had similar levels of UACR compared to those treated with control IgG after 4-week treatment and 8-weeks treatment (p = 0.49). Thus, anti-IL-1β IgG does not reduce urine albumin excretion in *db/db* mice with uninephrectomy.

5.2.5 Effects of interleukin-1β blockade on glomerular hypertrophy

From the onset of diabetes, glomeruli undergo hypertrophy, which is most likely an adaptive response to hyperfiltration driven by hyperglycemia, SGLT2-induced tubuloglomerular feedback disorder, and low nephron per body mass [141, 142]. In order to explore the potential effect of anti-IL-1β treatment on glomerular hypertrophy, tuft and Bowman's capsule size was measured in 15-25 cortex glomeruli per kidney in PAS-staining slides. In Figure 5.10 A, it showed representative images from each group. The size of glomerular tuft (yellow dot line) and Bowman's capsule (green line) was larger in DM-1K+IgG and DM-1K+anti-IL-1β group.

The glomeruli from all the mice in each group were pooled, and a density plot was generated to see the distribution of glomerular size in each group. As shown in Figure 5.10 B,

compared with healthy wild type controls (WT-2K), wild type mice with uninephrectomy (WT-1K) and diabetic mice showed a clear ”shift” towards bigger tuft, bigger Bowman’s capsule, and higher tuft/capsule ratio. This phenomenon was more obvious in diabetic mice with uninephrectomy (DM-1K+IgG and DM-1K+anti-IL-1β). The glomerular size distribution did not differ between DM-1K+IgG and DM-1K+anti-IL-1β.

Then the average size was calculated and the results were shown in Figure 5.10 C. Compared with IgG-treated mice, anti-IL-1β-treated mice displayed similar tuft area, capsule area, and tuft/capsule ratio. Thus, anti-IL-1β treatment does not alter glomerular hypertrophy in *db/db* mice with uninephrectomy.

5.2.6 Effects of interleukin-1β blockade on podocyte loss

In consequence of glomerular hyperfiltration and hypertrophy, glomerular filtration surface expands and post-mitotic podocytes accommodating to remain attached to the filtration membrane [142]. As glomerular hyperfiltration and hypertrophy persist, podocyte loss is inevitable, underlining the progression of DKD. In order to see whether anti-IL-1β had an effect on podocyte loss in *db/db* mice, we perform WT-1 staining in kidney sections (Figure 5.11 A) and counted glomerular WT-1 positive cells from 15-25 cortex glomeruli for each kidney section (Figure 5.11 B).

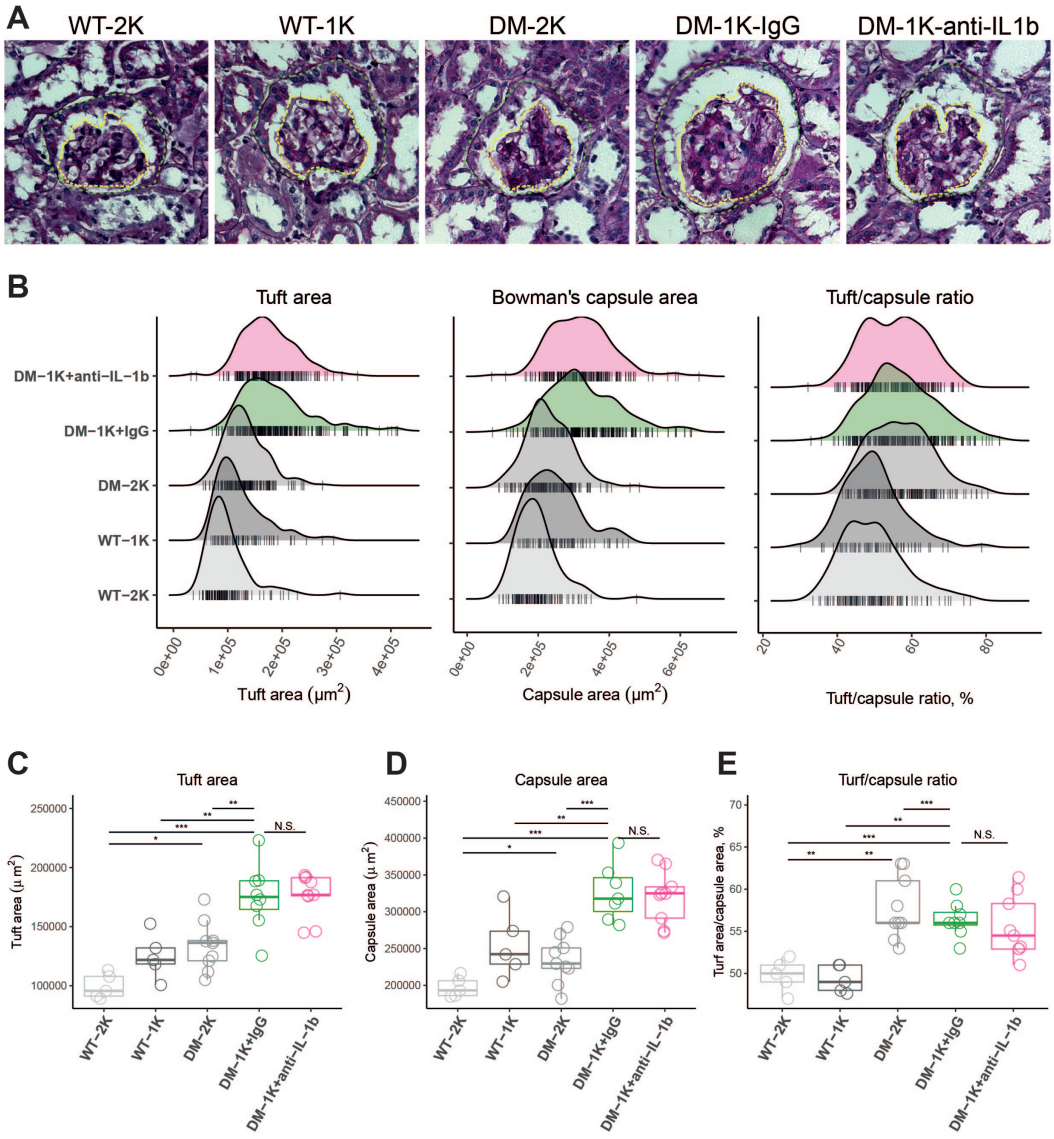

Figure 5.10: Effect of anti-IL-1β antibody on glomerular size in *db/db* mice. A, Tuft and Bowman's capsule area in PAS staining. Kidney sections were stained by PAS staining. Representative images of glomeruli from each group. Yellow dash line, tuft area. Green dash line, Bowman's capsule area. Original magnification 400x. B, Distribution of glomerular size. Area of tuft and capsule, as well as tuft over capsule ratio from 10-25 glomeruli per mouse was measured by software. Density plots were generated based on the pooled data from mice belonging to the same group. Each vertical short line beneath the histogram represents for the value of one glomerulus. C, Quantification of glomerular size. N.S., statistically not significant; **p* <0.05; ***p* <0.005; ****p* <0.001.

The number of WT-1 positive cells per glomerulus in anti-IL-1β-treated mice was significantly higher (11.8 ± 0.40) than IgG-treated mice (10.15 ± 0.27). WT-1/nephrin double staining was further performed, which has a higher specificity for podocyte, to confirm the result from WT-1 staining by the immunochemistry method. As shown in Figure 5.11 C, the number of WT-1 and nephrin double positive cells per glomerulus in anti-IL-1β-treated mice (10.72 ± 0.59) was significantly higher compared with IgG-treated mice (8.65 ± 0.35), which was consist with the result from WT-1 single staining.

For comparison of podocyte counts between other groups, WT-2K displayed significantly more WT-1 positive cells (16.86 ± 0.60) than WT-1K (13.78 ± 1.86). DM-2K (13.60 ± 0.29) also showed more WT-1 positive cells compared to DM-1K. Above indicates the effect of

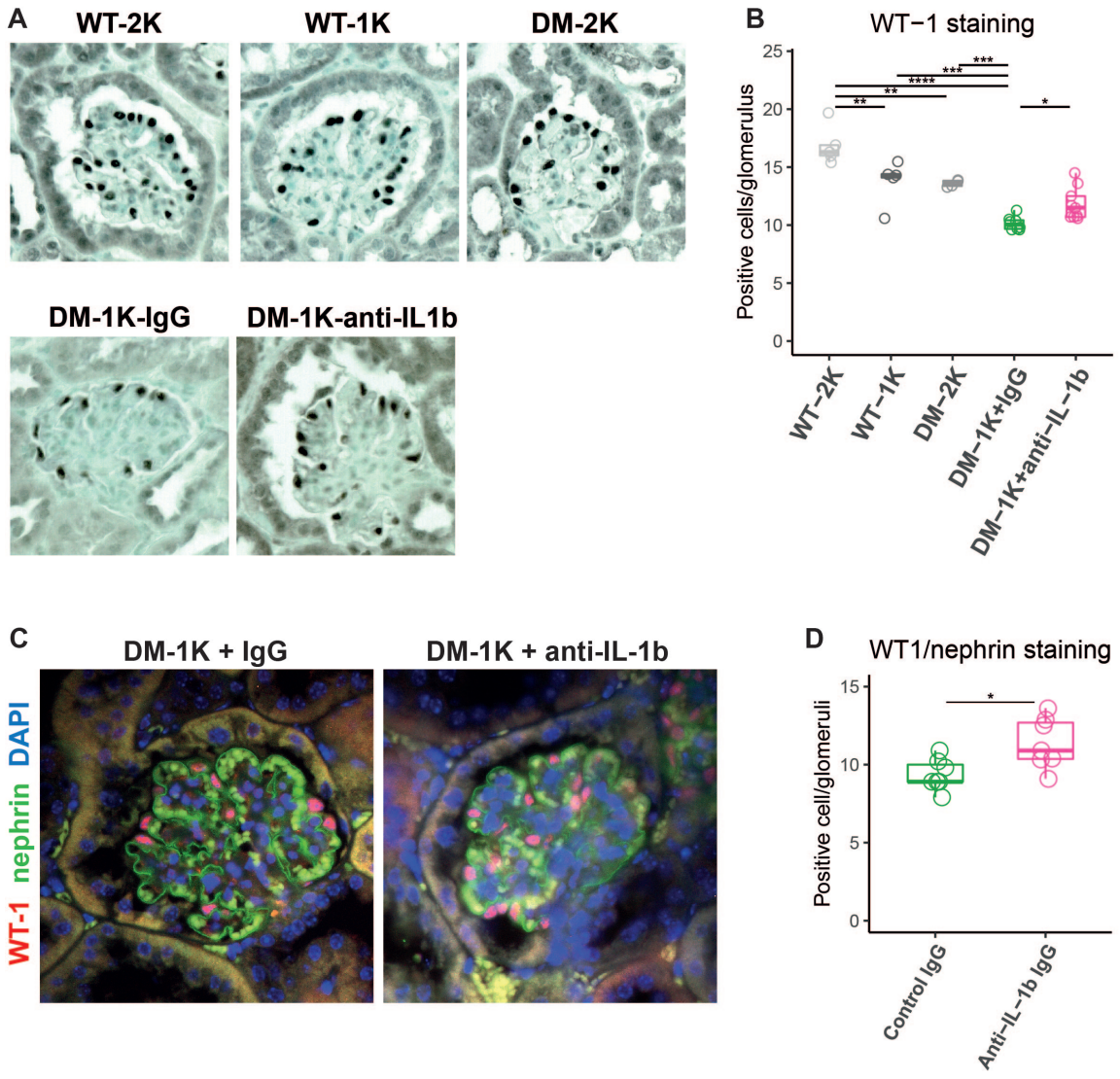

Figure 5.11: Effect of anti-IL-1β antibody on podocyte loss in *db/db* mice. A, WT-1 staining. Kidney sections were stained for WT-1. Representative images of each group. Original magnification 400x. B, Quantification of WT-1 positive cells. One dot represented the mean of WT-1 positive cells calculated from 15-25 cortex glomeruli per kidney section. C, WT-1/nephrin double staining. Original magnification 400x. D, Quantification of WT-1/nephrin double positive cells. *p <0.05.

compensatory hyperfiltration and podocyte loss secondary to uninephrectomy. WT-2K group showed more WT-1 positive cells than DM-2K group; WT-1K group also showed more WT-1 positive cells compared to DM-1K+IgG. Above indicates the effect of diabetes on podocyte loss.

To further evaluate the effects of anti-IL-1β treatment on podocyte loss, we performed RT-qPCR to quantify the transcription levels of podocyte marker genes. As represented in Figure 5.11 D, compared with IgG-treated mice, IL-1β-treated mice showed a significant upregulation of mRNA levels in *Synpo* and *Wt1* but not in .

Taken together, anti-IL-1β treatment ameliorates podocyte loss driven by diabetes and uninephrectomy.

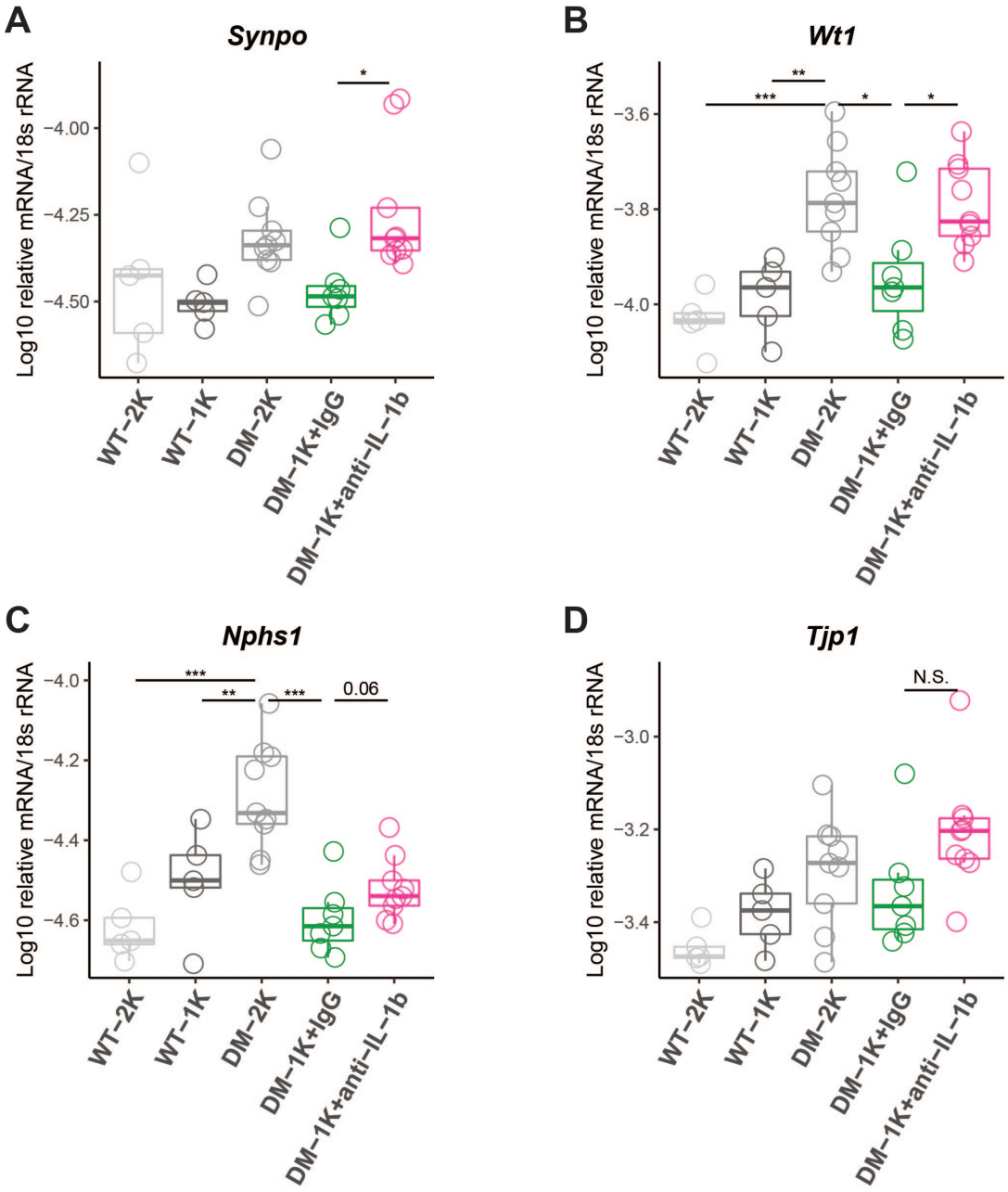

Figure 5.12: Effect of anti-IL-1β antibody on podocyte marker gene expression in *db/db* mice. RNA expression levels of podocyte markers in wild type mice and *db/db* mice with or without uninephrectomy. Kidney RNA was isolated and measured for *Synpo*, *Wt1*, *Nphs1*, and *Tjp1* expression levels by real-time quantitative PCR. N.S., not significant; **p* <0.05; ***p* <0.01; ****p* <0.001.

5.2.7 Effects of interleukin-1β blockade on kidney fibrosis

Kidney fibrosis is a hallmark of DKD. Collagen deposition in GBM and mesangium is the major contribution to intra-glomerular fibrosis. In order to analyse kidney fibrosis, kidney slides were stained with picro-sirius red to visualize the deposition of collagen type I and III. As shown in Figure 5.13, DM-1K+IgG mice had greater picro-sirius red area than DM-2K group (5.86 ± 0.48% vs. 1.49 ± 0.33%, $p<0.05$), indicating an effect of nephron loss in the context of diabetes. Nevertheless, picro-sirius red area in glomerular compartment in anti-IL-1β group was indistinguishable to control group. Besides, there was no significant difference between DM-2K, WT-1K, and WT-2K.

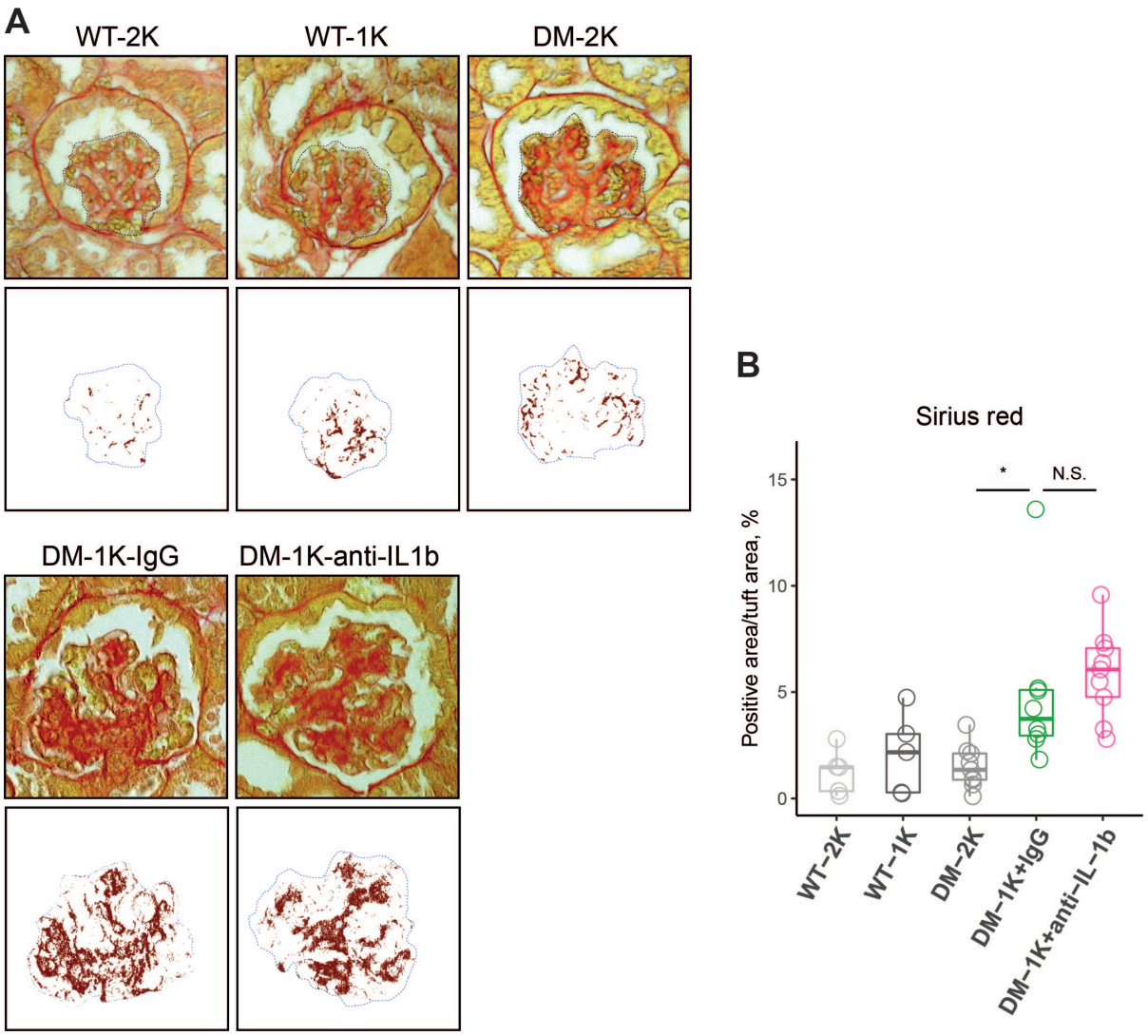

Figure 5.13: Effect of anti-IL-1β antibody on glomerulosclerosis in *db/db* mice. A, Picro-sirius red staining. Mouse kidney sections were stained for Picro-sirius red staining, which indicates collagen deposition. Representative pictures of glomeruli from each group. Original magnification 400x. B, Quantification of picro-sirius red. Results were presented as the ratio of picro-sirius red positive area over glomerular tuft area. N.S., statistically not significant; *p <0.05.

αSMA is another source for tissue fibrosis. Next, kidney fibrosis was analyzed by αSMA staining. As demonstrated in Figure 5.14 A, αSMA staining positive area located mainly in arteries, interstitial fibrosis area, as well as in mesangial matrices. To rule out the confounding factor from arteries, artery area was removed from the whole section and the remnant was quantified. As shown in Figure 5.14 B, αSMA staining was similar across all groups; DM-1K+IgG groups showed no increase in αSMA compared to healthy wild type mice (3.61% ± 0.39 vs. 2.80 ± 0.41%, p = 0.87), indicating αSMA deposition might be a later event in current model compared with hypertrophy and podocyte loss.

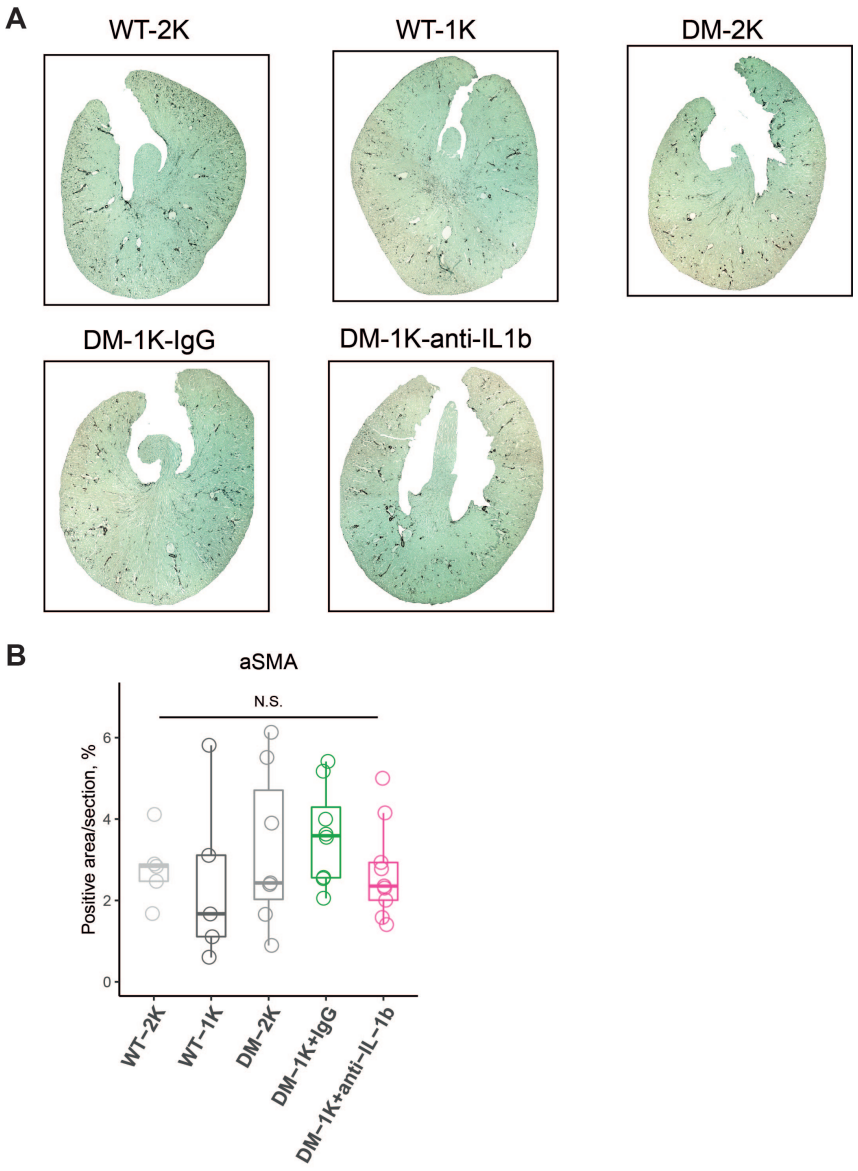

Figure 5.14: Effect of anti-IL-1β antibody on kidney α SMA accumulation in *db/db* mice. A, αSMA staining. Kidney sections were stained for αSMA. Representative images of kidney sections from each group. Original magnification 100x. B, Quantification of αSMA staining. Result was calculated as the percentage of αSMA positive area over kidney section (arteries area was omitted). N.S., statistically not significant.

Gene expression of fibrosis components were also measured to evaluate fibrosis levels. As shown in Figure 5.15 A-C, anti-IL-1β IgG treatment significantly reduced *Acta2* (gene encodes αSMA) and *Col4a3*.

Taken together, the overall fibrosis level in current model is not pronounced at protein level. Anti-IL-1β IgG reduces fibrosis-related gene expression in *db/db* mice with uninephrectomy.

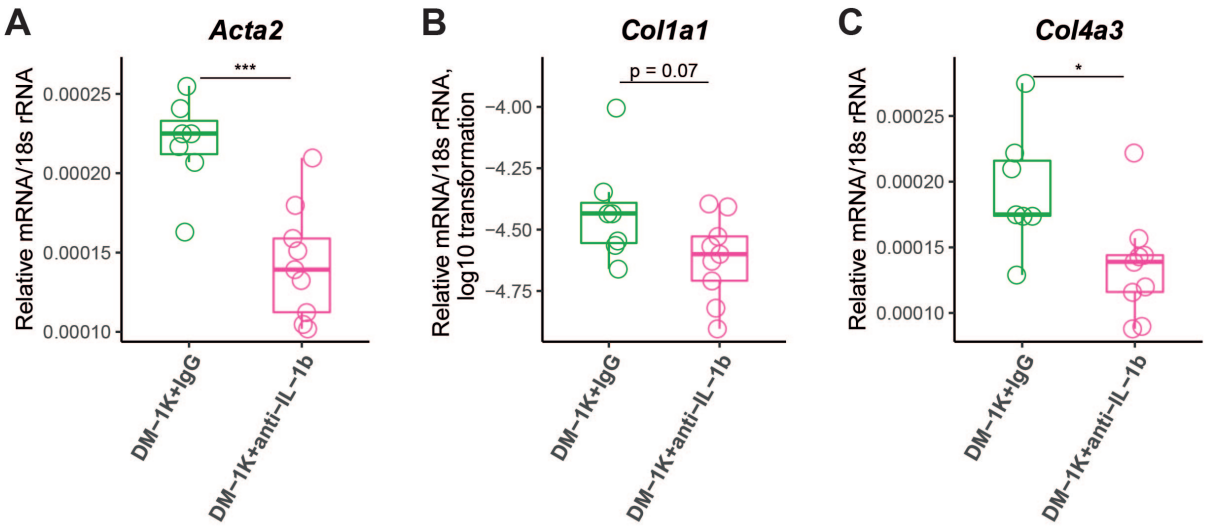

Figure 5.15: Effect of anti-IL-1β antibody on kidney fibrosis marker gene expressions in *db/db* mice. Kidney was analyzed for *Acta2*, *Col1a1*, and *Col4a3* mRNA expression by real-time quantitative PCR. *Acta2* encodes αSMA. **p* <0.05; ****p* <0.001.

5.2.8 Effects of interleukin-1β blockade on kidney inflammation

Kidney inflammation is a key event in DKD. In DKD, macrophages infiltrate into glomerular compartment and promote local inflammation. To visualize infiltrated macrophages in glomerular compartment, Mac-2 (galectin-3), a marker for macrophages, was stained and quantified. As demonstrated in Figure 5.16, nephron loss in combination with diabetes in DM-1K+IgG group (3.14 ± 0.40) induced a significantly greater number of infiltrated macrophages compared to DM-2K (1.53 ± 0.21), WT-1K (1.33 ± 0.35), and WT-2K (0.63 ± 0.18). Also, anti-IL-1β-treated mice had less Mac-2 positive cells compared to IgG control (1.74 ± 0.20 vs. 1.53 ± 0.21, $p = 0.003$).

To further analyze the inflammation levels, we performed RT-qPCR to examine the mRNA expression levels of inflammatory genes. As shown in Figure 5.17, neither *Il1b*-related genes, nor cytokine genes such as *Il6* and *Tgfb*, nor chemokine genes such as *Ccl2*, *Cx3cl1* and *Ccl5*, was significant between anti-IL-1β-treated mice and IgG-treated mice.

Taken together, anti-IL-1β IgG treatment reduces the number of infiltrating macrophages in diabetic mice compared with control group.

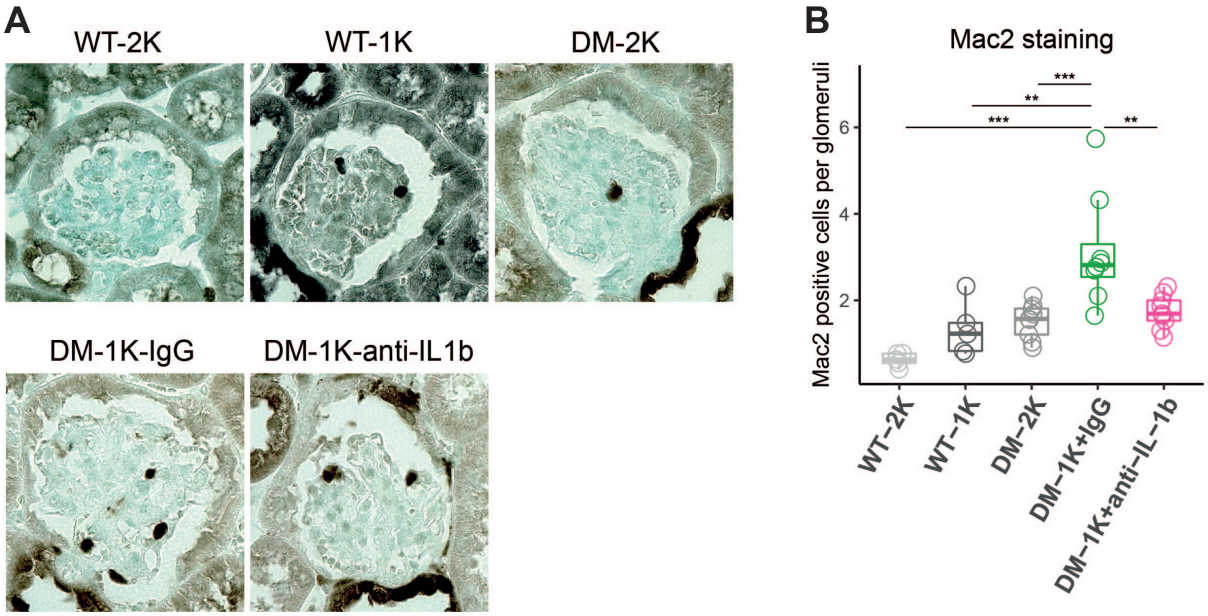

Figure 5.16: Macrophage staining in mouse glomeruli. A, Mac-2 staining. Kidney sections were stained for Mac-2. Representative images of glomerulus from each group. Original magnification 400x. B, Quantification of Mac-2 positive cells. Each dot represents the mean of Mac-2 positive cells from 15-25 cortex glomeruli per kidney section. $^{**}p$ <0.01; $^{***}p$ <0.001.

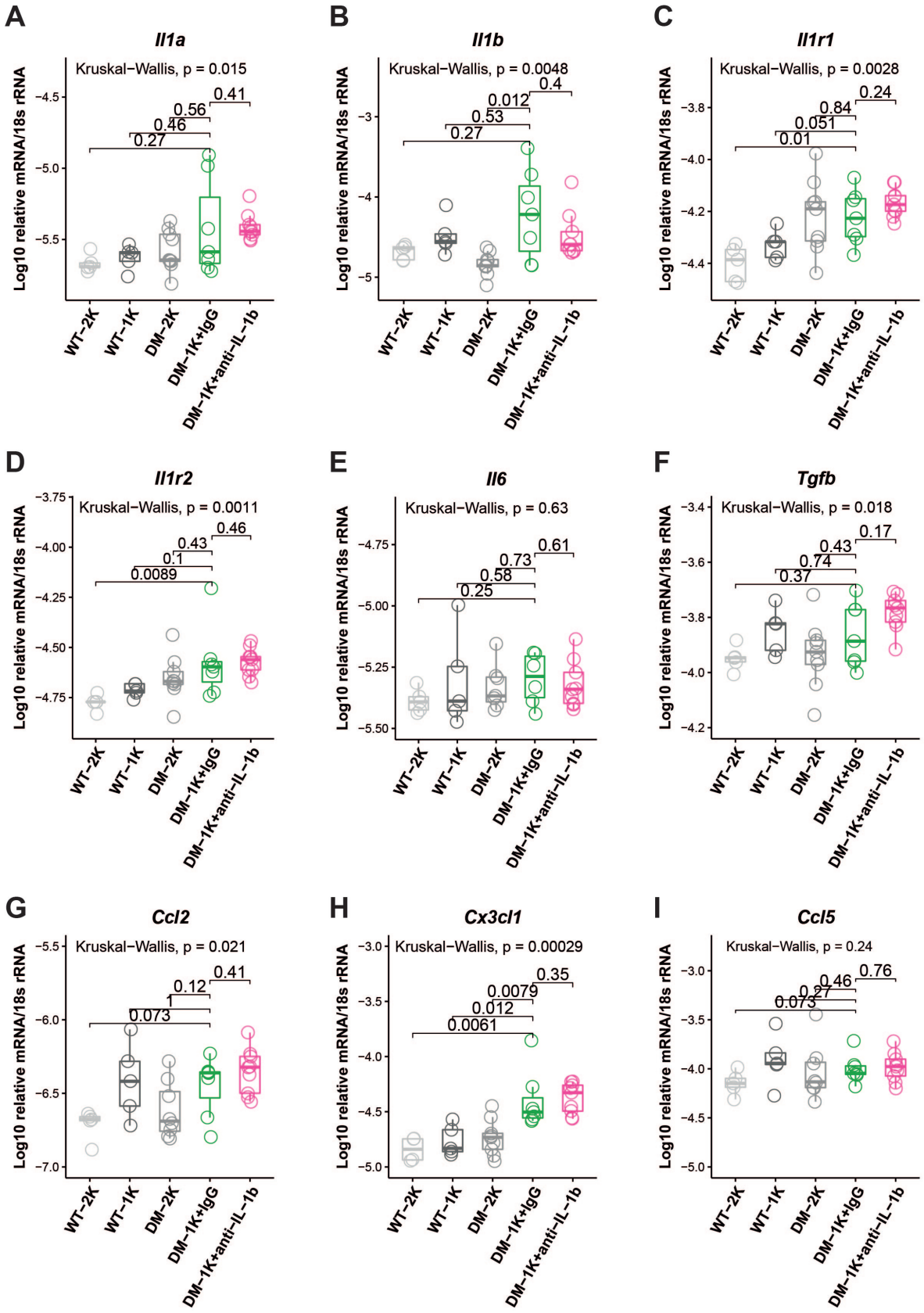

Figure 5.17: Mouse kidney inflammatory gene expressions. A-D, *Ilb*-related mRNA expression. E-F, Cytokine *Il6* and *Tgfb* expression. G-I, Chemokine *Ccl2*, *Cx3cl1*, and *Ccr5* expression. Data represent relative gene expression after $\log_{10}$ transformation from each group. N.S., not significant; **p* <0.05; ***p* < 0.01.

6 Discussion

We had hypothesized that:

1. An oxalate-rich diet could induce crystal deposition and GFR loss in *db/db* mice.
2. IL-1β blockade by a specific anti-IL-1β IgG would have renoprotective effects in a mouse model of DKD.

Testing these hypotheses experimentally gave the following results:

1. Oxalate-rich diet did not induce GFR deterioration on C57BL/Ks *db/db* mice because oxalate-rich diet did not lead to significant nephrocalcinosis.
2. Kidney IL-1β expression is induced in DKD. Specific blockade using an anti-IL-1β IgG did not alter glucose homeostasis. IL-1 blockade by anti-IL-1β IgG had statistically significant renoprotective effects on GFR, podocyte loss, fibrosis, and macrophage infiltration with a minor to moderate effect size but not on albuminuria or BUN levels.

6.1 Oxalate-rich diet does not induce crystal formation and GFR loss in *db/db* mice

Oxalate-rich food did not induce GFR loss and crystal deposition in kidneys of *db/db* C57BL/Ks mice, as reported from C57BL/6N mice [76, 77, 78, 79, 80, 81, 82]. One possible explanation is that this model is strain dependent. Marschner J.A., *et al* found that oxalate-rich diet-induced nephrocalcinosis and CKD was restricted to certain gender of certain mouse strains. For instance, both genders of C57BL/6N and male Balb/c mice were prone to develop mass crystal deposition in kidney upon oxalate-rich diet, while female Balb/c mice and both genders of CD-1 and 129SV mice was resistant to crystal deposition [82]. As mention before, C57BL/Ks carries ≈84% C57BL/6J-like and ≈14% DBA/2J-like alleles [70]. Another possible explanation is the osmotic diuresis in hyperglycemic *db/db* mice with the consequence of urine dilution, which might also lead to reduced crystal deposition in kidney. We decided not to perform a deeper analysis into the underlying causes, as obviously this approach turned out to be not useful to replace uninephrectomy to accelerate DKD in *db/db* C57BL/Ks mice.

6.2 Immune cells are the main source of interleukin-1β in diabetic kidneys

Previous studies have shown increased IL-1β gene expression by microarray [38] and increased IL-1β protein expression by immunohistology [118] in kidney biopsies from patients with diabetes. By analyzing the micro-dissected glomeruli and interstitium tissues from

diabetic patients, we found *IL1B* expression levels increased in both tissue compartments compared to healthy humans, which supports the previous finding that in human DKD IL-1β was significantly induced [38, 118]. As with human kidney, an enhanced IL-1β expression in both gene and protein levels was found in the *db/db* mouse model of DKD, which is also consistent with results reported by others using the same or other mouse models of DKD [38, 111, 118].

The cellular origin of IL-1β expression in DKD is not fully clear [115]. Even though immune cells are well-known to express IL-1β [88, 83, 90], there are debates on whether also kidney parenchymal cells can express IL-1β [87]. *In vitro* studies have shown IL-1β protein expression in response to various stimuli in several kidney cells, e.g. a human podocytes cell line [38], primary mouse podocytes [38], primary mouse glomerular endothelial cells [38], primary mouse collecting duct epithelial cells [112], and primary mouse proximal tubular cells (cell line [113], primary [114]). However, other studies performed on podocytes [143], pericytes [144], glomerular endothelial cells [144], tubular epithelial cells [145] did not detect production of mature IL-1β upon exposure to inflammasome-activating stimuli. According to a recent single-nucleus RNA-sequencing dataset of human DKD, *IL1B* expression was found in 1-2% of leukocytes, ≈0.5% of mesangial cells, <0.5% of epithelial cells in proximal convoluted tubule, ≈0.5% of epithelial cells in distal convoluted tubule, <0.5% of endothelial cells, and <0.5% of type A intercalated cells. Almost no podocytes tested expressed *IL1B*. Furthermore, kidney parenchymal cells expressed *IL1B* in a lesser extent than leukocytes [31]. In our immunostaining results, IL-1β was mainly expressed in infiltrated cells in both glomeruli and interstitium, most probably mononuclear phagocytes [146, 26], and occasionally expressed in tubular epithelial cells. Our results do not support endothelial cells or podocytes as IL-1β-expressing cells.

IL-1β expression can derive from inflammasome-dependent and -independent pathways [94]. Of various inflammasomes, NLRP3-inflammasome is the most characterized one [115]. We found NLRP3 was highly and diffusely expressed in tubular epithelial cells in human DKD. To a lesser extent, NLRP3 was expressed in infiltrated cells in interstitium, in glomerular parietal epithelial cells, and in glomerular cells, especially those closed to vascular pole. As infiltrated cells expressed both NLRP3 and IL-1β, one presumption could be that NLRP3-inflammasome dependent IL-1β is activated in infiltrated cells. However, a co-staining of IL-1β and NLRP3, or inflammasome-associated speck-like structure is needed to confirm such presumption [115]. Another notable observation from the human immunohistology is that, the abundance of NLRP3 and meanwhile absent of IL-1β expression in non-myeloid cells, e.g. most tubular epithelial cells and glomerular cells, indicate an IL-1β-independent role of NLRP3 in human DKD. Consisting with this observation, a previous study showed tubular cells did express NLRP3, ASC, and pro-caspase 1 but did not release IL-1β after canonical inflammasome stimuli. Instead, NLRP3 assembled a speck-like structure together with ASC

and caspase 8 in mitochondria during TNFα/cycloheximide induced apoptosis in proximal tubular epithelial cells [145]. Another study also indicated IL-1-independent role of NLRP3 in nephrocalcinosis-related CKD, including development of pro-inflammatory and -fibrotic phenotype in macrophages *in vivo*, and TGFβ-dependent fibrosis and proliferation in primary murine fibroblasts *in vitro* [78]. Considering the diffuse NLRP3 expression in kidney from diabetic patients, as well as kidney protective phenotypes from diabetic *Nlrp3*-/- mice [38], more research on the IL-1β-independent role of NLRP3 in DKD is needed.

6.3 Interleukin-1β blockade has moderate renoprotective effects

Treatment with the anti-IL-1β antibody preserved higher GFR in uninephrectomized *db/db* mice, indicating IL-1β is involved in kidney function decline in diabetes. The underlying mechanism might involve anti-IL-1β antibody blocking IL-1β-related kidney inflammation, fibrosis, and podocyte loss.

Firstly, the levels of various inflammation markers were reduced in diabetic kidneys treated with anti-IL-1β antibody such as macrophage inside glomeruli. Macrophage infiltration is a hallmark of inflammation in DKD. Fiona C, *et al.* characterized infiltrated macrophages in *db/+*, *db/db* mice at the age of 2 months, and *db/db* mice at the age of 8 months. They found glomerular macrophage infiltration correlated with albuminuria, glomerular hypertrophy, glomerular collagen IV accumulation. The number of infiltrated cells correlated with kidney gene expression of chemokines, e.g. *Ccl2*, *Spp1*, *Mif*, and *Csf1* [147]. Transcription levels of *Ccl2*, *Ccl5*, and *Cx3cl1* were measured in my study due to they are considered as the most important chemokines attracting macrophages in diabetic kidney disease [27, 148]. However, we did not find anti-IL-1β treatment reduced these gene expression in kidneys, indicating less infiltration of macrophage by anti-IL-1β antibody could be chemokine-independent. Non-kidney-related mechanism might be involved, e.g. in bone marrows, IL-1β is a mediator of promoting hematopoiesis through mechanisms such as increasing production of hematopoietic growth factors and regulating proliferation of primitive hematopoietic progenitor cells [149].

Second, anti-IL-1β antibody treatment reduced fibrosis. In IL-1β immunostaining of diabetic patients, IL-1β staining intensity correlated with kidney interstitial fibrosis and tubular atrophy, indicating IL-1β is associated with fibrosis. Indeed, a recent study revealed a mechanism by which IL-1β drives kidney fibrosis [43]. The authors found taht stimulation of IL-1β in kidney stromal cells resulted in an interleukin 1 receptor associated kinase 4-dependent activation of MYC, which is a transcription factor regulates genes of glycolysis, proliferation, and fibrosis. Inhibition of IL-1β downstream signaling, interleukin 1 receptor associated kinase 4 and MYC, resulted in less fibrosis in mice and in kidney organoids *in vitro*

[43]. Consistent with this study, we found reduced expression levels of fibrosis genes, e.g. *Acta2*, *Col1a1*, *Col4a1* in diabetic mice receiving anti-IL-1β treatment, which was likely the result from blocking IL-1β-induced fibrosis. However, we did not find difference in αSMA staining or collagen staining between control and treatment group, one possible explanation could be the overall fibrosis level was relatively low in this model. Whether IL-1β blockade can reduce overt kidney fibrosis needs further study in models with more advanced diabetic kidney disease, like eNOS$^{-/-}$ *db/db* mice.

Third, inhibition of IL-1β had a protective effect on podocyte loss. Mice receiving anti-IL-1β IgG treatment exhibited less podocyte loss as indicated by two independent immunostainings and higher gene expression levels of podocyte markers. IL-1R1 and IL1RAP are ubiquitous expressed on almost all cells and the latter is necessary for IL-1β signaling [87, 116]. Interestingly, according to single-nucleus RNA-sequencing dataset of human DKD [31], ≈40% and 20-30% glomerular parietal epithelial cells expressed *IL1R3*, in contrast only less than 10% endothelial cells and mesangial cells expressed *IL1R3*, suggesting that podocytes and glomerular parietal epithelial cells might be the major targets in glomeruli in response to IL-1β. The benefits of anti-IL-1β antibodies on podocyte loss might be associated with IL-1β neutralization and thus less IL-1β-IL-1R1-IL-1R3 complex formation on podocytes. But in our study, a higher number of podocyte in anti-IL-1β treated mice did not lead to a lower albuminuria level. The number of podocyte per glomerulus is one of the various structural parameters in DKD [150]. The correlation between glomerular structure alterations and function changes have been investigated in patients with T1D and t2d [151, 150, 152]. Meyer T.W., *et al.* analyzed biopsies from 16 American Indian with T2D and found that the podocyte number was tightly associated with albuminuria progression [150]. On the contrary, another study analyzed the correlation between kidney functional parameters (GFR and albuminuria) and kidney structural alterations in 48 diabetic American Indian patients with GFR > 90 mL/min/1.73m². These patients were followed up for around 9 years on average. The authors found that albuminuria progression was positively correlated with mesangial expansion, glomerular volume, GBM thickening, surface density of GBM, and glomerulosclerosis but not correlate with podocyte density [152]. Above studies suggested that podocyte number measured by two-dimensional method in present study could only partially explain albuminuria. Other structural alterations, like glomerular collagen deposition, αSMA accumulation, and glomerular size, which were similar between control group and anti-IL-1β antibody treated group, might also be associated with albuminuria progress and probably lead to a similar albuminuria level between these two groups.

Shahzad K, *et al.* also tested IL-1β blockade in DKD models. The authors treated *db/db* mice at the age of 8 weeks and 12 weeks with anakinra. The treatment lasted for 12 weeks and 8 weeks, respectively. The authors found that anakinra normalized albuminuria and mesangial expansion in above two study designs [38]. In present study, we did not find as

potent protective effects on albuminuria and mesangial expansion from anti-IL-1β in diabetic mice. The possible explanations are as follows. First, at the treatment initiation severity levels of DKD were different in these two studies. In study from Shahzad K. *et al.*, treatment started in 8- and 12-week-old *db/db* mice, whereas in current study treatment started in uninephrectomized *db/db* mice at the age of 18 weeks. Second, treatment lasted 12 and 8 weeks in study from Shahzad K, *et al.*. In present study it lasted 8 weeks. Third, anakinra exhibited kidney protection, indication the effects could be IL-1β- or/and IL-1α- dependent, while in our study, protection effects was only IL-1β specific. Nevertheless, it indicates that IL-1β contributes to kidney structural and functional changes since the early phase of DKD [38]. Thus, a preemptive and extended treatment might be needed to achieve better kidney outcomes.

6.4 Interleukin-1β blockade does not alter glucose homeostasis

From the previous literature, a glucose-lowering effect of IL-1β blockade was uncertain in patients with T2D, as shown in Table 1.3. For instance, treatment with IL-1β/IL-1R blockade induced a decrease [121, 122, 131], or an increase [127], or no change [124, 123] on HbA1c in patients with T2D. Similarly, animal models of diabetes or obesity also found inconsistent results. For instance, IL-1β/IL-1R blockade induced a decrease [153, 154, 155, 156, 157], or no change [158, 159] in blood glucose levels.

Many studies have unveiled how IL-1β affects glucose homeostasis. On one hand, IL-1β might be a mediator inducing β cell impairment and reducing insulin secretion [160, 161]. Boeni-Schnetzler M, *et al.* found that IL-1β can induce β cell dysfunction via the E2F1-Kir6.2 pathway. In mouse isolated islets, IL-1β suppressed the expression of Kir6.2, which is a potassium channel and regulates insulin secretion in β cells. The IL-1β-dependent downregulation of Kir6.2 was partially through E2F1, a transcription factor not only regulates cell cycle but also Kir6.2 [162]. On the other hand, IL-1β can induce insulin release by pancreatic islets *ex vivo* [163]. It can also increase serum GLP1 levels, resulting in hyperinsulinemia and hypoglycemia [164]. Similarly, a recent study found that macrophage-derived IL-1β is a physiological mediator in postprandium-induced insulin secretion [165]. In this study Dror E, *et al.* found that postprandial hyperglycemia can induce primed-macrophages releasing IL-1β. This activation and secretion of IL-1β was NLRP3-dependent. The postprandium-related IL-1β promoted β cells to secrete insulin. In turn, secreted insulin acted on macrophages via insulin recetpors and induced glucose uptake, IL-1β secretion, and ROS production. In contrast, *Il1b* deficient mice had impaired insulin secretion after feeding [165]. This study revealed a physiological role of IL-1β in glucose homeostasis that it acts as a mediator to mobilize glucose disposal after meals and

specifically fuel macrophages [166]. Together, IL-1β can have opposite roles on regulating glucose homeostasis.

In the present study, IL-1β blockade did not affect blood glucose levels. Further measurements could provide mechanistic insights, such as glucose tolerance test or insulin secretion but our animal clearance did not include a permission for these kinds of analyses.

6.5 Limitations

There are several limitations in the present study. Firstly, our *db/db* model with uninephrectomy still did not display advanced CKD. Though diabetic mice with uninephrectomy had ≈50 times higher albuminuria level compared to healthy wild type controls and ≈40% less GFR compared to their peak values. When the treatment finished, diabetic mice with uninephrectomy still had comparable GFR level compared to healthy controls. Further, fibrosis and glomerulosclerosis were not evident at the study end, which caused difficulty to evaluate the efficacy of anti-IL-1β on fibrosis and sclerosis. Thus, this model could only represent the disease scenario before CKD G3a. Second, our group size was relatively small, resulting in less power to detect the difference between each group, especially when comparing parameters with big variations, such as albuminuria. Third, the IL-1β biological activity upon anti-IL-1β antibody injection was not determined. We were not able to detect the pharmacokinetic profile of anti-IL-1β IgG in circulation or in kidney, which could be measured by mass spectrometry approaches [167]. Fourth, spot urine, but not 24-hour urine collected by metabolic cages, was used. Even though it was calibrated by creatinine levels, bias may still exist. Fifth, we measured podocyte loss basing on two-dimension images, which is a suboptimal approach [168]. Sixth, we lacked oxalate measurement in urine or serum to explore the causes of no crystal deposition in kidney.

7 Summary

An animal model with overt DKD is needed for preclinical study. Uninephrectomy is a common tool to accelerate kidney impairment but it has shortcomings such as lethality and kidney infection. Given that oxalate-rich diet is a convenient method to generate progressive nephrocalcinosis, tubular atrophy, and CKD in C56BL6 mice, we want to explore the possibility of using oxalate-rich diet as a substitutive and non-surgical approach to accelerate kidney impairment in *db/db*. We fed *db/db* mice of 14 weeks old with oxalate-rich diet or control diet for 30 days. We measured GFR every 10 days and analysed the crystal deposition in kidney after 30 days. We found that oxalate rich diet did not induce GFR loss and oxalate crystal deposition in kidney compared to mice with control diet.

Inflammation is one of the center mechanisms leading to DKD. Infiltrated immune cells as well as renal resident cells release various cytokines which contribute to kidney function loss and structural alterations. Of the cytokines, IL-1β is a key mediator in amplifying inflammation, such as upregulating chemokines and other cytokines. IL-1β also contributes to kidney fibrosis. Thus IL-1β serves as a potential target for DKD.

Previous studies have shown that NLRP3-dependent IL-1β from non-myeloid cell contribute to initiation and progression of DKD in diabetic mice, even though other studies suggested that non-myeloid cells may lack the ability to synthesis IL-1β. Our first aim was to investigate IL-1β expression and possible cellular location in kidney. We observed IL-1β expression was mildly increased in kidney biopsies from patients with diabetes at protein and mRNA level, as indicated by immunostaining and microarray, respectively. In a uninephrectomized *db/db* mice, IL-1β gene expression level was also increased. Furthermore, human biopsy immunostainings demonstrated that IL-1β was mainly located in infiltrated immune cells. Therefore, IL-1β expression was induced in DKD and was mainly expressed by immune cells.

Since we observed IL-1β expression is increased in DKD, we hypothesized that targeting IL-1β has a renal protective effect on DKD in animal model of DKD. To test this hypothesis, we treated 18-week-old *db/db* mice undergoing uninephrectomy at the age of 8 weeks with anti-IL-1β IgG antibody or control IgG for 8 weeks. Mice treated with anti-IL-1β IgG preserved higher glomerular filtration rate but comparable albuminuria level to those treated with control IgG. On glomerular structural changes, anti-IL-1β antibody treatment did not affect glomerular tuft and Bowman's capsule size, nor collagen deposition in glomeruli. However, anti-IL-1β showed higher podocyte account and higher expression levels of podocyte marker genes. IL-1β blockade also reduced infiltrated macrophages in glomeruli. On fibrosis, IL-1β blockade did not reduced alpha smooth muscle actin accumulation, but reduced fibrosis gene expression, such as *Acta2* and *Col4a3*.

In conclusion, (i) oxalate-rich diet did not induce massive oxalate crystal deposition in

kidney nor GFR loss, thus is not a suitable method to generate overt DKD in *db/db* model. (ii) kidney IL-1β expression mildly increased in human diabetes, and mainly originated from immune cells. Targeting IL-1β by antibody generated a moderate effect on glomerular filtration rate decline, podocyte loss, and renal inflammation in type 2 diabetic mice with CKD. Whether these findings can translate into better outcomes also in human DKD remains to be determined.

8 Zusammenfassung

In der präklinischen Forschung besteht der nicht erfüllte Bedarf nach einem Tiermodell für schwere diabetische Nephropathie. Die Uninephrektomie ist ein gebräuchliches Mittel zur Beschleunigung der Nierenschädigung, hat jedoch Mängel wie Letalität und Niereninfektionen. Angesichts der Tatsache, dass eine oxalatreiche Ernährung eine geeignete Methode ist, um progressive Nephrokalzinose, tubuläre Atrophie und chronische Nierenerkrankung bei C56BL6-Mäusen zu induzieren, wollen wir die Möglichkeit untersuchen, oxalatreiche Ernährung als substitutiven und nicht-chirurgischen Ansatz zur Beschleunigung der Nierenschädigung im db/db-Modell einzusetzen. Db/db-Mäuse im Alter von 14 Wochen wurden 30 Tage lang mit oxalatreicher Nahrung bzw. einer Kontrolldiät gefüttert. Die glomeruläre Filtrationsrate wurde alle 10 Tage, Kristallablagerungen in der Niere nach 30 Tagen bestimmt. Die Ergebnisse zeigten, dass oxalatreiches Futter im Vergleich zur Kontrolldiät keinen GFR-Verlust und keine Oxalatkristallablagerung in der Niere induzierte.

Die Entzündung ist einer der zentralen Mechanismen, die zu einer diabetischen Nephropathie führen. Infiltrierte Immunzellen sowie nierenresidente Zellen setzen verschiedene Zytokine frei, die zum Verlust der Nierenfunktion und zu strukturellen Veränderungen beitragen. Unter den Zytokinen ist IL-1b ein Schlüsselmediator bei der Verstärkung der Entzündung, wie z.B. durch die Hochregulierung von Chemokinen und anderen Zytokinen. IL-1b trägt auch zur Nierenfibrose bei. Somit stellt IL-1b ein potentielles therapeutisches Ziel bei diabetischer Nephropathie dar.

Vorangegangene Studien haben gezeigt, dass NLRP3-abhängiges IL-1b aus nicht-myeloiden Zellen zur Auslösung und zum Fortschreiten einer diabetischen Nephropathie in diabetischen Mäusen beiträgt, obwohl andere Studien darauf hindeuteten, dass nicht-myeloide Zellen möglicherweise nicht die Fähigkeit zur Synthese von IL-1b besitzen. Das erste Ziel der vorliegenden Studie war daher die Untersuchung der IL-1b-Expression und seiner möglichen zellulären Lokalisation in der Niere. Es zeigte sich, dass die IL-1b-Expression in Nierenbiopsien von Patienten mit Diabetes auf Protein- und mRNA-Ebene leicht erhöht war, wie durch Immunfärbung bzw. Microarray gezeigt werden konnte. In uninephrektomierten db/db-Mäusen war die IL-1b-Genexpression ebenfalls erhöht. Darüber hinaus zeigten Immunfärbungen in menschlichen Biopsien, dass IL-1b hauptsächlich in infiltrierten Immunzellen lokalisiert war. Daraus kann geschlussfolgert werden, dass die IL-1b-Expression bei diabetischer Nephropathie hauptsächlich in Immunzellen induziert wird.

In Anbetracht der Tatsache, dass IL-1b bei der diabetischen Nephropathie erhöht exprimiert ist, sollte nachfolgend die Hypothese überprüft werden, dass die gezielte Inhibierung von IL-1b im Tiermodell der diabetischen Nephropathie einenprotektiven renalen Effekt auf aufweist. Hierzu wurden 18 Wochen alte db/db-Mäuse, die im Alter von 8 Wochen einer Uninephrektomie unterzogen wurden, 8 Wochen lang mit Anti-IL-1b-IgG-Antikörpern bzw. Kontroll-IgG behandelt. Mit Anti-IL-1b-IgG behandelte Mäuse zeigten im Vergleich zu

den Kontroll-IgG behandelten Mäusen eine höhere glomeruläre Filtrationsrate, aber eine vergleichbar ausgeprägte Albuminurie. Im Hinblick auf glomeruläre Strukturveränderungen beeinflusste die Behandlung mit Anti-IL-1b-Antikörpern weder die Größe des glomerulären Kapillarknäuls und der Bowman'schen Kapsel noch die Kollagendeposition in den Glomeruli. Die Behandlung mit Anti-IL-1b-Antikörpern führte jedoch zu einem geringeren Podozyten-Verlust und einer höheren Expressions von Podozyten-Markergenen. Die IL-1b-Blockade reduzierte auch die Zahl infiltrierter Makrophagen in den Glomeruli. Im Hinblick auf fibrotische Veränderungen verringerte die IL-1b-Blockade nicht die Ablagerung von Alpha-Aktin-2 , dafür aber die Expression von Fibrose-Markergenen wie Acta2 und Col4a3.

Zusammenfassend lässt sich festhalten, dass (i) oxalatreiche Ernährung weder eine massive Oxalatkristallablagerung in der Niere noch einen Verlust der glomerulären Filtrationsrate induzierte und somit keine geeignete Methode ist, um eine schwere diabetische Nephropathie im db/db-Modell zu erzeugen. (ii) Die IL-1b-Expression in der Niere war bei Diabetes im Menschen leicht erhöht und stammte hauptsächlich von Immunzellen. Die gezielte Beeinflussung von IL-1b durch Antikörper erzeugte eine moderate Wirkung auf den Rückgang der glomerulären Filtrationsrate, den Podozytenverlust und die Nierenentzündung bei diabetischen Mäusen vom Typ 2 mit chronischer Nephropathie. Ob diese Ergebnisse auch auf die diabetische Nephropathie im Menschen übertragen werden können, muss erst noch untersucht werden.

9 List of tables

10 List of figures

11 Abbreviation

BKS C57BL/Ks.

BUN blood urea nitrogen.

CKD chronic kidney disease.

CT cycle threshold.

DAMPs danger-associated molecular patterns.

DKD diabetic kidney disease.

DM diabetes mellitus.

DM-1K+anti-IL-1β DM-1K+anti-IL-1β.

DM-1K+IgG DM-1K+IgG.

FITC fluorescein isothiocyanate.

GBM glomerular basement membrane.

GFR glomerular filtration rate.

GLP1 glucagon-like peptide 1.

HbA1c hemoglobin A1C.

hsCRP high-sensitivity C-reaction protein.

IFTA interstitial fibrosis and tubular atrophy.

IL-1R1 IL-1 receptor type I.

IL-1R2 IL-1 receptor type II.

IL-1Ra interleukin-1 receptor antagonist.

IL-1α interleukin-1α.

IL-1β interleukin-1β.

IL1RAP IL-1 receptor accessory protein.

KFRT kidney failure with replacement therapy.

KRT kidney replacement treatment.

LPS lipopolysaccharide.

NF-κB cytokine-dependent nuclear factor kappa-light-chain-enhancer of activated B cells.

NLRP3 nucleotide-binding domain and leucine-rich repeat pyrin containing protein-3.

PAMPs pathogen-associated molecular patterns.

PBMCs peripheral blood mononuclear cells.

PRRs pattern recognition receptors.

ROS reactive oxygen species.

SD standard deviation.

SGLT sodium-glucose cotransporter.

SGLT2i sodium-glucose cotransporter 2 inhibitors.

STZ streptozotocin.

T1D type 1 diabetes.

T2D type 2 diabetes.

TIR Toll-IL-1 resistance.

TLR Toll-like receptor.

TNFα tumor necrosis factor α.

UACR urinary albumin-creatinine ratio.

Unx uninephrectomy.

WT-1 Wilms Tumor-1.

12 Reference

[1] *Summary of Recommendation Statements*. [Online; accessed 27. Jun. 2019]. Jan. 2013. DOI: 10.1038/kisup.2012.77.

[2] Andrew S. Levey, Kai-Uwe Eckardt, Yusuke Tsukamoto, Adeera Levin, Josef Coresh, Jerome Rossert, Dick D. E. Zeeuw, Thomas H. Hostetter, Norbert Lameire, and Garabed Eknoyan. "Definition and classification of chronic kidney disease: A position statement from Kidney Disease: Improving Global Outcomes (KDIGO)". In: *Kidney International* 67.6 (June 2005), pp. 2089–2100. ISSN: 0085-2538. DOI: 10.1111/j.1523-1755.2005.00365.x.

[3] Andrew S. Levey, Kai-Uwe Eckardt, Nijsje M. Dorman, Stacy L. Christiansen, Ewout J. Hoorn, Julie R. Ingelfinger, Lesley A. Inker, Adeera Levin, Rajnish Mehrotra, Paul M. Palevsky, et al. "Nomenclature for kidney function and disease: report of a Kidney Disease: Improving Global Outcomes (KDIGO) Consensus Conference". In: *Kidney International* 0.0 (Mar. 2020). ISSN: 0085-2538. DOI: 10.1016/j.kint.2020.02.010.

[4] Kitty J. Jager, Csaba Kovesdy, Robyn Langham, Mark Rosenberg, Vivekanand Jha, and Carmine Zoccali. "A single number for advocacy and communication—worldwide more than 850 million individuals have kidney diseases". In: *Kidney International* 96.5 (Nov. 2019), pp. 1048–1050. ISSN: 0085-2538. DOI: 10.1016/j.kint.2019.07.012.

[5] Thaminda Liyanage et al. "Worldwide access to treatment for end-stage kidney disease: a systematic review". In: *Lancet* 385.9981 (May 2015), pp. 1975–1982. ISSN: 1474-547X. DOI: 10.1016/S0140-6736(14)61601-9.

[6] Boris Bikbov, Caroline A. Purcell, Andrew S. Levey, Mari Smith, Amir Abdoli, Molla Abebe, Oladimeji M. Adebayo, Mohsen Afarideh, Sanjay Kumar Agarwal, Marcela Agudelo-Botero, et al. "Global, regional, and national burden of chronic kidney disease, 1990–2017: a systematic analysis for the Global Burden of Disease Study 2017". In: *Lancet* 395.10225 (Feb. 2020), pp. 709–733. ISSN: 0140-6736. DOI: 10.1016/S0140-6736(20)30045-3.

[7] Mark J. Sarnak, Andrew S. Levey, Anton C. Schoolwerth, Josef Coresh, Bruce Culleton, L. Lee Hamm, Peter A. McCullough, Bertram L. Kasiske, Ellie Kelepouris, Michael J. Klag, et al. "Kidney Disease as a Risk Factor for Development of Cardiovascular Disease: A Statement From the American Heart Association Councils on Kidney in Cardiovascular Disease, High Blood Pressure Research, Clinical Cardiology, and Epidemiology and Prevention". In: *Hypertension* 42.5 (Nov. 2003), pp. 1050–1065. ISSN: 1524-4563. DOI: 10.1161/01.HYP.0000102971.85504.7c.

[8] J. L. Zelmer. "The economic burden of end-stage renal disease in Canada". In: *Kidney International* 72.9 (Nov. 2007), pp. 1122–1129. ISSN: 0085-2538. DOI: 10.1038/sj.ki.5002459.

[9] Pouya Saeedi, Inga Petersohn, Paraskevi Salpea, Belma Malanda, Suvi Karuranga, Nigel Unwin, Stephen Colagiuri, Leonor Guariguata, Ayesha A. Motala, Katherine Ogurtsova, et al. “Global and regional diabetes prevalence estimates for 2019 and projections for 2030 and 2045: Results from the International Diabetes Federation Diabetes Atlas, 9th edition”. In: *Diabetes Research and Clinical Practice* 157 (Nov. 2019). ISSN: 0168-8227. DOI: 10.1016/j.diabres.2019.107843.

[10] United States Renal Data System. “2018 USRDS annual data report: Epidemiology of kidney disease in the United States. National Institutes of Health, National Institute of Diabetes and Digestive and Kidney Diseases, Bethesda, MD”. In: (2018).

[11] American Diabetes Association. “Diagnosis and Classification of Diabetes Mellitus”. In: *Diabetes Care* 37.Supplement 1 (Jan. 2014), S81–S90. ISSN: 0149-5992. DOI: 10.2337/dc14-S081.

[12] American Diabetes Association. “2. Classification and Diagnosis of Diabetes: Standards of Medical Care in Diabetes—2018”. In: *Diabetes Care* 41.Supplement 1 (Jan. 2018), S13–S27. ISSN: 0149-5992. DOI: 10.2337/dc18-S002.

[13] Hans-Joachim Anders, Tobias B. Huber, Berend Isermann, and Mario Schiffer. “CKD in diabetes: diabetic kidney disease versus nondiabetic kidney disease”. In: *Nat. Rev. Nephrol.* 14.6 (Apr. 2018), pp. 361–377. ISSN: 1759-507X. DOI: 10.1038/s41581-018-0001-y.

[14] C. E. Mogensen, C. K. Christensen, and E. Vittinghus. “The Stages in Diabetic Renal Disease: With Emphasis on the Stage of Incipient Diabetic Nephropathy”. In: *Diabetes* 32.Supplement 2 (June 1983), pp. 64–78. ISSN: 0012-1797. DOI: 10.2337/diab.32.2.S64.

[15] Merlin C. Thomas, Andrew J. Weekes, Olivia J. Broadley, Mark E. Cooper, and Tim H. Mathew. “The burden of chronic kidney disease in Australian patients with type 2 diabetes (the NEFRON study)”. In: *Medical Journal of Australia* 185.3 (Aug. 2006), pp. 140–144. DOI: 10.5694/j.1326-5377.2006.tb00499.x.

[16] Esteban Porrini, Piero Ruggenenti, Carl Erik Mogensen, Drazenka Pongrac Barlovic, Manuel Praga, Josep M. Cruzado, Radovan Hojs, Manuela Abbate, and Aiko P. J. de Vries. “Non-proteinuric pathways in loss of renal function in patients with type 2 diabetes”. In: *Lancet Diabetes Endocrinol.* 3.5 (May 2015), pp. 382–391. ISSN: 2213-8587. DOI: 10.1016/S2213-8587(15)00094-7.

[17] Lennart Tonneijck, Marcel H. A. Muskiet, Mark M. Smits, Erik J. van Bommel, Hiddo J. L. Heerspink, Danil H. van Raalte, and Jaap A. Joles. “Glomerular Hyperfiltration in Diabetes: Mechanisms, Clinical Significance, and Treatment”. In: *JASN* 28.4 (Apr. 2017), pp. 1023–1039. ISSN: 1046-6673. DOI: 10.1681/ASN.2016060666.

[18] Julie R. Ingelfinger. “Nephron Protection in Diabetic Kidney Disease”. In: *N. Engl. J. Med.* (Nov. 2016), pp. 2096–2098. ISSN: 1533-4406. DOI: 10.1056/NEJMcibr1608564.

[19] Radica Z. Alicic, Emily J. Johnson, and Katherine R. Tuttle. “SGLT2 Inhibition for the Prevention and Treatment of Diabetic Kidney Disease: A Review”. In: *American Journal of Kidney Diseases* 72.2 (Aug. 2018), pp. 267–277. ISSN: 0272-6386. DOI: 10.1053/j.ajkd.2018.03.022.

[20] Radica Z. Alicic, Michele T. Rooney, and Katherine R. Tuttle. “Diabetic Kidney Disease: Challenges, Progress, and Possibilities”. In: *CJASN* (May 2017). ISSN: 1555-9041. DOI: 10.2215/CJN.11491116.

[21] Sara Conti, Norberto Perico, Rubina Novelli, Camillo Carrara, Ariela Benigni, and Giuseppe Remuzzi. “Early and late scanning electron microscopy findings in diabetic kidney disease”. In: *Sci. Rep.* 8.4909 (Mar. 2018), pp. 1–14. ISSN: 2045-2322. DOI: 10.1038/s41598-018-23244-2.

[22] Thijs W. Cohen Tervaert et al. “Pathologic Classification of Diabetic Nephropathy”. In: *JASN* 21.4 (Apr. 2010), pp. 556–563. ISSN: 1046-6673. DOI: 10.1681/ASN.2010010010.

[23] Ying Qian, Eva Feldman, Subramanian Pennathur, Matthias Kretzler, and Frank C. Brosius. “From Fibrosis to Sclerosis: Mechanisms of Glomerulosclerosis in Diabetic Nephropathy”. In: *Diabetes* 57.6 (June 2008), pp. 1439–1445. ISSN: 0012-1797. DOI: 10.2337/db08-0061.

[24] Radica Z. Alicic, Michele T. Rooney, and Katherine R. Tuttle. “Diabetic Kidney Disease: Challenges, Progress, and Possibilities”. In: *CJASN* 12.12 (Dec. 2017), pp. 2032–2045. ISSN: 1555-9041. DOI: 10.2215/CJN.11491116.

[25] *IDF Diabetes Atlas 9th edition 2019*. [Online; accessed 29. Jan. 2020]. Jan. 2020. URL: https://www.diabetesatlas.org/en.

[26] Raimund Pichler, Maryam Afkarian, Brad P. Dieter, and Katherine R. Tuttle. “Immunity and inflammation in diabetic kidney disease: translating mechanisms to biomarkers and treatment targets”. In: *American Journal of Physiology-Renal Physiology* (Apr. 2017). URL: https://www.physiology.org/doi/full/10.1152/ajprenal.00314.2016.

[27] Radica Z. Alicic, Emily J. Johnson, and Katherine R. Tuttle. “Inflammatory Mechanisms as New Biomarkers and Therapeutic Targets for Diabetic Kidney Disease”. In: *Advances in Chronic Kidney Disease* 25.2 (Mar. 2018), pp. 181–191. ISSN: 1548-5595. DOI: 10.1053/j.ackd.2017.12.002.

[28] Juan F. Navarro-Gonzlez, Carmen Mora-Fernndez, Mercedes Muros de Fuentes, and Javier Garca-Prez. “Inflammatory molecules and pathways in the pathogenesis of diabetic nephropathy”. In: *Nat. Rev. Nephrol.* 7.6 (May 2011), pp. 327–340. ISSN: 1759-507X. DOI: 10.1038/nrneph.2011.51.

[29] Julie A. D. Van, James W. Scholey, and Ana Konvalinka. “Insights into Diabetic Kidney Disease Using Urinary Proteomics and Bioinformatics”. In: *JASN* 28.4 (Apr. 2017), pp. 1050–1061. ISSN: 1046-6673. DOI: 10.1681/ASN.2016091018.

[30] Monika A. Niewczas et al. “A signature of circulating inflammatory proteins and development of end-stage renal disease in diabetes”. In: *Nat. Med.* 25.5 (Apr. 2019), pp. 805–813. ISSN: 1546-170X. DOI: 10.1038/s41591-019-0415-5.

[31] Parker C. Wilson, Haojia Wu, Yuhei Kirita, Kohei Uchimura, Nicolas Ledru, Helmut G. Rennke, Paul A. Welling, Sushrut S. Waikar, and Benjamin D. Humphreys. “The single-cell transcriptomic landscape of early human diabetic nephropathy”. In: *Proc. Natl. Acad. Sci. U.S.A.* 116.39 (Sept. 2019), pp. 19619–19625. ISSN: 0027-8424. DOI: 10.1073/pnas.1908706116.

[32] Jun Wada and Hirofumi Makino. “Innate immunity in diabetes and diabetic nephropathy”. In: *Nat. Rev. Nephrol.* 12.1 (Nov. 2015), pp. 13–26. ISSN: 1759-507X. DOI: 10.1038/nrneph.2015.175.

[33] Manjula Darshi, Benjamin Van Espen, and Kumar Sharma. “Metabolomics in Diabetic Kidney Disease: Unraveling the Biochemistry of a Silent Killer”. In: *AJN* 44.2 (2016), pp. 92–103. ISSN: 0250-8095. DOI: 10.1159/000447954.

[34] Avry Chagnac, Boris Zingerman, Benaya Rozen-Zvi, and Michal Herman-Edelstein. “Consequences of Glomerular Hyperfiltration: The Role of Physical Forces in the Pathogenesis of Chronic Kidney Disease in Diabetes and Obesity”. In: *NEF* 143.1 (2019), pp. 38–42. ISSN: 1660-8151. DOI: 10.1159/000499486.

[35] Josephine M. Forbes and David R. Thorburn. “Mitochondrial dysfunction in diabetic kidney disease”. In: *Nat. Rev. Nephrol.* 14.5 (Feb. 2018), pp. 291–312. ISSN: 1759-507X. DOI: 10.1038/nrneph.2018.9.

[36] Johannes Schdel and Peter J. Ratcliffe. “Mechanisms of hypoxia signalling: new implications for nephrology”. In: *Nat. Rev. Nephrol.* 15.10 (Sept. 2019), pp. 641–659. ISSN: 1759-507X. DOI: 10.1038/s41581-019-0182-z.

[37] Diane L. Rosin and Mark D. Okusa. “Dangers Within: DAMP Responses to Damage and Cell Death in Kidney Disease”. In: *JASN* 22.3 (Mar. 2011), pp. 416–425. ISSN: 1046-6673. DOI: 10.1681/ASN.2010040430.

[38] Khurrum Shahzad et al. “Nlrp3-inflammasome activation in non-myeloid-derived cells aggravates diabetic nephropathy”. In: *Kidney Int.* 87.1 (Jan. 2015), pp. 74–84. ISSN: 1523-1755. DOI: 10.1038/ki.2014.271.

[39] Rui Wu, Xuanchen Liu, Jianyong Yin, Huijuan Wu, Xiulei Cai, Niansong Wang, Youcun Qian, and Feng Wang. “IL-6 receptor blockade ameliorates diabetic nephropathy via inhibiting inflammasome in mice”. In: *Metab. Clin. Exp.* 83 (June 2018), pp. 18–24. ISSN: 0026-0495. DOI: 10.1016/j.metabol.2018.01.002.

[40] Keisuke Omote, Tomohito Gohda, Maki Murakoshi, Yu Sasaki, Saiko Kazuno, Tsutomu Fujimura, Masanori Ishizaka, Yuji Sonoda, and Yasuhiko Tomino. “Role of the TNF pathway in the progression of diabetic nephropathy in KK-Ay mice”. In: *American Journal of Physiology-Renal Physiology* (June 2014). URL: https://www.physiology.org/doi/full/10.1152/ajprenal.00509.2013.

[41] Alaa S. Awad, Hanning You, Ting Gao, Timothy K. Cooper, Sergei A. Nedospasov, Jean Vacher, Patrick F. Wilkinson, Francis X. Farrell, and W. Brian Reeves. “Macrophage-derived Tumor Necrosis Factor-α mediates diabetic renal injury”. In: *Kidney international* 88.4 (Oct. 2015), p. 722. DOI: 10.1038/ki.2015.162.

[42] Dongsheng Cheng, Rulian Liang, Baorui Huang, Jiasheng Hou, Jianyong Yin, Ting Zhao, Lu Zhou, Rui Wu, Youcun Qian, and Feng Wang. “Tumor necrosis factor-α blockade ameliorates diabetic nephropathy in rats”. In: *ckj.* (Nov. 2019). ISSN: 2048-8505. DOI: 10.1093/ckj/sfz137.

[43] Dario R. Lemos, Michael McMurdo, Gamze Karaca, Julia Wilflingseder, Irina A. Leaf, Navin Gupta, Tomoya Miyoshi, Koichiro Susa, Bryce G. Johnson, Kirolous Soliman, et al. “Interleukin-1β Activates a MYC-Dependent Metabolic Switch in Kidney Stromal Cells Necessary for Progressive Tubulointerstitial Fibrosis”. In: *JASN* 29.6 (June 2018), pp. 1690–1705. ISSN: 1046-6673. DOI: 10.1681/ASN.2017121283.

[44] Bernard Zinman et al. “Empagliflozin, Cardiovascular Outcomes, and Mortality in Type 2 Diabetes”. In: *N. Engl. J. Med.* 373.22 (Sept. 2015), pp. 2117–2128. ISSN: 1533-4406. DOI: 10.1056/NEJMoa1504720.

[45] Christoph Wanner, Silvio E. Inzucchi, John M. Lachin, David Fitchett, Maximilian von Eynatten, Michaela Mattheus, Odd Erik Johansen, Hans J. Woerle, Uli C. Broedl, and Bernard Zinman. “Empagliflozin and Progression of Kidney Disease in Type 2 Diabetes”. In: *N. Engl. J. Med.* 375.4 (June 2016), pp. 323–334. ISSN: 1533-4406. DOI: 10.1056/NEJMoa1515920.

[46] Bruce Neal, Vlado Perkovic, Kenneth W. Mahaffey, Dick de Zeeuw, Greg Fulcher, Ngozi Erondu, Wayne Shaw, Gordon Law, Mehul Desai, and David R. Matthews. “Canagliflozin and Cardiovascular and Renal Events in Type 2 Diabetes”. In: *N. Engl. J. Med.* 377.7 (June 2017), pp. 644–657. ISSN: 1533-4406. DOI: 10.1056/NEJMoa1611925.

[47] Vlado Perkovic et al. “Canagliflozin and renal outcomes in type 2 diabetes: results from the CANVAS Program randomised clinical trials”. In: *PubMed. comprises. more. than. 30 million. citations. for. biomedical. literature. from. MEDLINE, life. science. journals., and. online. books.* 6.9 (Sept. 2018), pp. 691–704. ISSN: 2213-8595. DOI: 10.1016/S2213-8587(18)30141-4.

[48] Stephen D. Wiviott et al. “Dapagliflozin and Cardiovascular Outcomes in Type 2 Diabetes”. In: *N. Engl. J. Med.* 380.4 (Nov. 2018), pp. 347–357. ISSN: 1533-4406. DOI: 10.1056/NEJMoa1812389.

[49] Carol Pollock, Bergur Stefnsson, Daniel Reyner, Peter Rossing, C. David Sjstrm, David C. Wheeler, Anna Maria Langkilde, and Hiddo J. L. Heerspink. “Albuminuria-lowering effect of dapagliflozin alone and in combination with saxagliptin and effect of dapagliflozin and saxagliptin on glycaemic control in patients with type 2 diabetes and chronic kidney disease (DELIGHT): a randomised, double-blind, placebo-controlled trial”. In: *Lancet Diabetes & Endocrinology* 7.6 (June 2019), pp. 429–441. ISSN: 2213-8587. DOI: 10.1016/S2213-8587(19)30086-5.

[50] Steven P. Marso, Gilbert H. Daniels, Kirstine Brown-Frandsen, Peter Kristensen, Johannes F. E. Mann, Michael A. Nauck, Steven E. Nissen, Stuart Pocock, Neil R. Poulter, Lasse S. Ravn, et al. “Liraglutide and Cardiovascular Outcomes in Type 2 Diabetes”. In: *N. Engl. J. Med.* 375.4 (June 2016), pp. 311–322. ISSN: 1533-4406. DOI: 10.1056/NEJMoa1603827.

[51] Steven P. Marso et al. “Semaglutide and Cardiovascular Outcomes in Patients with Type 2 Diabetes”. In: *N. Engl. J. Med.* 375.19 (Sept. 2016), pp. 1834–1844. ISSN: 1533-4406. DOI: 10.1056/NEJMoa1607141.

[52] Katherine R. Tuttle, Mark C. Lakshmanan, Brian Rayner, Robert S. Busch, Alan G. Zimmermann, D. Bradley Woodward, and Fady T. Botros. “Dulaglutide versus insulin glargine in patients with type 2 diabetes and moderate-to-severe chronic kidney disease (AWARD-7): a multicentre, open-label, randomised trial”. In: *Lancet Diabetes & Endocrinology* 6.8 (Aug. 2018), pp. 605–617. ISSN: 2213-8587. DOI: 10.1016/S2213-8587(18)30104-9.

[53] Benjamin M. Scirica et al. “Saxagliptin and Cardiovascular Outcomes in Patients with Type 2 Diabetes Mellitus”. In: *N. Engl. J. Med.* 369.14 (Sept. 2013), pp. 1317–1326. ISSN: 1533-4406. DOI: 10.1056/NEJMoa1307684.

[54] William B. White et al. “Alogliptin after Acute Coronary Syndrome in Patients with Type 2 Diabetes”. In: *N. Engl. J. Med.* 369.14 (Sept. 2013), pp. 1327–1335. ISSN: 1533-4406. DOI: 10.1056/NEJMoa1305889.

[55] Jennifer B. Green et al. “Effect of Sitagliptin on Cardiovascular Outcomes in Type 2 Diabetes”. In: *N. Engl. J. Med.* 373.3 (June 2015), pp. 232–242. ISSN: 1533-4406. DOI: 10.1056/NEJMoa1501352.

[56] Julio Rosenstock et al. “Effect of Linagliptin vs Placebo on Major Cardiovascular Events in Adults With Type 2 Diabetes and High Cardiovascular and Renal Risk: The CARMELINA Randomized Clinical Trial”. In: *PubMed. comprises. more. than. 30 million. citations. for.*

biomedical. literature. from. MEDLINE, life. science. journals., and. online. books. 321.1 (Jan. 2019), pp. 69–79. ISSN: 1538-3598. DOI: 10.1001/jama.2018.18269.

[57] Morten Lindhardt et al. “Proteomic prediction and Renin angiotensin aldosterone system Inhibition prevention Of early diabetic nephRopathy in Type 2 diabetic patients with normoalbuminuria (PRIORITY): essential study design and rationale of a randomised clinical multicentre trial”. In: *BMJ Open* 6.3 (2016). DOI: 10.1136/bmjopen-2015-010310.

[58] Vlado Perkovic et al. “Canagliflozin and Renal Outcomes in Type 2 Diabetes and Nephropathy”. In: *N. Engl. J. Med.* 380.24 (Apr. 2019), pp. 2295–2306. ISSN: 1533-4406. DOI: 10.1056/NEJMoa1811744.

[59] Hiddo J. L. Heerspink et al. “Atrasentan and renal events in patients with type 2 diabetes and chronic kidney disease (SONAR): a double-blind, randomised, placebo-controlled trial”. In: *PubMed. comprises. more. than. 30 million. citations. for. biomedical. literature. from. MEDLINE, life. science. journals., and. online. books.* 393.10184 (May 2019), pp. 1937–1947. ISSN: 1474-547X. DOI: 10.1016/S0140-6736(19)30772-X.

[60] Susanne Brenner and Christoph Wanner. “Diabetes mellitus Typ 2: Wie schtzen wir die Nieren am besten?” In: *Dtsch. med. Wochenschr.* 144.11 (June 2019), pp. 710–714. ISSN: 0012-0472. DOI: 10.1055/a-0662-1919.

[61] Kengo Azushima, Susan B. Gurley, and Thomas M. Coffman. “Modelling diabetic nephropathy in mice”. In: *Nat. Rev. Nephrol.* 14 (Oct. 2017), pp. 48–56. ISSN: 1759-507X. DOI: 10.1038/nrneph.2017.142.

[62] Frank C. Brosius, Charles E. Alpers, Erwin P. Bottinger, Matthew D. Breyer, Thomas M. Coffman, Susan B. Gurley, Raymond C. Harris, Masao Kakoki, Matthias Kretzler, Edward H. Leiter, et al. “Mouse Models of Diabetic Nephropathy”. In: *JASN* 20.12 (Dec. 2009), pp. 2503–2512. ISSN: 1046-6673. DOI: 10.1681/ASN.2009070721.

[63] E. J. Michaud, S. J. Bultman, M. L. Klebig, M. J. van Vugt, L. J. Stubbs, L. B. Russell, and R. P. Woychik. “A molecular model for the genetic and phenotypic characteristics of the mouse lethal yellow (Ay) mutation.” In: *Proc. Natl. Acad. Sci. U.S.A.* 91.7 (Mar. 1994), p. 2562. DOI: 10.1073/pnas.91.7.2562.

[64] Zhonghua Qi, Hiroki Fujita, Jianping Jin, Linda S. Davis, Yihan Wang, Agnes B. Fogo, and Matthew D. Breyer. “Characterization of susceptibility of inbred mouse strains to diabetic nephropathy”. In: *Diabetes* 54.9 (Sept. 2005), pp. 2628–2637. ISSN: 0012-1797. DOI: 10.2337/diabetes.54.9.2628.

[65] Susan B. Gurley, Sharon E. Clare, Kamie P. Snow, Ann Hu, Timothy W. Meyer, and Thomas M. Coffman. “Impact of genetic background on nephropathy in diabetic mice”. In: *Am. J. Physiol. Renal Physiol.* 290.1 (Jan. 2006), pp. 214–222. ISSN: 1931-857X. DOI: 10.1152/ajprenal.00204.2005.

[66] D. L. Coleman. “Obese and diabetes: two mutant genes causing diabetes-obesity syndromes in mice”. In: *Diabetologia* 14.3 (Mar. 1978), pp. 141–148. ISSN: 0012-186X. DOI: 10.1007/bf00429772.

[67] D. L. Coleman and K. P. Hummel. “The influence of genetic background on the expression of the obese (Ob) gene in the mouse”. In: *Diabetologia* 9.4 (Aug. 1973), pp. 287–293. ISSN: 0012-186X. DOI: 10.1007/bf01221856.

[68] Mette V. Østergaard, Vanda Pinto, Kirsty Stevenson, Jesper Worm, Lisbeth N. Fink, and Richard J. M. Coward. “DBA2J db/db mice are susceptible to early albuminuria and glomerulosclerosis that correlate with systemic insulin resistance”. In: *American Journal of Physiology - Renal Physiology* 312.2 (Feb. 2017), F312. DOI: 10.1152/ajprenal.00451.2016.

[69] Streamson Chua, Yifu Li, Shun Mei Liu, Ruijie Liu, Ka Tak Chan, Jeremiah Martino, Zongyu Zheng, Katalin Susztak, Vivette D. D’Agati, and Ali G. Gharavi. “A susceptibility gene for kidney disease in an obese mouse model of type II diabetes maps to chromosome 8”. In: *Kidney International* 78.5 (Sept. 2010), pp. 453–462. ISSN: 0085-2538. DOI: 10.1038/ki.2010.160.

[70] J. K. Naggert, J. L. Mu, W. Frankel, D. W. Bailey, and B. Paigen. “Genomic analysis of the C57BL/Ks mouse strain”. In: *Mamm. Genome* 6.2 (Feb. 1995), pp. 131–133. ISSN: 0938-8990. DOI: 10.1007/bf00303258.

[71] Kelly L. Hudkins, Warangkana Pichaiwong, Tomasz Wietecha, Jolanta Kowalewska, Miriam C. Banas, Min W. Spencer, Anja Mhlfeld, Mariko Koelling, Jeffrey W. Pippin, Stuart J. Shankland, et al. “BTBR Ob/Ob Mutant Mice Model Progressive Diabetic Nephropathy”. In: *JASN* 21.9 (Sept. 2010), pp. 1533–1542. ISSN: 1046-6673. DOI: 10.1681/ASN.2009121290.

[72] Takahiko Nakagawa, Waichi Sato, Olena Glushakova, Marcelo Heinig, Tracy Clarke, Martha Campbell-Thompson, Yukio Yuzawa, Mark A. Atkinson, Richard J. Johnson, and Byron Croker. “Diabetic Endothelial Nitric Oxide Synthase Knockout Mice Develop Advanced Diabetic Nephropathy”. In: *JASN* 18.2 (Feb. 2007), pp. 539–550. ISSN: 1046-6673. DOI: 10.1681/ASN.2006050459.

[73] Hui John Zhao, Suwan Wang, Huifang Cheng, Ming-zhi Zhang, Takamune Takahashi, Agnes B. Fogo, Matthew D. Breyer, and Raymond C. Harris. “Endothelial Nitric Oxide Synthase Deficiency Produces Accelerated Nephropathy in Diabetic Mice”. In: *JASN* 17.10 (Oct. 2006), pp. 2664–2669. ISSN: 1046-6673. DOI: 10.1681/ASN.2006070798.

[74] Shannon M. Harlan, Kathleen M. Heinz-Taheny, John M. Sullivan, Tao Wei, Hana E. Baker, Dianna L. Jaqua, Zhonghua Qi, Martin S. Cramer, Tatiyana L. Shiyanova, Matthew D. Breyer, et al. “Progressive Renal Disease Established by Renin-Coding Adeno-Associated Virus–Driven Hypertension in Diverse Diabetic Models”. In: *JASN* 29.2 (Feb. 2018), pp. 477–491. ISSN: 1046-6673. DOI: 10.1681/ASN.2017040385.

[75] Jean-Francois Thibodeau, Chet E. Holterman, Dylan Burger, Naomi C. Read, Timothy L. Reudelhuber, and Christopher R. J. Kennedy. “A Novel Mouse Model of Advanced Diabetic Kidney Disease”. In: *PLoS One* 9.12 (2014). DOI: 10.1371/journal.pone.0113459.

[76] Shrikant R. Mulay, Jonathan N. Eberhard, Victoria Pfann, Julian A. Marschner, Murthy N. Darisipudi, Christoph Daniel, Simone Romoli, Jyaysi Desai, Melissa Grigorescu, Santhosh V. Kumar, et al. “Oxalate-induced chronic kidney disease with its uremic and cardiovascular complications in C57BL/6 mice”. In: *PubMed. comprises. more. than. 30 million. citations. for. biomedical. literature. from. MEDLINE, life. science. journals., and. online. books.* 310.8 (Apr. 2016), pp. 785–795. ISSN: 1522-1466. DOI: 10.1152/ajprenal.00488.2015.

[77] Shrikant R. Mulay, Jonathan N. Eberhard, Jyaysi Desai, Julian A. Marschner, Santhosh V. R. Kumar, Marc Weidenbusch, Melissa Grigorescu, Maciej Lech, Nuru Eltrich, Lisa Mller, et al. “Hyperoxaluria Requires TNF Receptors to Initiate Crystal Adhesion and Kidney Stone Disease”. In: *JASN* 28.3 (Mar. 2017), pp. 761–768. ISSN: 1046-6673. DOI: 10.1681/ASN.2016040486.

[78] Hans-Joachim Anders, Beatriz Suarez-Alvarez, Melissa Grigorescu, Orestes Foresto-Neto, Stefanie Steiger, Jyaysi Desai, Julian A. Marschner, Mohsen Honarpisheh, Chongxu Shi, Jutta Jordan, et al. “The macrophage phenotype and inflammasome component NLRP3 contributes to nephrocalcinosis-related chronic kidney disease independent from IL-1-mediated tissue injury”. In: *Kidney Int.* 93.3 (Mar. 2018), pp. 656–669. ISSN: 1523-1755. DOI: 10.1016/j.kint.2017.09.022.

[79] Mohsen Honarpisheh, Jyaysi Desai, Julian A. Marschner, Marc Weidenbusch, Maciej Lech, Volker Vielhauer, Hans-Joachim Anders, and Shrikant R. Mulay. “Regulated necrosis-related molecule mRNA expression in humans and mice and in murine acute tissue injury and systemic autoimmunity leading to progressive organ damage, and progressive fibrosis”. In: *Biosci. Rep.* 36.6 (Dec. 2016). ISSN: 0144-8463. DOI: 10.1042/BSR20160336.

[80] Melda Onal, Alex H. Carlson, Jeff D. Thostenson, Nancy A. Benkusky, Mark B. Meyer, Seong M. Lee, and J. Wesley Pike. “A Novel Distal Enhancer Mediates Inflammation-, PTH-, and Early Onset Murine Kidney Disease-Induced Expression of the Mouse Fgf23 Gene”. In: *JBMR Plus* 2.1 (Jan. 2018), pp. 31–46. ISSN: 2475-0328. DOI: 10.1002/jbm4.10023.

[81] Stefanie Steiger, Julia Felicitas Grill, Qiuyue Ma, Tobias Buerle, Jutta Jordan, Michaela Smolle, Claudia Bhland, Maciej Lech, and Hans-Joachim Anders. "Anti-Transforming Growth Factor β IgG Elicits a Dual Effect on Calcium Oxalate Crystallization and Progressive Nephrocalcinosis-Related Chronic Kidney Disease". In: *Front. Immunol.* 9 (Mar. 2018). ISSN: 1664-3224. DOI: 10.3389/fimmu.2018.00619.

[82] Julian A. Marschner et al. "The Long Pentraxin PTX3 Is an Endogenous Inhibitor of Hyperoxaluria-Related Nephrocalcinosis and Chronic Kidney Disease". In: *Front. Immunol.* 9 (Sept. 2018), p. 2173. ISSN: 1664-3224. DOI: 10.3389/fimmu.2018.02173.

[83] Charles A. Dinarello. "Immunological and inflammatory functions of the interleukin-1 family". In: *Annu. Rev. Immunol.* 27 (2009), pp. 519–50. ISSN: 0732-0582. DOI: 10.1146/annurev.immunol.021908.132612.

[84] Paul M. Ridker, Brendan M. Everett, Tom Thuren, Jean G. MacFadyen, William H. Chang, Christie Ballantyne, Francisco Fonseca, Jose Nicolau, Wolfgang Koenig, Stefan D. Anker, et al. "Antiinflammatory Therapy with Canakinumab for Atherosclerotic Disease". In: *N. Engl. J. Med.* 377.12 (Aug. 2017), pp. 1119–1131. ISSN: 1533-4406. DOI: 10.1056/NEJMoa1707914.

[85] C. A. Dinarello, N. P. Goldin, and S. M. Wolff. "Demonstration and characterization of two distinct human leukocytic pyrogens". In: *J. Exp. Med.* 139.6 (June 1974), pp. 1369–1381. ISSN: 0022-1007. URL: https://www.ncbi.nlm.nih.gov/.

[86] C. J. March, B. Mosley, A. Larsen, D. P. Cerretti, G. Braedt, V. Price, S. Gillis, C. S. Henney, S. R. Kronheim, and K. Grabstein. "Cloning, sequence and expression of two distinct human interleukin-1 complementary DNAs". In: *Nature* -26;315.6021 (June 1985), pp. 641–647. ISSN: 0028-0836. URL: https://www.ncbi.nlm.nih.gov/pubmed/2989698?dopt=Abstract$%5C&$holding=npg.

[87] Hans-Joachim Anders. "Of Inflammasomes and Alarmins: IL-1β and IL-1α in Kidney Disease". In: *J. Am. Soc. Nephrol.* 27.9 (Sept. 2016), pp. 2564–2575. ISSN: 1533-3450. DOI: 10.1681/ASN.2016020177.

[88] Alberto Mantovani, Charles A. Dinarello, Martina Molgora, and Cecilia Garlanda. "Interleukin-1 and Related Cytokines in the Regulation of Inflammation and Immunity". In: *Immunity* 50.4 (Apr. 2019), pp. 778–795. ISSN: 1097-4180. DOI: 10.1016/j.immuni.2019.03.012.

[89] Charles A. Dinarello. "Overview of the IL-1 family in innate inflammation and acquired immunity". In: *Immunol. Rev.* 281.1 (Jan. 2018), pp. 8–27. ISSN: 1600-065X. DOI: 10.1111/imr.12621.

[90] Brian Krumm, Yan Xiang, and Junpeng Deng. “Structural biology of the IL-1 superfamily: Key cytokines in the regulation of immune and inflammatory responses”. In: *Protein Sci.* 23.5 (May 2014), p. 526. DOI: 10.1002/pro.2441.

[91] S. A. Greenfeder, P. Nunes, L. Kwee, M. Labow, R. A. Chizzonite, and G. Ju. “Molecular cloning and characterization of a second subunit of the interleukin 1 receptor complex”. In: *J. Biol. Chem.* 270.23 (June 1995), pp. 13757–13765. ISSN: 0021-9258. URL: https://www.ncbi.nlm.nih.gov/pubmed/7775431.

[92] C. Korherr, R. Hofmeister, H. Wesche, and W. Falk. “A critical role for interleukin-1 receptor accessory protein in interleukin-1 signaling”. In: *Eur. J. Immunol.* 27.1 (Jan. 1997), pp. 262–267. ISSN: 0014-2980. DOI: 10.1002/eji.1830270139.

[93] C. J. McMahan, J. L. Slack, B. Mosley, D. Cosman, S. D. Lupton, L. L. Brunton, C. E. Grubin, J. M. Wignall, N. A. Jenkins, and C. I. Brannan. “A novel IL-1 receptor, cloned from B cells by mammalian expression, is expressed in many cell types”. In: *EMBO J.* 10.10 (Oct. 1991), pp. 2821–2832. ISSN: 0261-4189. URL: https://www.ncbi.nlm.nih.gov/pubmed/1833184.

[94] Charles A. Dinarello. “Interleukin-1 in the pathogenesis and treatment of inflammatory diseases”. In: *Blood* 117.14 (Apr. 2011), pp. 3720–3732. ISSN: 1528-0020. DOI: 10.1182/blood-2010-07-273417.

[95] Petr Broz and Vishva M. Dixit. “Inflammasomes: mechanism of assembly, regulation and signalling”. In: *Nat. Rev. Immunol.* 16.7 (July 2016), pp. 407–420. ISSN: 1474-1741. DOI: 10.1038/nri.2016.58.

[96] Karen V. Swanson, Meng Deng, and Jenny P.-Y. Ting. “The NLRP3 inflammasome: molecular activation and regulation to therapeutics”. In: *Nat. Rev. Immunol.* 19.8 (Apr. 2019), pp. 477–489. ISSN: 1474-1741. DOI: 10.1038/s41577-019-0165-0.

[97] Dave Boucher et al. “Caspase-1 self-cleavage is an intrinsic mechanism to terminate inflammasome activity”. In: *J. Exp. Med.* 215.3 (Mar. 2018), pp. 827–840. ISSN: 0022-1007. DOI: 10.1084/jem.20172222.

[98] Fabio Martinon, Kimberly Burns, and Jrg Tschopp. “The inflammasome: a molecular platform triggering activation of inflammatory caspases and processing of proIL-beta”. In: *PubMed. comprises. more. than. 30 million. citations. for. biomedical. literature. from. MEDLINE, life. science. journals., and. online. books.* 10.2 (Aug. 2002), pp. 417–426. ISSN: 1097-2765. DOI: 10.1016/s1097-2765(02)00599-3.

[99] Wan-ting He, Haoqiang Wan, Lichen Hu, Pengda Chen, Xin Wang, Zhe Huang, Zhang-Hua Yang, Chuan-Qi Zhong, and Jiahuai Han. “Gasdermin D is an executor of pyroptosis and required for interleukin-1β secretion”. In: *Cell Res.* 25.12 (Dec. 2015), pp. 1285–1298. ISSN: 1748-7838. DOI: 10.1038/cr.2015.139.

[100] Jianjin Shi, Yue Zhao, Kun Wang, Xuyan Shi, Yue Wang, Huanwei Huang, Yinghua Zhuang, Tao Cai, Fengchao Wang, and Feng Shao. “Cleavage of GSDMD by inflammatory caspases determines pyroptotic cell death”. In: *PubMed. comprises. more. than. 30 million. citations. for. biomedical. literature. from. MEDLINE, life. science. journals., and. online. books.* 526.7575 (Oct. 2015), pp. 660–665. ISSN: 1476-4687. DOI: 10.1038/nature15514.

[101] Uwe Schnbeck, Franois Mach, and Peter Libby. “Generation of Biologically Active IL-1β by Matrix Metalloproteinases: A Novel Caspase-1-Independent Pathway of IL-1β Processing”. In: *J. Immunol.* 161.7 (Oct. 1998), pp. 3340–3346. ISSN: 0022-1767. URL: http://www.jimmunol.org/content/161/7/3340.short.

[102] Kate Schroder and Jurg Tschopp. “The Inflammasomes”. In: *Cell* 140.6 (Mar. 2010), pp. 821–832. ISSN: 0092-8674. DOI: 10.1016/j.cell.2010.01.040.

[103] Franz G. Bauernfeind et al. “Cutting edge: NF-kappaB activating pattern recognition and cytokine receptors license NLRP3 inflammasome activation by regulating NLRP3 expression”. In: *PubMed. comprises. more. than. 30 million. citations. for. biomedical. literature. from. MEDLINE, life. science. journals., and. online. books.* 183.2 (July 2009), pp. 787–791. ISSN: 1550-6606. DOI: 10.4049/jimmunol.0901363.

[104] Luigi Franchi, Tatjana Eigenbrod, and Gabriel Nez. “Cutting edge: TNF-alpha mediates sensitization to ATP and silica via the NLRP3 inflammasome in the absence of microbial stimulation”. In: *PubMed. comprises. more. than. 30 million. citations. for. biomedical. literature. from. MEDLINE, life. science. journals., and. online. books.* 183.2 (July 2009), pp. 792–796. ISSN: 1550-6606. DOI: 10.4049/jimmunol.0900173.

[105] Moritz M. Gaidt, Thomas S. Ebert, Dhruv Chauhan, Tobias Schmidt, Jonathan L. Schmid-Burgk, Francesca Rapino, Avril A. B. Robertson, Matthew A. Cooper, Thomas Graf, and Veit Hornung. “Human Monocytes Engage an Alternative Inflammasome Pathway”. In: *Immunity* 44.4 (Apr. 2016), pp. 833–846. ISSN: 1074-7613. DOI: 10.1016/j.immuni.2016.01.012.

[106] Mihai G. Netea et al. “Differential requirement for the activation of the inflammasome for processing and release of IL-1beta in monocytes and macrophages”. In: *PubMed. comprises. more. than. 30 million. citations. for. biomedical. literature. from. MEDLINE, life. science. journals., and. online. books.* 113.10 (Mar. 2009), pp. 2324–2335. ISSN: 1528-0020. DOI: 10.1182/blood-2008-03-146720.

[107] C. A. Dinarello. “Biologic basis for interleukin-1 in disease”. In: *Blood* 87.6 (Mar. 1996), pp. 2095–2147. ISSN: 0006-4971. URL: https://www.ncbi.nlm.nih.gov/pubmed/8630372.

[108] Hye-Mi Lee, Jwa-Jin Kim, Hyun Jin Kim, Minho Shong, Bon Jeong Ku, and Eun-Kyeong Jo. “Upregulated NLRP3 inflammasome activation in patients with type 2 diabetes”. In: *Diabetes* 62.1 (Jan. 2013), pp. 194–204. ISSN: 1939-327X. DOI: 10.2337/db12-0420.

[109] Kehong Chen, Jianguo Zhang, Weiwei Zhang, Jinhua Zhang, Jurong Yang, Kailong Li, and Yani He. “ATP-P2X4 signaling mediates NLRP3 inflammasome activation: A novel pathway of diabetic nephropathy”. In: *Int. J. Biochem. Cell Biol.* 45.5 (May 2013), pp. 932–943. ISSN: 1357-2725. DOI: 10.1016/j.biocel.2013.02.009.

[110] Takanori Komada, Hyunjae Chung, Arthur Lau, Jaye M. Platnich, Paul L. Beck, Hallgrimur Benediktsson, Henry J. Duff, Craig N. Jenne, and Daniel A. Muruve. “Macrophage Uptake of Necrotic Cell DNA Activates the AIM2 Inflammasome to Regulate a Proinflammatory Phenotype in CKD”. In: *JASN* 29.4 (Apr. 2018), pp. 1165–1181. ISSN: 1046-6673. DOI: 10.1681/ASN.2017080863.

[111] Khurrum Shahzad et al. “Caspase-1, but Not Caspase-3, Promotes Diabetic Nephropathy”. In: *J. Am. Soc. Nephrol.* 27.8 (Aug. 2016), pp. 2270–2275. ISSN: 1533-3450. DOI: 10.1681/ASN.2015060676.

[112] Takanori Komada, Fumitake Usui, Koumei Shirasuna, Akira Kawashima, Hiroaki Kimura, Tadayoshi Karasawa, Satoshi Nishimura, Junji Sagara, Tetsuo Noda, Shun’ichiro Taniguchi, et al. “ASC in renal collecting duct epithelial cells contributes to inflammation and injury after unilateral ureteral obstruction”. In: *Am. J. Pathol.* 184.5 (May 2014), pp. 1287–1298. ISSN: 1525-2191. DOI: 10.1016/j.ajpath.2014.01.014.

[113] Yibo Zhuang, Guixia Ding, Min Zhao, Mi Bai, Lingyun Yang, Jiajia Ni, Rong Wang, Zhanjun Jia, Songming Huang, and Aihua Zhang. “NLRP3 inflammasome mediates albumin-induced renal tubular injury through impaired mitochondrial function”. In: *J. Biol. Chem.* 289.36 (Sept. 2014), pp. 25101–25111. ISSN: 1083-351X. DOI: 10.1074/jbc.M114.578260.

[114] Hyun-Jung Kim, Dong Won Lee, Kameswaran Ravichandran, Daniel O. Keys, Ali Akcay, Quocan Nguyen, Zhibin He, Alkesh Jani, Danica Ljubanovic, and Charles L. Edelstein. “NLRP3 Inflammasome Knockout Mice Are Protected against Ischemic but Not Cisplatin-Induced Acute Kidney Injury”. In: *J. Pharmacol. Exp. Ther.* 346.3 (Sept. 2013), pp. 465–472. ISSN: 0022-3565. DOI: 10.1124/jpet.113.205732.

[115] Takanori Komada and Daniel A. Muruve. “The role of inflammasomes in kidney disease”. In: *Nat. Rev. Nephrol.* 15.8 (Aug. 2019), pp. 501–520. ISSN: 1759-507X. DOI: 10.1038/s41581-019-0158-z.

[116] *The interleukin-1 Receptor Family*. [Online; accessed 3. Feb. 2020]. Dec. 2013. DOI: 10.1016/j.smim.2013.10.023.

[117] Hong Feng, Junling Gu, Fang Gou, Wei Huang, Chenlin Gao, Guo Chen, Yang Long, Xueqin Zhou, Maojun Yang, Shuang Liu, et al. “High Glucose and Lipopolysaccharide Prime NLRP3 Inflammasome via ROS/TXNIP Pathway in Mesangial Cells”. In: *J. Diabetes Res.* J.Diabetes (Jan. 2016), Res. ISSN: 2314-6753. DOI: 10.1155/2016/6973175.

[118] Yachun Han, Xiaoxuan Xu, Chengyuan Tang, Peng Gao, Xianghui Chen, Xiaofen Xiong, Ming Yang, Shikun Yang, Xuejing Zhu, Shuguang Yuan, et al. “Reactive oxygen species promote tubular injury in diabetic nephropathy: The role of the mitochondrial ros-txnip-nlrp3 biological axis”. In: *Redox Biol.* 16 (June 2018), pp. 32–46. ISSN: 2213-2317. DOI: 10.1016/j.redox.2018.02.013.

[119] Kenshi Yamasaki et al. “NLRP3/cryopyrin is necessary for interleukin-1beta (IL-1beta) release in response to hyaluronan, an endogenous trigger of inflammation in response to injury”. In: *J. Biol. Chem.* 284.19 (May 2009), pp. 12762–12771. ISSN: 0021-9258. DOI: 10.1074/jbc.M806084200.

[120] Stuart Jones, Suzanne Jones, and Aled Owain Phillips. “Regulation of renal proximal tubular epithelial cell hyaluronan generation: Implications for diabetic nephropathy”. In: *Kidney International* 59.5 (May 2001), pp. 1739–1749. ISSN: 0085-2538. DOI: 10.1046/j.1523-1755.2001.0590051739.x.

[121] Claus M. Larsen, Mirjam Faulenbach, Allan Vaag, Aage Vølund, Jan A. Ehses, Burkhardt Seifert, Thomas Mandrup-Poulsen, and Marc Y. Donath. “Interleukin-1-receptor antagonist in type 2 diabetes mellitus”. In: *N. Engl. J. Med.* 356.15 (Apr. 2007), pp. 1517–1526. ISSN: 1533-4406. DOI: 10.1056/NEJMoa065213.

[122] Maria G. Ramos-Zavala, Manuel Gonzlez-Ortiz, Esperanza Martnez-Abundis, Jos A. Robles-Cervantes, Roberto Gonzlez-Lpez, and Nestor J. Santiago-Hernndez. “Effect of Diacerein on Insulin Secretion and Metabolic Control in Drug-Nave Patients With Type 2 Diabetes: A randomized clinical trial”. In: *Diabetes Care* 34.7 (July 2011), pp. 1591–1594. ISSN: 0149-5992. DOI: 10.2337/dc11-0357.

[123] Joanne Sloan-Lancaster, Eyas Abu-Raddad, John Polzer, Jeffrey W. Miller, Joel C. Scherer, Andrea De Gaetano, Jolene K. Berg, and William H. Landschulz. “Double-Blind, Randomized Study Evaluating the Glycemic and Anti-inflammatory Effects of Subcutaneous LY2189102, a Neutralizing IL-1β Antibody, in Patients With Type 2 Diabetes”. In: *Diabetes Care* 36.8 (Aug. 2013), p. 2239. DOI: 10.2337/dc12-1835.

[124] Paul M. Ridker, Campbell P. Howard, Verena Walter, Brendan Everett, Peter Libby, Johannes Hensen, and Tom Thuren. “Effects of interleukin-1β inhibition with canakinumab on hemoglobin A1c, lipids, C-reactive protein, interleukin-6, and fibrinogen: a phase IIb randomized, placebo-controlled trial”. In: *PubMed. comprises.*

more. than. 30 million. citations. for. biomedical. literature. from. MEDLINE, life. science. journals., and. online. books. 126.23 (Dec. 2012), pp. 2739–2748. ISSN: 1524-4539. DOI: 10.1161/CIRCULATIONAHA.112.122556.

[125] Brendan M. Everett, Marc Y. Donath, Aruna D. Pradhan, Tom Thuren, Prem Pais, Jose C. Nicolau, Robert J. Glynn, Peter Libby, and Paul M. Ridker. "Anti-Inflammatory Therapy With Canakinumab for the Prevention and Management of Diabetes". In: *PubMed. comprises. more. than. 30 million. citations. for. biomedical. literature. from. MEDLINE, life. science. journals., and. online. books.* 71.21 (May 2018), pp. 2392–2401. ISSN: 1558-3597. DOI: 10.1016/j.jacc.2018.03.002.

[126] Kristen L. Nowak et al. "IL-1 Inhibition and Vascular Function in CKD". In: *J. Am. Soc. Nephrol.* 28.3 (Mar. 2017), p. 971. DOI: 10.1681/ASN.2016040453.

[127] Piero Ruscitti et al. "Anti-interleukin-1 treatment in patients with rheumatoid arthritis and type 2 diabetes (TRACK): A multicentre, open-label, randomised controlled trial". In: *PLoS Med.* 16.9 (Sept. 2019), e1002901. ISSN: 1549-1676. DOI: 10.1371/journal.pmed.1002901.

[128] Claudia Cavelti-Weder, Katharina Timper, Eleonora Seelig, Cornelia Keller, Martin Osranek, Ute Lssing, Gunther Spohn, Patrik Maurer, Philipp Mller, Gary T. Jennings, et al. "Development of an Interleukin-1β Vaccine in Patients with Type 2 Diabetes". In: *PubMed. comprises. more. than. 30 million. citations. for. biomedical. literature. from. MEDLINE, life. science. journals., and. online. books.* 24.5 (May 2016), pp. 1003–1012. ISSN: 1525-0024. DOI: 10.1038/mt.2015.227.

[129] A. Rissanen, C. P. Howard, J. Botha, and T. Thuren. "Effect of anti-IL-1β antibody (canakinumab) on insulin secretion rates in impaired glucose tolerance or type 2 diabetes: results of a randomized, placebo-controlled trial". In: *Diabetes Obes. Metab.* 14.12 (Dec. 2012), pp. 1088–1096. ISSN: 1462-8902. DOI: 10.1111/j.1463-1326.2012.01637.x.

[130] Robin P. Choudhury et al. "Arterial Effects of Canakinumab in Patients With Atherosclerosis and Type 2 Diabetes or Glucose Intolerance". In: *PubMed. comprises. more. than. 30 million. citations. for. biomedical. literature. from. MEDLINE, life. science. journals., and. online. books.* 68.16 (Oct. 2016), pp. 1769–1780. ISSN: 1558-3597. DOI: 10.1016/j.jacc.2016.07.768.

[131] Claudia Cavelti-Weder, Andrea Babians-Brunner, Cornelia Keller, Marc A. Stahel, Malaika Kurz-Levin, Hany Zayed, Alan M. Solinger, Thomas Mandrup-Poulsen, Charles A. Dinarello, and Marc Y. Donath. "Effects of gevokizumab on glycemia and inflammatory markers in type 2 diabetes". In: *PubMed. comprises. more. than. 30 million. citations. for. biomedical. literature. from. MEDLINE, life. science. journals.,*

and. online. books. 35.8 (Aug. 2012), pp. 1654–1662. ISSN: 1935-5548. DOI: 10.2337/dc11-2219.

[132] Andrea Schreiber et al. “Transcutaneous measurement of renal function in conscious mice”. In: *Am. J. Physiol. Renal Physiol.* 303.5 (Sept. 2012), pp. 783–788. ISSN: 1522-1466. DOI: 10.1152/ajprenal.00279.2012.

[133] Murthy N. Darisipudi et al. “Dual blockade of the homeostatic chemokine CXCL12 and the proinflammatory chemokine CCL2 has additive protective effects on diabetic kidney disease”. In: *Am. J. Pathol.* 179.1 (July 2011), pp. 116–124. ISSN: 1525-2191. DOI: 10.1016/j.ajpath.2011.03.004.

[134] Volha Ninichuk et al. “Late Onset of Ccl2 Blockade with the Spiegelmer mNOX-E36–3′PEG Prevents Glomerulosclerosis and Improves Glomerular Filtration Rate in db/db Mice”. In: *Am. J. Pathol.* 172.3 (Mar. 2008), p. 628. DOI: 10.2353/ajpath.2008.070601.

[135] Sufyan G. Sayyed, Anil Bhanudas Gaikwad, Julia Lichtnekert, Onkar Kulkarni, Dirk Eulberg, Sven Klussmann, Kulbhushan Tikoo, and Hans-Joachim Anders. “Progressive glomerulosclerosis in type 2 diabetes is associated with renal histone H3K9 and H3K23 acetylation, H3K4 dimethylation and phosphorylation at serine 10”. In: *Nephrol. Dial. Transplant* 25.6 (June 2010), pp. 1811–1817. ISSN: 1460-2385. DOI: 10.1093/ndt/gfp730.

[136] Yutian Lei, Satish K. Devarapu, Manga Motrapu, Clemens D. Cohen, Maja T. Lindenmeyer, Solange Moll, Santhosh V. Kumar, and Hans-Joachim Anders. “Interleukin-1β Inhibition for Chronic Kidney Disease in Obese Mice With Type 2 Diabetes”. In: *Front. Immunol.* 10 (2019). DOI: 10.3389/fimmu.2019.01223.

[137] Clemens D. Cohen, Karin Frach, Detlef Schlndorff, and Matthias Kretzler. “Quantitative gene expression analysis in renal biopsies: A novel protocol for a high-throughput multicenter application”. In: *Kidney International* 61.1 (Jan. 2002), pp. 133–140. ISSN: 0085-2538. DOI: 10.1046/j.1523-1755.2002.00113.x.

[138] Kumar Sharma, Bethany Karl, Anna V. Mathew, Jon A. Gangoiti, Christina L. Wassel, Rintaro Saito, Minya Pu, Shoba Sharma, Young-Hyun You, Lin Wang, et al. “Metabolomics Reveals Signature of Mitochondrial Dysfunction in Diabetic Kidney Disease”. In: *JASN* 24.11 (Nov. 2013), pp. 1901–1912. ISSN: 1046-6673. DOI: 10.1681/ASN.2013020126.

[139] Holger Schmid, Anissa Boucherot, Yoshinari Yasuda, Anna Henger, Bodo Brunner, Felix Eichinger, Almut Nitsche, Eva Kiss, Markus Bleich, Hermann-Josef Grne, et al. “Modular Activation of Nuclear Factor-κB Transcriptional Programs in Human Diabetic Nephropathy”. In: *Diabetes* 55.11 (Nov. 2006), pp. 2993–3003. ISSN: 0012-1797. DOI: 10.2337/db06-0477.

[140] Virginia Goss Tusher, Robert Tibshirani, and Gilbert Chu. “Significance analysis of microarrays applied to the ionizing radiation response”. In: *Proc. Natl. Acad. Sci. U.S.A.* 98.9 (Apr. 2001), pp. 5116–5121. ISSN: 0027-8424. DOI: 10.1073/pnas.091062498.

[141] Lennart Tonneijck, Marcel H.A. Muskiet, Mark M. Smits, Erik J. van Bommel, Hiddo J.L. Heerspink, Daniël H. van Raalte, and Jaap A. Joles. “Glomerular Hyperfiltration in Diabetes: Mechanisms, Clinical Significance, and Treatment”. In: *Journal of the American Society of Nephrology* 28.4 (2017), pp. 1023–1039. ISSN: 1046-6673. DOI: 10.1681/ASN.2016060666. eprint: https://jasn.asnjournals.org/content/28/4/1023.full.pdf. URL: https://jasn.asnjournals.org/content/28/4/1023.

[142] L. Anguiano Gomez, Y. Lei, S. Kumar Devarapu, and H. J. Anders. “The diabetes pandemic suggests unmet needs for ’CKD with diabetes’ in addition to ’diabetic nephropathy’-implications for pre-clinical research and drug testing”. In: *Nephrol Dial Transplant* 33.8 (2018), pp. 1292–1304. ISSN: 0931-0509. DOI: 10.1093/ndt/gfx219.

[143] Julia Lichtnekert, Onkar P. Kulkarni, Shrikant R. Mulay, Khader Valli Rupanagudi, Mi Ryu, Ramanjaneyulu Allam, Volker Vielhauer, Dan Muruve, Maja T. Lindenmeyer, Clemens D. Cohen, et al. “Anti-GBM Glomerulonephritis Involves IL-1 but Is Independent of NLRP3/ASC Inflammasome-Mediated Activation of Caspase-1”. In: *PLoS One* 6.10 (Oct. 2011), e26778. ISSN: 1932-6203. DOI: 10.1371/journal.pone.0026778.

[144] Arthur Lau, Hyunjae Chung, Takanori Komada, Jaye M. Platnich, Christina F. Sandall, Saurav Roy Choudhury, Justin Chun, Victor Naumenko, Bas Gj Surewaard, Michelle C. Nelson, et al. “Renal immune surveillance and dipeptidase-1 contribute to contrast-induced acute kidney injury”. In: *J. Clin. Invest.* 128.7 (July 2018), pp. 2894–2913. ISSN: 1558-8238. DOI: 10.1172/JCI96640.

[145] H. Chung et al. “NLRP3 regulates a non-canonical platform for caspase-8 activation during epithelial cell apoptosis”. In: *Cell Death Differ.* 23.8 (Feb. 2016), pp. 1331–1346. ISSN: 1476-5403. DOI: 10.1038/cdd.2016.14.

[146] Peter J. Nelson, Andrew J. Rees, Matthew D. Griffin, Jeremy Hughes, Christian Kurts, and Jeremy Duffield. “The Renal Mononuclear Phagocytic System”. In: *JASN* 23.2 (Feb. 2012), pp. 194–203. ISSN: 1046-6673. DOI: 10.1681/ASN.2011070680.

[147] Fiona Chow, Elyce Ozols, David J. Nikolic-Paterson, Robert C. Atkins, and Gregory H. Tesch. “Macrophages in mouse type 2 diabetic nephropathy: Correlation with diabetic state and progressive renal injury”. In: *Kidney International* 65.1 (Jan. 2004), pp. 116–128. ISSN: 0085-2538. DOI: 10.1111/j.1523-1755.2004.00367.x.

[148] Arthur C. K. Chung and Hui Y. Lan. “Chemokines in Renal Injury”. In: *JASN* 22.5 (May 2011), pp. 802–809. ISSN: 1046-6673. DOI: 10.1681/ASN.2010050510.

[149] W. E. Fibbe and R. Willemze. “The Role of Interleukin-1 in Hematopoiesis”. In: *AHA* 86.3 (1991), pp. 148–154. ISSN: 0001-5792. DOI: 10.1159/000204824.

[150] T. W. Meyer, P. H. Bennett, and R. G. Nelson. “Podocyte number predicts long-term urinary albumin excretion in Pima Indians with Type II diabetes and microalbuminuria”. In: *Diabetologia* 42.11 (Oct. 1999), pp. 1341–1344. ISSN: 1432-0428. DOI: 10.1007/s001250051447.

[151] Michael Mauer, Maria Luiza Caramori, Paola Fioretto, and Behzad Najafian. “Glomerular structural–functional relationship models of diabetic nephropathy are robust in type 1 diabetic patients”. In: *ndt.* 30.6 (Sept. 2014), pp. 918–923. ISSN: 0931-0509. DOI: 10.1093/ndt/gfu279.

[152] Helen C. Looker, Michael Mauer, Pierre-Jean Saulnier, Jennifer L. Harder, Viji Nair, Carine M. Boustany-Kari, Paolo Guarnieri, Jon Hill, Cordell A. Esplin, Matthias Kretzler, et al. “Changes in Albuminuria But Not GFR are Associated with Early Changes in Kidney Structure in Type 2 Diabetes”. In: *JASN* 30.6 (June 2019), pp. 1049–1059. ISSN: 1046-6673. DOI: 10.1681/ASN.2018111166.

[153] O. Osborn, SE Brownell, M. Sanchez-Alavez, D. Salomon, H. Gram, and T. Bartfai. “Treatment with an Interleukin 1 beta antibody improves glycemic control in diet induced obesity”. In: *Cytokine* 44.1 (Oct. 2008), p. 141. DOI: 10.1016/j.cyto.2008.07.004.

[154] Helena Cucak, Gitte Hansen, Niels Vrang, Torben Skarsfeldt, Eva Steiness, and Jacob Jelsing. “The IL-1β Receptor Antagonist SER140 Postpones the Onset of Diabetes in Female Nonobese Diabetic Mice”. In: *J. Diabetes Res.* 2016 (2016). DOI: 10.1155/2016/7484601.

[155] J. A. Ehses, G. Lacraz, M.-H. Giroix, F. Schmidlin, J. Coulaud, N. Kassis, J.-C. Irminger, M. Kergoat, B. Portha, F. Homo-Delarche, et al. “IL-1 antagonism reduces hyperglycemia and tissue inflammation in the type 2 diabetic GK rat”. In: *Proc. Natl. Acad. Sci. U.S.A.* 106.33 (Aug. 2009), pp. 13998–14003. ISSN: 0027-8424. DOI: 10.1073/pnas.0810087106.

[156] Jun Zha, Xiao-wei Chi, Xiao-lin Yu, Xiang-meng Liu, Dong-qun Liu, Jie Zhu, Hui Ji, and Rui-tian Liu. “Interleukin-1β-Targeted Vaccine Improves Glucose Control and β-Cell Function in a Diabetic KK-Ay Mouse Model”. In: *PLoS One* 11.5 (May 2016), e0154298. ISSN: 1932-6203. DOI: 10.1371/journal.pone.0154298.

[157] Nadine S. Sauter, Fabienne T. Schulthess, Ryan Galasso, Lawrence W. Castellani, and Kathrin Maedler. “The Antiinflammatory Cytokine Interleukin-1 Receptor Antagonist Protects from High-Fat Diet-Induced Hyperglycemia”. In: *endo.* 149.5 (May 2008), pp. 2208–2218. ISSN: 0013-7227. DOI: 10.1210/en.2007-1059.

[158] Philippe P. Pagni, Damien Bresson, Teresa Rodriguez-Calvo, Amira Bel Hani, Yulia Manenkova, Natalie Amirian, Alecia Blaszczak, Sina Faton, Sowbarnika Sachithanantham, and Matthias G. von Herrath. “Combination Therapy With an Anti–IL-1β Antibody and GAD65 DNA Vaccine Can Reverse Recent-Onset Diabetes in the RIP-GP Mouse Model”. In: *Diabetes* 63.6 (June 2014), pp. 2015–2025. ISSN: 0012-1797. DOI: 10.2337/db13-1257.

[159] Vitaly Ablamunits, Octavian Henegariu, Jakob Bondo Hansen, Lynn Opare-Addo, Paula Preston-Hurlburt, Pere Santamaria, Thomas Mandrup-Poulsen, and Kevan C. Herold. “Synergistic Reversal of Type 1 Diabetes in NOD Mice With Anti-CD3 and Interleukin-1 Blockade: Evidence of Improved Immune Regulation”. In: *Diabetes* 61.1 (Jan. 2012), pp. 145–154. ISSN: 0012-1797. DOI: 10.2337/db11-1033.

[160] Alexander M. Owyang et al. “XOMA 052, an anti-IL-1{beta} monoclonal antibody, improves glucose control and {beta}-cell function in the diet-induced obesity mouse model”. In: *PubMed. comprises. more. than. 30 million. citations. for. biomedical. literature. from. MEDLINE, life. science. journals., and. online. books.* 151.6 (June 2010), pp. 2515–2527. ISSN: 1945-7170. DOI: 10.1210/en.2009-1124.

[161] Yue Zhang, Xiao-Lin Yu, Jun Zha, Li-Zhen Mao, Jia-Qian Chai, and Rui-Tian Liu. “Therapeutic vaccine against IL-1β improved glucose control in a mouse model of type 2 diabetes”. In: *Life Sci.* 192 (Jan. 2018), pp. 68–74. ISSN: 1879-0631. DOI: 10.1016/j.lfs.2017.11.021.

[162] Marianne Bni-Schnetzler et al. “β Cell-Specific Deletion of the IL-1 Receptor Antagonist Impairs β Cell Proliferation and Insulin Secretion”. In: *Cell Reports* 22.7 (Feb. 2018), pp. 1774–1786. ISSN: 2211-1247. DOI: 10.1016/j.celrep.2018.01.063.

[163] M. R. Yelich. “In vivo endotoxin and IL-1 potentiate insulin secretion in pancreatic islets”. In: *PubMed. comprises. more. than. 30 million. citations. for. biomedical. literature. from. MEDLINE, life. science. journals., and. online. books.* 258.4 (Apr. 1990), Pt. ISSN: 0002-9513. DOI: 10.1152/ajpregu.1990.258.4.R1070.

[164] Florian Kahles et al. “GLP-1 Secretion Is Increased by Inflammatory Stimuli in an IL-6–Dependent Manner, Leading to Hyperinsulinemia and Blood Glucose Lowering”. In: *Diabetes* 63.10 (Oct. 2014), pp. 3221–3229. ISSN: 0012-1797. DOI: 10.2337/db14-0100.

[165] Erez Dror et al. “Postprandial macrophage-derived IL-1β stimulates insulin, and both synergistically promote glucose disposal and inflammation”. In: *Nat. Immunol.* 18 (Jan. 2017), pp. 283–292. ISSN: 1529-2916. DOI: 10.1038/ni.3659.

[166] David Holmes. “Immunometabolism: Physiologic role of IL-1β in glucose homeostasis”. In: *Nat. Rev. Endocrinol.* 13 (Feb. 2017), p. 128. ISSN: 1759-5037. DOI: 10.1038/nrendo.2017.11.

[167] Paula M. Ladwig, David R. Barnidge, and Maria A. V. Willrich. “Mass Spectrometry Approaches for Identification and Quantitation of Therapeutic Monoclonal Antibodies in the Clinical Laboratory”. In: *Clin. Vaccine Immunol.* 24.5 (May 2017). DOI: 10.1128/CVI.00545-16.

[168] Victor G. Puelles, James W. van der Wolde, Keith E. Schulze, Kieran M. Short, Milagros N. Wong, Jonathan G. Bensley, Luise A. Cullen-McEwen, Georgina Caruana, Stacey N. Hokke, Jinhua Li, et al. “Validation of a Three-Dimensional Method for Counting and Sizing Podocytes in Whole Glomeruli”. In: *JASN* 27.10 (Oct. 2016), pp. 3093–3104. ISSN: 1046-6673. DOI: 10.1681/ASN.2015121340.

13 Declaration

I hereby declare that I have written the present thesis entitled ”Interleukin-1β Inhibition for Chronic Kidney Disease in Obese Mice with Type 2 Diabetes” independently, without assistance from external parties and without use of other resources than those indicated. The ideas taken directly or indirectly from external sources are duly acknowledged in the text. The material, either in full or in part, has not been previously submitted for grading at this or any other academic institution.

Part of the work was done by others, as mentioned below:

1. PD Maja T. Lindenmeyer, University of Munich, Germany. She performed the analysis of human kidney biopsy transcriptomics. The data is presented in the results part II, section 5.2.1 (IL-1β gene expression in patients with DKD) of this thesis.
2. Dr. Solange Moll, Institute of Clinical Pathology, University Hospital Geneva, Geneva, Switzerland. She performed the human immunostaining. The data is presented in the results part II, section 5.2.1 (IL-1β protein expression in patients with DKD) of this thesis.

Munich, 17.07.2021	Yutian Lei
Date, place	Signature

14 Acknowledgement

There are many colleagues who have contributed to this project, helped and inspired me during my study. I would like to convey my gratitude to all of them.

First, I would like to thank my supervisor Prof. Hans-Joachim Anders. He patiently provided the vision, encouragement,W and advice necessary for me to proceed through the doctoral program. Thank you very much for giving me the opportunity to work at Anders Lab. I would like to thank my co-supervisor on my first year Dr. rer. hum. biol. Santhosh Kumar Vankayala Ramaiah. Thank you for your sharing, guidance, and encouragement.

I would also like to thank people for their work and cooperation to complete this thesis. Thank Dr. Stefan Dengl, Roche Diagnostics, Penzberg, Germany for developing and sharing anti-IL-1β IgG. I thank Dr. Sabine Grüner, Roche Pharma Research & Early Development, Basel, Switzerland, for providing the antibody and supporting logistics. Thank Dan Draganovici and Janina Mandelbaum for performing the histology of animal studies. Thank Yvonne Minor, Narci Izidoro da Rocha, and Martrez Nabil Zaki Ebrahim for their technique support on animal care. Thank Dr. Julian Marschner and Dr. Satish Kumar Devarapu for their help on mouse surgery. Thank Manga Motrapu for support in analyzing the sirius red staining. Thank Dr. Stefanie Steiger, Dr. Lidia Anguiano Gómez, and Dr. Laura Martinez Valenzuela for their support and assistance of animal study.

I thank all my lab members. Thank Julian, Lidia, Steffi, Mohsen, Qiuyue, Shishi, Yao, Daigo, Taka, Shrikant, Maciej, Manga, Julia, and Lina for their teaching, sharing, help, and encouragement. Thank all the lab buddies, who I could not enumerate here, for generating such a friendly and scientific environment. Thank PD Dr. Bruno Luckow for his excellent organization and management of our lab, sharing experience, and providing technique supports. Thank Kathi, Ewa, and Anna for all the arrangement.

I would like to thank CSC-LMU scholarship for their financial support and giving me an opportunity to study abroad.

I would like to thank my family and friends, who are the pillar of my life and whose advice and encouragement I greatly appreciate.

It is my duty to express my humble respect to the animals, which had to involved in the experiment for the betterment of human being.